Progress in Materials Science xxx (xxxx) xxx

Contents lists available at ScienceDirect

Progress in Materials Science

journal homepage: www.elsevier.com/locate/pmatsci

(Ba, Sr)TiO_3/polymer dielectric composites–progress and perspective

Feng Gao [a,*], Kena Zhang [a], Yiting Guo [a], Jie Xu [a], Mikołaj Szafran [b]

[a] State Key Laboratory of Solidification Processing, MIIT Key Laboratory of Radiation Detection Materials and Devices, NPU – QMUL Joint Research Institute of Advanced Materials and Structures (JRI-AMAS), School of Materials Science and Engineering, Northwestern Polytechnical University, Xi'an, Shaanxi 710072, PR China

[b] Faculty of Chemistry, Warsaw University of Technology, Noakowskiego 3, 00-664 Warsaw, Poland

ARTICLE INFO

Keywords:
BST/polymer composites
Fabrication processing
Permittivity
Dielectric tunability
Energy storage
Theoretical models

ABSTRACT

This paper reviews recent developments and challenges of (Ba,Sr)TiO_3/polymer functional composites. The microstructure of barium-strontium titanate (Ba,Sr)TiO_3(BST)/polymer composites with different polymer matrices and the nature of the interface between the BST and polymer matrix is critical in the final dielectric properties. The effects of concentration, particle size and BST filler shape on the dielectric properties of BST/polymer composites are discussed. A theoretical model for the dielectric constants of ceramic/polymer composites and the fabrication of BST/polymer composites are described briefly. The development of a dielectric tunability for the BST/polymer composites is summarized. A dielectric tunability theoretical model is proposed based on our previous research results and the effects of several factors on the dielectric tunability of the composites are discussed, which contributes to a prediction of the dielectric tunability of the composites and provides important theoretical and research significance for future work.

1. Introduction

Barium-strontium titanate $Ba_{1-x}Sr_xTiO_3$ or $Ba_xSr_{1-x}TiO_3$ (BST) is a ferroelectric solid-solution that is composed of $BaTiO_3$ (BT) and $SrTiO_3$ (ST) with a perovskite structure [1–2]. Because of its outstanding properties, such as its high dielectric constant, low dielectric loss, well-controlled Curie temperature by Ba/Sr ratio adjustment and its strong dielectric nonlinearity in an applied direct-current (DC) electric field, the application of BST materials has been investigated in several fields, including microwave phase shifters [3–5], memory storage [6–9], super dielectric capacitor [10–11] and other functional sensor components [12–13]. BST has some drawbacks, such as its brittleness, high sintering temperature, poor processing conditions and low dielectric strength because of the presence of residual pores, which impedes its widespread application.

Polymers have advantages of an easy fabrication, light weight, mechanical flexibility, low dielectric loss, convenient processing and high dielectric strength. However, polymers have a low dielectric constant compared with inorganic materials [14], which limits their application in the production of electrical devices. Thus, functional composites that combine the advantages of BST ceramics and polymer are expected to be desirable materials for dielectric devices [15–18]. The connectivity of individual phases influences the composite properties. Newnham [19–20] proposed the concept of connectivity to describe the connection between filler and matrix. In a diphasic system, each phase has a continuous state with 0, 1, 2 or 3 dimensions and the connectivity can be marked as 0–3, 2–2, in

* Corresponding author.
E-mail address: gaofeng@nwpu.edu.cn (F. Gao).

https://doi.org/10.1016/j.pmatsci.2021.100813
Received 5 May 2019; Received in revised form 3 March 2021; Accepted 9 April 2021
Available online 3 May 2021

Nomenclature

Symbols	Description
T_c	Curie temperature
E_c	coercive electric field
P_r	remanent polarization
E_a	activation energy
K_B	Boltzmann constant
$\varepsilon_{(0)}$	permittivity under zero direct current
$\varepsilon_{(E)}$	permittivity under a specific applied electric bias
T_u	dielectric tunability under a specific applied electric bias
T_0	dielectric tunability under unit electric field
E	a specific applied electric bias
J	energy storage density
ε_0	vacuum permittivity (8.854×10^{-12}F/m)
$\varepsilon_{r(E)}$	dielectric constant under a specific applied electric bias
E_b	dielectric breakdown strength
$\boldsymbol{\varepsilon_r}$	dielectric constant
tanδ	dielectric loss
ε_c	dielectric constant of ceramic
ε_p	dielectric constant of polymer
δ_c	volume fraction of ceramic
δ_p	volume fraction of polymer
T_{u1}	dielectric tunability of composites
ε_1	dielectric constant of composites
T_{u2}	dielectric tunability of ceramic
ε_2	dielectric constant of ceramic
β_1	phenomenological coefficient of composites
β_2	phenomenological coefficient of ceramics

which the first and second digits correspond to the filler and matrix phases, respectively. Among the composites studied so far, extensive research has been conducted on the simplest 0–3 connectivity, which consists of a three-dimensional connected polymer matrix filled with ceramic particles.

In recent years, the focus on BST/polymer 0–3-type composites has included their fabrication, microstructure and dielectric properties. Noticeable issues for BST/polymer composites are related to the interface between the BST and polymer phases. An excessively high content of ceramic particles will result in a poorer bonding force of the two-phase interface in the composite material, which results in a microstructure with more defects. BST filler modification yields an improved microstructure and enhanced dielectric properties. For example, BST filler was modified by a silane coupling agent or functionalized by a specific group [21–23] to optimize the microstructure and improve the dielectric properties. Nanofibers [22,24–26], nanotubes [27] and nanowires [28–29] impart better microstructural and dielectric properties to composites with a relatively low BST filler content. Among these composites, BST powders with a larger surface area and aspect ratio contribute to superior dielectric properties. Besides the 0–3-types composites, other composites types can be investigated in these BST/polymer composites. In some three-phase composites, the ultra-high composite dielectric constant does not stem directly from the intrinsic dielectric constant of the filler and polymer. An enhanced interfacial polarization and growing number of microcapacitors in the inner composite structure is often considered a reason for high dielectric constant. Therefore, the composite microstructure and the interface between two phases are important, and affect the dielectric properties of the composite. Similarly, the type, concentration, size, BST filler shape and composite material preparation process have an important influence on the dielectric properties of the composite material. All factors are correlated and should be considered systematically when BST/polymer materials are investigated.

BST materials have another important property, namely, the dielectric tunability. The dielectric tunability of BST-based ceramics has been studied extensively [30–40]. These ceramics have a high dielectric tunability, which means a percentage change in permittivity under a DC bias. For application in microwave tunable devices, a lower permittivity and a higher dielectric tunability are most appropriate for impedance matching [41–42]. Nevertheless, the real performance does not provide the dielectrics with a high tunability but usually corresponds to a high permittivity. BST/polymer composites have been optimized for microwave tunable devices because of their suitable performance: (1) a moderate dielectric constant, (2) a low dielectric loss and (3) a high dielectric tunability. Thus, it is worth investigating the dielectric tunability of BST/polymer composites.

This paper aims to review progress in the field of BST/polymer composites from BST-based single-phase materials to final composites, and aims to provide a comprehensive and systematic analysis of BST/polymer composites and their potential applications. The paper consists of seven sections, including an overview of BST-based ceramics, the effects of BST/polymer composite microstructure and theoretical models for the ceramic/polymer composite dielectric constant, the fabrication approach for BST/polymer composites,

the effect of BST fillers on the dielectric properties of the BST/polymer composites, the development of a BST/polymer composite dielectric tunability, the potential applications of BST/polymer composites in different fields, and remarks and future perspectives.

2. Overview of (Ba,Sr)TiO_3 materials

2.1. Crystal structure

$Ba_{1-x}Sr_xTiO_3$ is an infinite solid-solution that is formed by $BaTiO_3$ and $SrTiO_3$, and has a typical perovskite-type (ABO_3) structure. The ideal perovskite [43] shows a simple ionic arrangement as shown in Fig. 1(a). The Ba^{2+} and Sr^{2+} ions are located at the vertex angle of the cube (A-site), the Ti^{4+} cations occupy the center of the cube (B-site) and the O^{2-} occupy the centers of the six cube faces and form $[TiO_6]^{2-}$ octahedra with adjacent Ti^{4+} cations. Each Ba^{2+} and Sr^{2+} ion occupies the $[TiO_6]^{2-}$ octahedra gap, as shown in Fig. 1(b). The $[TiO_6]^{2-}$ octahedron, with a perfect 90° angle and six Ti–O bonds of equal bond length, can be extended repeatedly in three dimensions and has three fourfold rotational axes, four threefold rotational axes and six twofold axes.

The basic BST perovskite unit is the $[TiO_6]^{2-}$ octahedra. The spontaneous polarization of BST originates from the movement of Ti^{4+} positive ions away from the $[TiO_6]^{2-}$ octahedra center. No spontaneous polarization occurs because of the coincidence between the positive and negative charge within the undistorted TiO_6 octahedron with central symmetry when BST crystals exist in a cubic phase under a relatively high temperature. With a decreasing temperature, the $Ba_{1-x}Sr_xTiO_3$ crystal has a tetragonal phase and Ti^{4+} cations are offset along a fourfold axis and cannot maintain the balanced position of the $[TiO_6]^{2-}$ octahedra center, which can form a strong dipole moment. Spontaneous polarization along the misalignment direction of the Ti^{4+} cations has been generated. When the temperature is reduced further, the Ti^{4+} cations are displaced from the $[TiO_6]^{2-}$ octahedra center with a two- and threefold axis and corresponding spontaneous polarization in the same direction.

2.2. Dielectric properties

2.2.1. Composition dependence of dielectric properties

The chemical composition of the $Ba_xSr_{1-x}TiO_3$ is an important parameter that affects the ferroelectric properties. **Reverón et al.** [44] prepared $Ba_xSr_{1-x}TiO_3$ with different x values by a conventional mixed-oxide method. The XRD interval of 2θ in the 29~35° range shows two effects (as shown in Fig. 2). The decreasing unit cell parameter with an increasing strontium content prompted a peak shift toward a high angle. Crystallization of smaller coherent domains was observed from a slightly increasing line width with the strontium content. In the BT crystal, when Sr^{2+} was introduced at a perovskite structure A-site, the ions entered the Ba^{2+} site substitutions, and a decrease in lattice constant occurred as the Sr^{2+} content increased (as shown in Fig. 3). Similar results were obtained by other researchers [45–47].

The BST Curie temperature covers a wide temperature range. A paraelectric–ferroelectric phase transition at 403 K from the cubic to the tetragonal phase resulted for pure $BaTiO_3$ (BT) ceramic, as a typical first-order phase transition of displacement type [48]. $SrTiO_3$ (ST) changes from a simple cubic phase to a tetragonal phase near 105 K and retains the phase at absolute zero [49]. The main result of Sr^{2+} ion addition into the BT is to promote the Curie temperature shift towards room temperature (RT) and stabilize the BST with a paraelectric phase at a low temperature. As shown in Fig. 4, **Kim et al.** [50] investigated the phase structure and dielectric properties of $Ba_{1-x}Sr_xTiO_3$ ceramics with various stoichiometric percentages of strontium. The strontium content did not change the perovskite structure. Diffraction peaks shifted to higher angles with an increase in Sr content because of the gradual decrease in lattice constants, as shown in Fig. 4(a). BST with $x < 0.3$ exhibited ferroelectric properties, whereas BST with $x > 0.3$ exhibited paraelectric properties. These results match the structural investigation, which indicate a tetragonal structure for $x < 0.3$ and a cubic structure for $x > 0.3$, as shown in Fig. 4(b). For ferroelectric BST, the remnant polarization P_r and coercive electric field E_c decrease with an increase in Sr^{2+} concentration. With an increase in ST content, the Curie temperature of BST decreased gradually, and the corresponding maximum dielectric constant decreased. The Curie temperature of the BST was 305 K (near RT). It was difficult to determine the T_c and maximum dielectric constant of ST ceramics because ST is a quantum paraelectric.

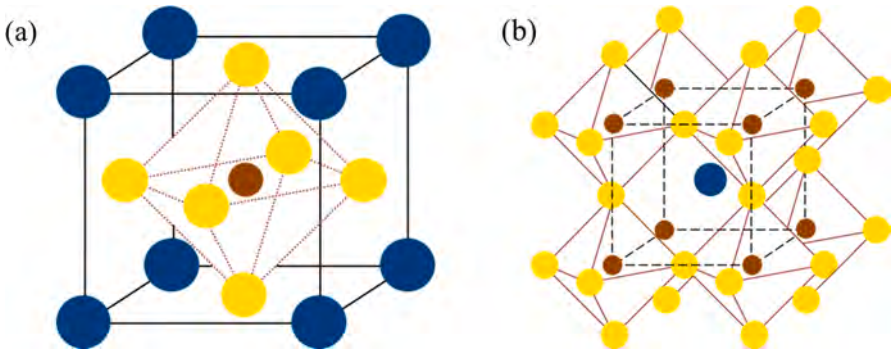

Fig. 1. (a) Perovskite structure and (b) oxygen octahedral connection in perovskite structure.

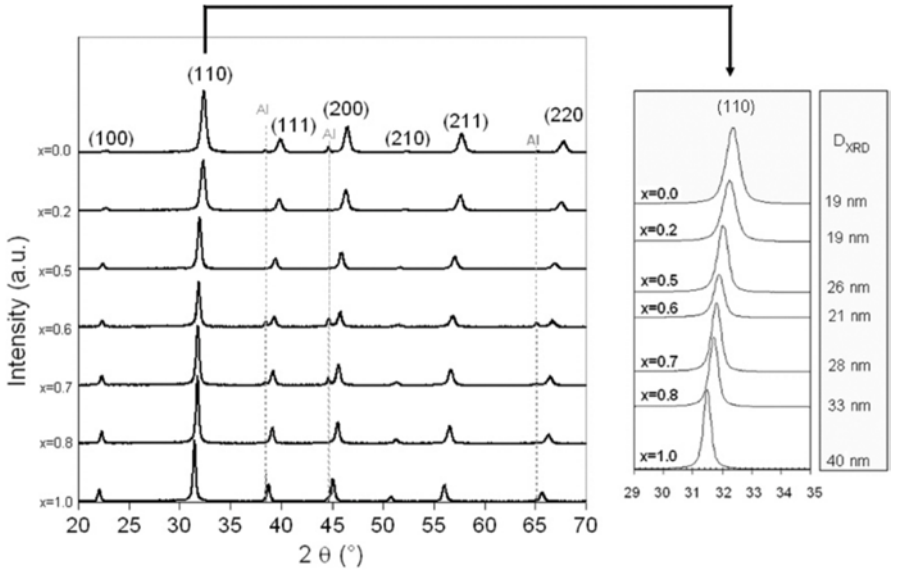

Fig. 2. XRD pattern of $Ba_xSr_{1-x}TiO_3$ powders, zoom in 29–35° range and estimated mean crystalline size from Scherrer's equation [33].

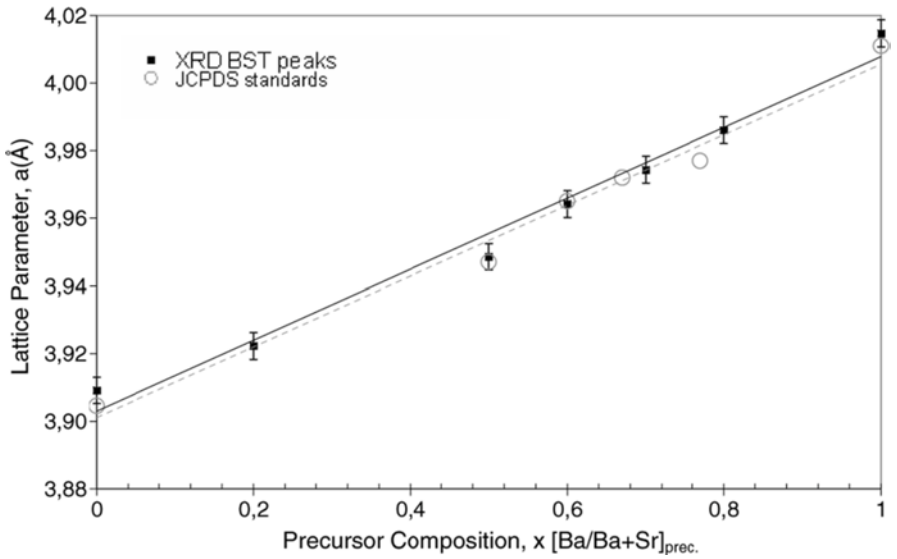

Fig. 3. Lattice parameter of as-synthesized BST powders calculated from XRD patterns versus corresponding feed solution compositions and (**o**) JCPDS values [44].

The influence of Ba/Sr ratio on the Curie temperature is described in Refs [51–53]. **Fu et al.** [54] summarized the dependence of Curie temperatures on x (x = Ba/(Ba + Sr)) and the direct linear relationship between the stoichiometric percentage of barium and Curie temperature was proposed as:

$$T_c(^{\circ}\mathrm{C}) = -195 + 322.2x \quad (1)$$

The Ba/Sr ratio dependence of the coercive electric field (E_c) and the remanent polarization (P_r) of $Ba_xSr_{1-x}TiO_3$ ceramics under the same sintering conditions were discussed where the values of E_c and P_r increased as the Ba/Sr ratio increased [40,54]. $Ba_{1-x}Sr_xTiO_3$ materials can be used as electroluminescent devices with a highly transparent insulation. Some authors have investigated the optical properties of BST powders [55–60], which are dependent on the chemical composition. **Rashad et al.** [60] reported the transmittance of $Ba_{1-x}Sr_xTiO_3$ nanopowders with different Sr^{2+} ion contents of 0.3, 0.5 and 0.7. The higher Sr^{2+} content yielded a larger $Ba_{1-x}Sr_xTiO_3$ nanopowder transmittance for a 200 to 800 nm wavelength, which was attributed to a decrease in band gap energy of $Ba_{1-x}Sr_xTiO_3$ with an increase in Sr^{2+} content. Therefore, the structure and dielectric properties can be tailored by controlling the $Ba_{1-x}Sr_xTiO_3$ composition.

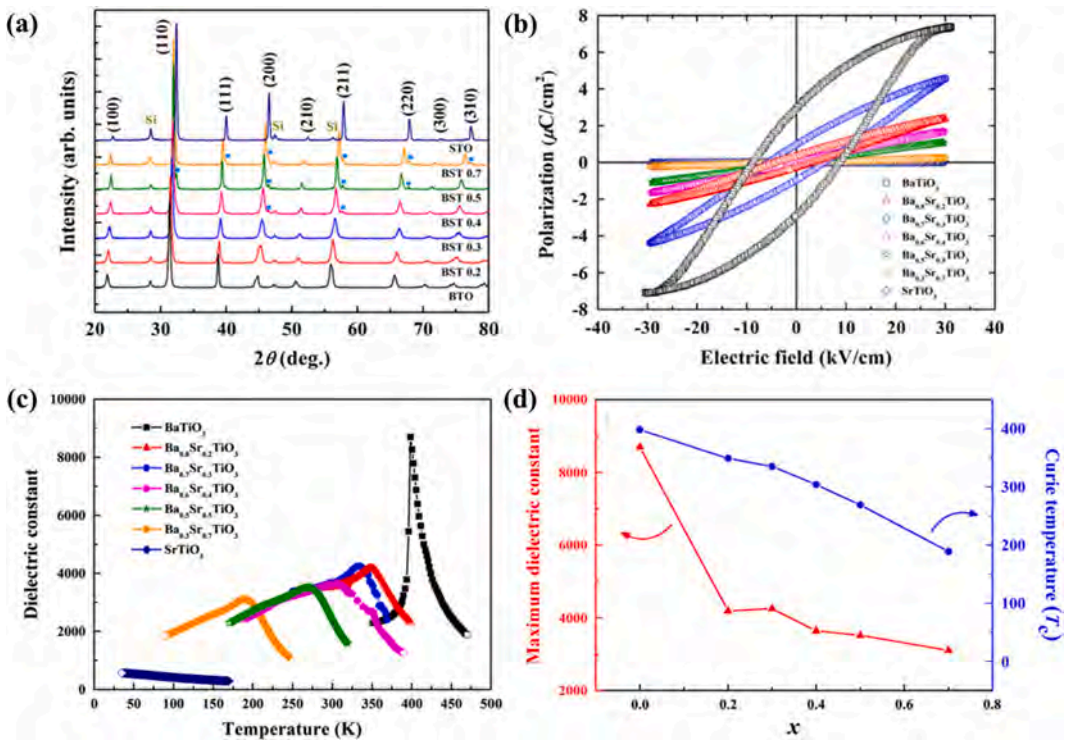

Fig. 4. (a) XRD pattern of $Ba_{1-x}Sr_xTiO_3$, (b) P–E loops of $Ba_{1-x}Sr_xTiO_3$, (c) temperature dependence of dielectric constant for $Ba_{1-x}Sr_xTiO_3$, (d) maximum dielectric constant and Curie temperature for $Ba_{1-x}Sr_xTiO_3$ [40].

2.2.2. *Temperature dependence of dielectric properties*

$Ba_xSr_{1-x}TiO_3$ materials are complex compounds and their macroscopic properties may differ when the temperature changes. The change in $Ba_xSr_{1-x}TiO_3$ dielectric behavior is studied often. A typical relaxor dielectric response has been detected in the $Ba_xSr_{1-x}TiO_3$ system [61–63]. For example, the variation of dielectric constant and dielectric loss of Ba_{1-x} Sr_xTiO_3 ceramics (x = 0.5, 0.55, 0.60, 0.70) with a higher temperature at different frequencies is shown in Fig. 5 [64]. At a low temperature, the dielectric constant and dielectric loss maintain a steady value and increase with an increase in temperature. A peak was visible from the temperature dependence of the dielectric loss data, which shows a shift to a higher temperature with an increase in frequency. Other BST ceramics with different compositions show a similar performance. The activation energy of the dielectric relaxation behaviors, which characterize the effective energy barriers that impede the polaron transfer and make them orientate under an external electric field, could be calculated from the temperature dependence of the dielectric loss of the BST ceramics from the following:

$$\ln f = \ln f_0 + \frac{-E_a}{K_B}\frac{1}{T} \tag{2}$$

where f is the measurement frequency at a certain measurement temperature, E_a is the activation energy for the relaxation process, K_B is the Boltzmann constant and T is the absolute temperature at the extreme point of each dielectric loss peak. As shown in Fig. 6, the activation energy of Ba_{1-x} Sr_xTiO_3 for relaxation was 1.172, 1.217 and 1.231 eV for x = 0.5, 0.6 and 0.7, respectively [64]. Free charge transfer and orientation was more difficult with an increase in Sr^{2+} content. E_a corresponds to the relaxation of space charge, which

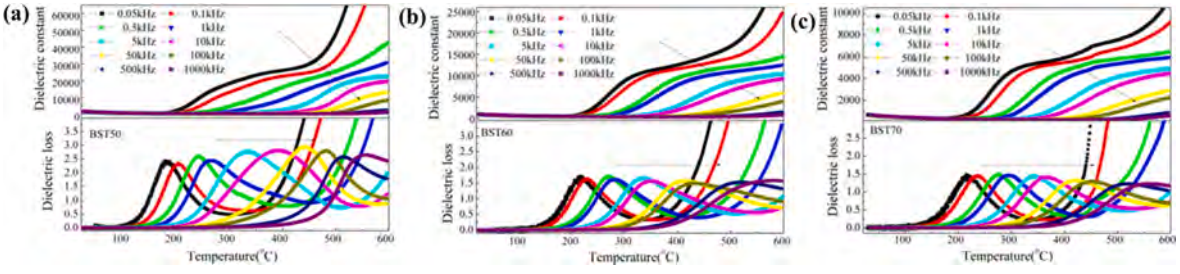

Fig. 5. Variation of dielectric constant and dielectric loss with temperature measured at different frequencies for BST ceramics: (a) $Ba_{0.5}Sr_{0.5}TiO_3$, (b) $Ba_{0.4}Sr_{0.6}TiO_3$, (c) $Ba_{0.3}Sr_{0.7}TiO_3$ [64].

characterizes the effective energy barriers that impeded free-charge transfer and yielded an orientation under an external electric field. The grain size decreased with an increase in Sr/Ba ratio, which resulted in an increased grain boundary and space charge in the BST ceramics. It was difficult for free-charge transfer and orientation provision under an external electric field, which led to an increase in activation energy.

2.2.3. Frequency dependence of dielectric properties

The variation in dielectric properties of the BST materials depends on the frequency because of different response characteristics in different frequency ranges. The frequency dependence of the dielectric constant of $Ba_{1-x}Sr_xTiO_3$ ($x = 0.5{\sim}0.7$) ceramics from 10 Hz to 1 MHz was investigated [64]. As shown in Fig. 7, all BST ceramics had a good frequency stability. The dielectric constant decreased with an increase in Sr^{2+} concentration because of the smaller radius of the Sr^{2+} with a lower contribution to the dielectric constant with ion-polarization. The gradual decrease in dielectric loss with an increase in frequency may be ascribed to the $Ba_{1-x}Sr_xTiO_3$ ($x = 0.5{\sim}0.7$) having a paraelectric phase at RT and the primary contribution to the dielectric loss of conduction loss at a low frequency.

The frequency dependence of the dielectric properties is complex because the $Ba_{1-x}Sr_xTiO_3$ ceramics have a relatively high temperature dependence. When the temperature range changed, the dielectric behavior was not similar. It is likely that the frequency had a strong influence on the dielectric constant at a higher temperature. Fig. 8 shows the dielectric constant and dielectric loss as a function of frequency (1 kHz to 1 MHz) at 225, 300 and 500 °C higher than T_c. A dispersive behavior results at low frequencies, which reflects the blocking effects. The dispersion variation in dielectric constant is caused mainly by the polarization structure of the BST ceramic and its mobile carriers [65]. At a lower frequency, the high dielectric constant is related to the presence of many polarizations types (such as dipolar, electronic, ionic orientation and interfacial). The dielectric constant decreases with an increase in frequency mainly because some polarization types in ferroelectric materials cannot maintain the electric field change at a higher frequency, which displays the typical dielectric material performance. For the dielectric loss, the presence of peaks was visible at a higher temperature (≥300 °C) and shifted towards a higher frequency when the temperature increased. This feature indicated that a dielectric relaxation occurred in the BST ceramics.

Dielectric properties at different dielectric measurements are always diverse. At low frequency conditions, the typical performance of the dielectric constants and anomalies corresponded to the cubic–tetragonal transition at $T_c = 273$ K and revealed the tetragonal-orthorhombic transition near 210 K and the orthorhombic-rhombohedral transition near 160 K. A broadband dielectric response in the $Ba_{0.6}Sr_{0.4}TiO_3$ solid-solution was investigated by **Ostapchuk et al.** [66]. The frequency dependence of the dielectric properties and the secondary electric phase and other ferroelectric phases over a wide temperature range (with microwaves and a low frequency) was also studied. Fig. 9 shows the broadband spectra of BST above and below T_c. When the temperature exceeded T_c, no appreciable dispersion resulted below the phonon frequencies in the paraelectric phase, but a broad relaxation appeared in the GHz range when the temperature was close to T_c, as shown in Fig. 9(a). Below T_c, the dielectric spectra was dominated by GHz dispersion. The data were fitted to the dotted line to describe the GHz and MHz dispersion. A strong and broad relaxation in the GHz range resulted below T_c, which narrowed gradually with a decrease in temperature and approaches the simple Debye relaxation. The presence of a weaker relaxation at or below 1 MHz was also detected. The additional presence of dispersion in the GHz range below T_c showed that the BST ceramics with a paraelectric phase were suitable candidates for microwave application in a wide frequency range [67].

2.3. Dielectric tunability properties

$Ba_{1-x}Sr_xTiO_3$ ceramics show an excellent dielectric tunability under an external applied DC biasing. The dielectric tunability (T_u) is a nonlinear characteristic of the dielectric constant under a changing applied electric field from:

$$T_u = \frac{\varepsilon_{(0)} - \varepsilon_{(E)}}{\varepsilon_{(0)}} \times 100\% \tag{3}$$

where $\varepsilon_{(0)}$ and $\varepsilon_{(E)}$ are the dielectric constant at zero-DC electric field and under a specific applied electric bias, respectively. **Liou et al.** [68] investigated the dielectric tunability (at 5 kV/mm) of doped $Ba_{1-x}Sr_xTiO_3$ bulk ceramics at T_c and $T_c + 10$ °C. The DC bias influenced the dielectric constant in the ferroelectric and paraelectric states as shown in Fig. 10. An unpredictable variation in dielectric characteristics usually occurred because of domain movement and hysteresis at a DC bias in the ferroelectric state, which suggested that the working temperature should be 5~15 °C above the T_c to prevent the dielectric behavior instability for a phase

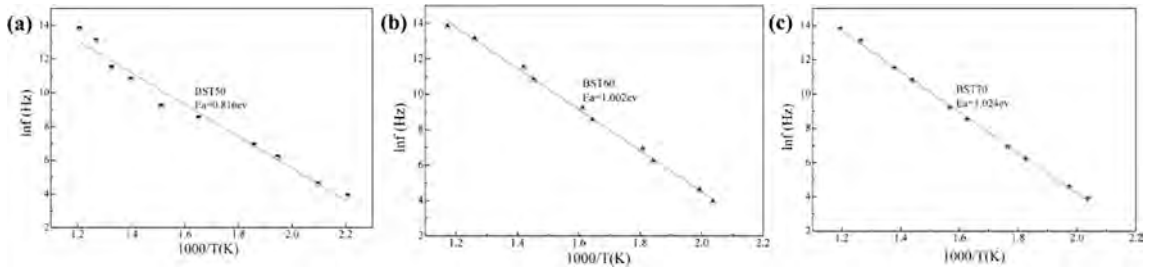

Fig. 6. Relaxation time as a function of 1000/T for BST ceramics: (a) $Ba_{0.5}Sr_{0.5}TiO_3$, (b) $Ba_{0.4}Sr_{0.6}TiO_3$, (c) $Ba_{0.3}Sr_{0.7}TiO_3$ [64].

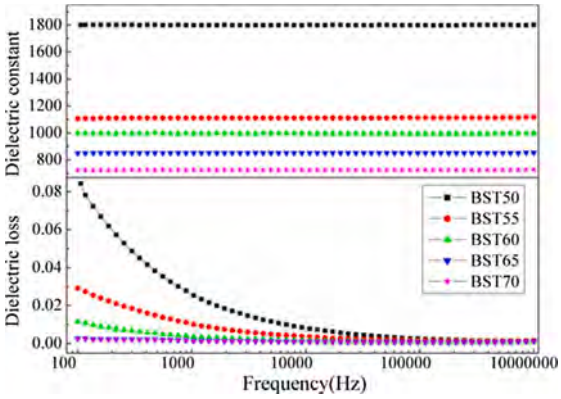

Fig. 7. Frequency dependence of dielectric constant and dielectric loss for BST ceramics with varying Sr/Ba ratios [64].

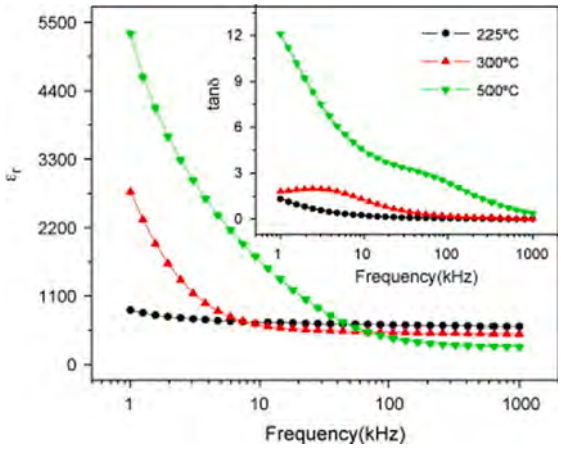

Fig. 8. Variation of ε_r and tanδ (inset) as a function of frequency at 225, 300 and 500 °C [65].

transition at ~T_c. **Qiu et al.** [69] fabricated $Ba_{1-x}Sr_xTiO_3$ thin films by a combined pulsed-laser deposition, and the effect of Sr^{2+} concentration on the dielectric tunability was investigated as shown in Fig. 11. Almost all measured BST films showed butterfly C-V loops (Fig. 11 (a)), especially for those with x from 0.1 to 0.7, which confirmed the existence of ferroelectricity in part of the BST films. Fig. 11(b) shows the dependence of tunability on the BST Sr content. The dielectric tunability of $Ba_{1-x}Sr_xTiO_3$ changed simultaneously with Sr^{2+} content and reached a maximum of ~85% for 0.4~0.5.

$Ba_{0.6}Sr_{0.4}TiO_3$ is denoted one of the most promising candidates for electronic tunable devices because of its relatively high dielectric tunability. Numerous studies have focused on the influence of microstructure, crystallinity, strain effects, ion doping and forming composite on the dielectric tunability of $Ba_{0.6}Sr_{0.4}TiO_3$ materials. However, work on dielectric tunability was measured at different conditions and it was difficult to compare results. For example, $Ba_{0.6}Sr_{0.4}TiO_3/Mg_2SiO_4$/MgO composite ceramics have a tunability of 10.5% at an applied electric field of 2.0 kV/mm [70]. The tunability of $Ba_{0.6}Sr_{0.4}TiO_3$ (Mn)/MgO was 27.3% at an electric field of 8.0 kV/mm [71]. $Ba_{0.6}Sr_{0.4}TiO_3$/MgO ceramics that were sintered by spark plasma sintering have a tunability of 50% at a 2.0 kV/mm biasing. [72]. The $Ba_{0.6}Sr_{0.4}TiO_3/Mg_{0.7}Zn_{0.3}TiO_3$ composite ceramic tunability was 33.5% at a 3.0 kV/mm biasing [73]. The $Ba_{0.6}Sr_{0.4}TiO_3/Mg_2TiO_4$ composite ceramic tunability reached 38.5% at an electric field of 2.0 kV/mm at 10 kHz [74]. A comparison standard for the tunability of materials was proposed by **Hu et al.** [75]. They defined T_0 as the tunability under a unit applied electric bias, as shown by:

$$T_0 = \frac{T}{E} \tag{4}$$

where T is the dielectric tunability at a specific applied electric bias, T_0 is the dielectric tunability at a unit electric field and E is a specific applied electric bias ($E \geq 0.5$ kV/mm). The calculated dielectric tunability values of some BST-based ceramics according to Eq. (4) are summarized in Table 1. The unit dielectric tunability of the BST ceramics existed between 0 and 0.3.

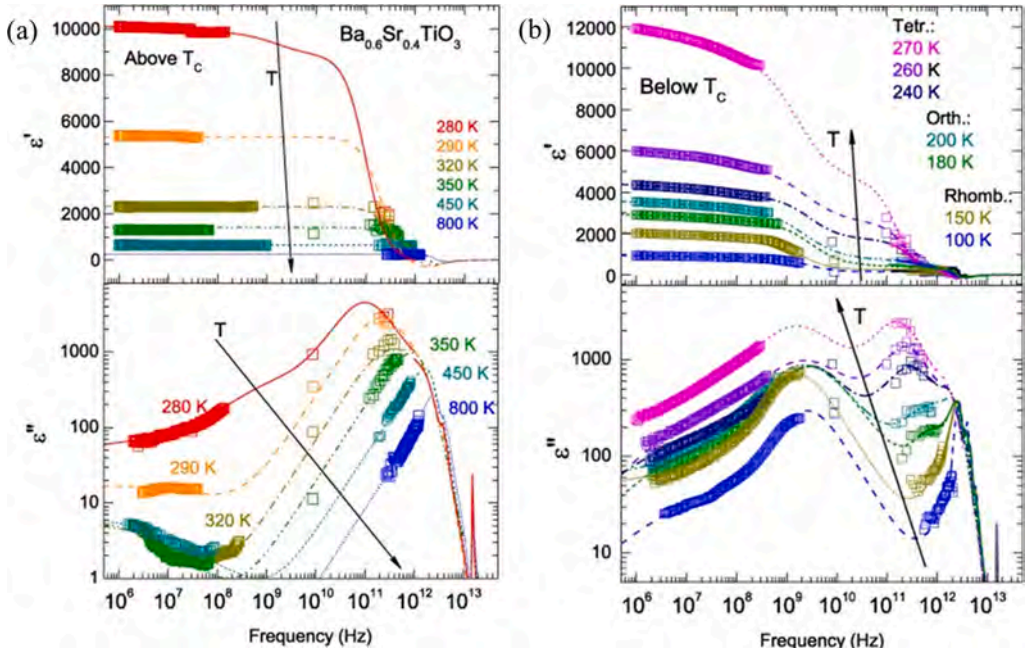

Fig. 9. Broadband spectra of BST at selected temperatures (a) above and (b) below T_C [66].

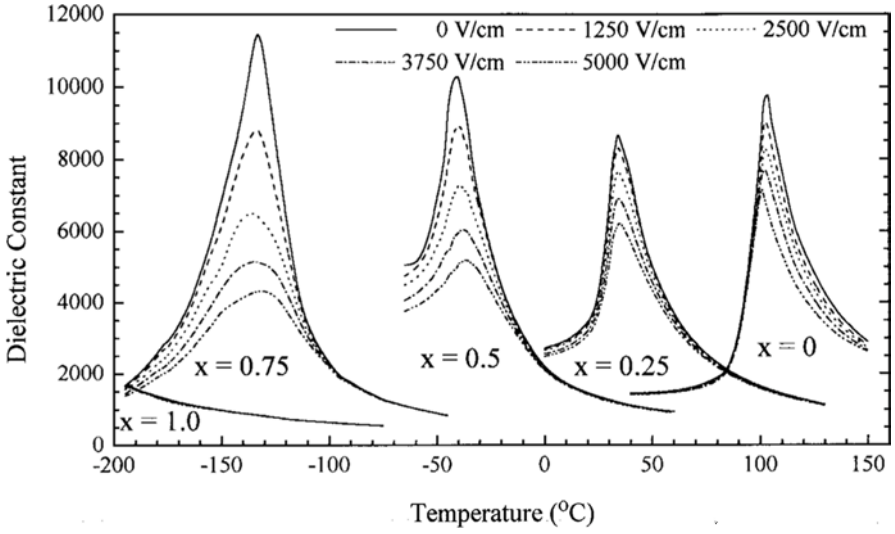

Fig. 10. Temperature dependence of dielectric constant as a function of DC-biasing field for doped $Ba_{1-x}Sr_xTiO_3$ system (10 kHz) [68].

2.4. *Energy storage properties*

Electric energy storage materials have received much attention because they are key in efficient, clean and versatile energy use. BST has been recognized as a promising candidate for energy storage because of its favorable properties. The energy storage density J is described by:

$$J = \int_0^E Edp = \int_0^E \varepsilon_0 \varepsilon_r(E) E dE \tag{5}$$

where J is the energy storage density (J/cm^3), E is the applied electric field (V/m), ε_0 is the vacuum permittivity (8.854×10^{-12}F/m), dp is the change in polarization induced in the dielectric by the applied field and $\varepsilon_r(E)$ is the electric-field-dependent dielectric constant. For linear dielectrics, the dielectric constant is not electric-field-dependent, and the energy storage density can be derived as:

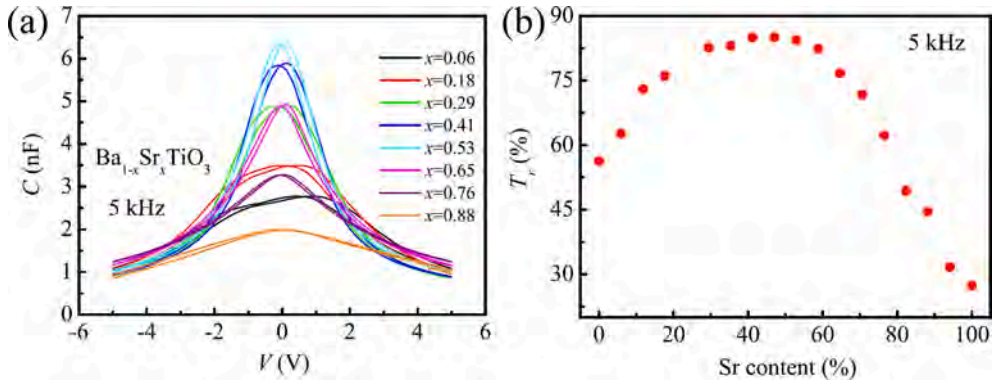

Fig. 11. (a) Capacitance–voltage characteristics at RT for BST films (5 kHz) and (b) dielectric tunability dependence of Sr concentration [69].

Table 1
T_u and T_0 in some $Ba_{0.6}Sr_{0.4}TiO_3$-based materials.

Materials	T_u (%)	E (kV/mm)	T_o (mm/kV)	Reference
$Ba_{0.6}Sr_{0.4}TiO_3/Mg_2SiO_4/MgO$	10.5	2.0	0.053	[70]
$Ba_{0.6}Sr_{0.4}TiO_3$(Mn)/MgO	27.3	8.0	0.034	[71]
$Ba_{0.6}Sr_{0.4}TiO_3$/MgO(3D)	50.0	2.0	0.250	[72]
$Ba_{0.6}Sr_{0.4}TiO_3/Mg_{0.7}Zn_{0.3}TiO_3$	33.5	3.0	0.112	[73]
$Ba_{0.6}Sr_{0.4}TiO_3/Mg_2TiO_4$	38.5	2.0	0.193	[74]
$Ba_{0.6}Sr_{0.4}TiO_3/MgO/Al_2O_3/ZnO$	27.4	1.0	0.274	[75]

$$J = \frac{1}{2}\varepsilon_0\varepsilon_r E_b^2 \tag{6}$$

where E_b is the dielectric breakdown strength. According to Eq. (6), the energy storage density was affected significantly by the dielectric breakdown strength (E_b) and dielectric constant. E_b is a key element to improve the energy storage property.

Previous studies showed that the E_b of BST ceramics was influenced by the composition [76,77], grain size [78,79], porosity [80], introduction of a second phase [81–83], preparation [84] and interfacial polarization [85]. For example, para-electric $Ba_{1-x}Sr_xTiO_3$ ceramics with a composition $x \geq 0.3$ and a T_c below RT, are considered a good energy storage material for electronic devices because of the higher breakdown strength. The dielectric constant of $Ba_{1-x}Sr_xTiO_3$ ceramics decreased as the strontium content increases, whereas the breakdown strength increased. The contradiction was balanced when $x = 0.6$, which meant that $Ba_{0.4}Sr_{0.6}TiO_3$ that was prepared by a conventional solid-state method and sintering temperature of 1350 °C had the highest energy density in the BST ceramics [86]. A comprehensive study of the grain size effect on the energy storage properties of $Ba_{0.4}Sr_{0.6}TiO_3$ prepared by the conventional solid-state reaction method was reported by **Song et al.** [87]. The E_b improved visibly from 114 kV/cm to 243 kV/cm with a grain size decrease from 5.6 to 0.5 μm. $Ba_{0.4}Sr_{0.6}TiO_3$ ceramics with a minimum grain size of 0.5 μm showed the maximum storage energy density (1.28 J/cm^3). Therefore, the significantly enhanced E_b of the $Ba_{0.4}Sr_{0.6}TiO_3$ ceramics was associated with grain boundaries [88].

A lower porosity tends to yield a higher E_b. Glass ceramics with fewer pores based on the ferroelectric materials can improve the energy storage density because of the sufficient dielectric constant and relatively high E_b of the glass state. The strong interactions between the existing glass and crystallized BST are critical to the energy storage density. BST ferroelectric glass-ceramics with the BaO-SrO-TiO_2-Al_2O_3-SiO_2 system using melt-casting and crystallization were fabricated by **Zhang et al.** [89]. The optimal discharged energy storage density was 1.8 J/cm^3. Therefore, a low released energy density in glass ceramics was caused mainly by interfacial polarization. **Wang et al.** [90] added AlF_3 into the BaO-SrO-TiO_2-Al_2O_3-SiO_2 system, and the charged and discharged energy storage densities increased with an increase in AlF_3 content (1~2 mol%) and decreased with a higher AlF_3 content. Extensive research has been conducted to improve the energy storage density included doping [91,92], powder refinement [93] and sintering with a special method, such as spark plasma sintering [94].

Three main forms of solid-dielectric breakdown include electrothermal, electrochemical and electrical breakdown. The first two forms of breakdown develop slowly over time, whereas electrical breakdown occurs in a relatively short time (10^{-7} s or less). Electrical breakdown tends to occur at pores and voids where the electric current can penetrate the grain interior.

3. BST/Polymer composites with different matrix materials

BST ceramics are used extensively in electronic devices because of their excellent dielectric properties, high stiffness and outstanding thermal stability [2–7]. However, their brittleness, low dielectric breakdown strength and challenging processing conditions impede their real applications. Compared with BST ceramics, polymers have advantages of a good mechanical flexibility, easy processing and low cost, which make them suitable for use as a ceramic/polymer functional composite matrix. The composites provide

an ideal solution to combine the dielectric materials and mechanical properties of the matrix.

3.1. Microstructure and dielectric properties of BST/Polymer composites

3.1.1. Two-phase composites

BST/polymer composite are a two-phase composite that consists of BST and a polymer matrix. It is unsystematic to understand and analyze the properties of ceramic/polymer composites based on the intrinsic properties of the individual phases. In addition to the content, type and size of ceramic particles mentioned above, the polymer is of great importance to the composite properties. The properties of the polymer matrix material affect the ceramic particle dispersion and compatibility and interface bonding of the two phases. The matrix microstructure should be considered critically when the ceramic/polymer composite performance is evaluated. The interfacial reaction between ceramic particles that participate in the formation of composite materials and between the polymer matrix is another important aspect that determines the composite material microstructure. Therefore, besides the ceramic fillers, the polymer matrix also dominated the electrical characteristics of the composites.

The polymer matrices that were selected for dielectric functional composites in the field of electronic equipment include PVDF [24–27,95–100], silicon–rubber [101], polyimide (PI) [102–104], polyacrylonitrile [17], polyvinyl chloride [105], cyanoethylated cellulose polymer [106], polystyrene [107], acrylonitrile butadiene styrene (ABS) [108], polyurethane [109], epoxy [110], cyclic olefin copolymer (COC) [111,112], polyphenylene sulfide (PPS) [113], polymethyl methacrylate (PMMA) [18,114,115] and others

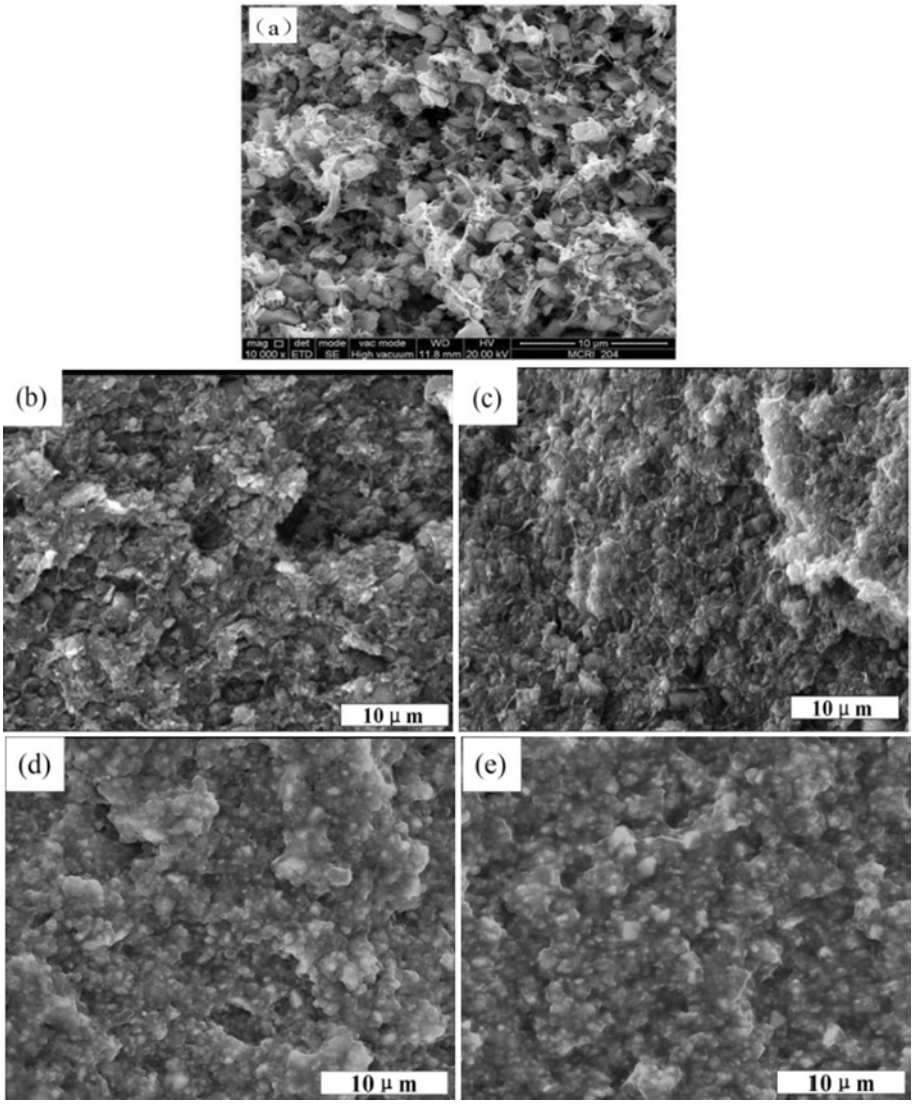

Fig. 12. SEM images of 40 vol% BST/PVDF composites modified with different mass fractions of KH550 coupling agent: (a) 0 wt%, (b) 1 wt%, (c) 2 wt%, (d) 4 wt%, (e) 8 wt% [122].

[116–120]. These polymers offer unique advantages over ceramics, such as their flexibility and therefore can be formed easily. Among these polymers, PVDF and PVDF-based polymers have been identified as a matrix of dielectric composites because they possess high dielectric and piezoelectric properties [16,121–133]. **Hu et al.** [121] prepared PVDF/$Ba_{0.6}Sr_{0.4}TiO_3$ composites by solution casting. The surface of BST micron amorphous particles was modified chemically by H_2O_2 through introduce many hydroxyl groups and improve the interface bonding between BST particles and the PVDF matrix. A strong interaction resulted between BST ceramic powder and the PVDF matrix. Hydrogen bonds can be obtained between the F atoms of PVDF molecular chains and the –OH groups on the BST particle surfaces, and the BST powders were dispersed uniformly in the matrix without any agglomeration. The dispersion stability of particles in polymers and the adhesion interface between fillers and polymers are important in the microstructure and final dielectric properties. To improve the interaction between BST and the polymer matrix, many surface modifications were used on the BST conventional powders. **Zhang et al.** [122] used aminopropyl triethoxy silane (KH550) as coupling agent to improve the $Ba_{0.6}Sr_{0.4}TiO_3$/PVDF composite interface, which improved the dielectric properties. The KH550 had a remarkable effect on the composite microstructure and the interfacial bonding force between the ceramic powder and polymer as shown in Fig. 12. The incompatibility of the unmodified fillers with the PVDF polymer matrix was obvious and the improved compatibility and uniform distribution were visible with an increase in KH550 content. They obtained an improved KH550 content of 4 wt%. Excessive KH500 will result in a self-condensation reaction, which makes it difficult to form a monolayer film of silane coupling agent on the ceramic surface, and is not conducive to improving the BST particle dispersion in the matrix. The importance of the KH550 is that it can be attached to the BST particle surface and form Si–O bonding by the dehydration condensation reaction as shown in Fig. 13. They confirmed that KH550 improved the dielectric properties and energy storage density of the BST/PVDF.

BST powders were dispersed in polypropylene–*graft*- poly(styrene-*stat*-divinylbenzene) (ER) to prepare ceramic/polymer composites by **Sonoda et al.** [134]. In their work, stearic acid was selected to modify the $Ba_{0.55}Sr_{0.45}TiO_3$ fillers, which improved the filler dispersion condition in the composites considerably, because the –COOH functional group attaches easily to Ba or Ti filler ions. Surface coating with stearic acid increases the relative permittivity of the composites without increasing their dielectric loss. **Sonoda et al.** prepared a series of $Ba_{0.55}Sr_{0.45}TiO_3$/ER composites that were modified by various linear aliphatic carboxylic acids with different carbon chains [135]. They showed that the surfactant moles were bound to the BST surface chemically and not physically. A better dispersion in the BST filler polymer matrix can be found by using surface modification with longer-chain aliphatic carboxylic acids. Carboxylic acids with longer carbon chains may enhance the relative permittivity of the composite because of the improved interface connection.

The microstructure of the two-phase BST/polymer composites depends on the preparation process. The composite uniformity is usually poor, and a hot treatment process is used to eliminate porosity and improve the composite uniformity [136–138]. **Wang et al.** [123] prepared 40 vol% $Ba_{0.6}Sr_{0.4}TiO_3$/PVDF composite films by tape casting followed by hot processing (HP), in which the BST micro-amorphous powders were modified by KH550. Details of the effect of HP temperature from RT to 140 °C on the microstructure are provided in Fig. 14. The porosity and defects were eliminated gradually as the HP temperature increased. An enhanced dielectric property was obtained at an HP temperature of 120 °C, which indicated that the HP method is a simple and effective strategy to enhance the dielectric properties in ceramic/polymer composites. The influence of configuration of the as-cast composite stack in the HP process on the structure and dielectric properties of the composite is reported in [123], where two sheets of $B_{0.5}Sr_{0.5}TiO_3$/P(VDF-CTFE) nanocomposite films were stacked into one layer film with two different configurations, followed by the HP process. After the HP process, the composite films were dense and of a better uniformity in microstructure and morphology. There was no clear difference in microstructure and uniformity of the composites that were prepared by using two configurations.

The polymer microstructure and properties depend on the distribution of fillers in the polymer matrix and on their coupling

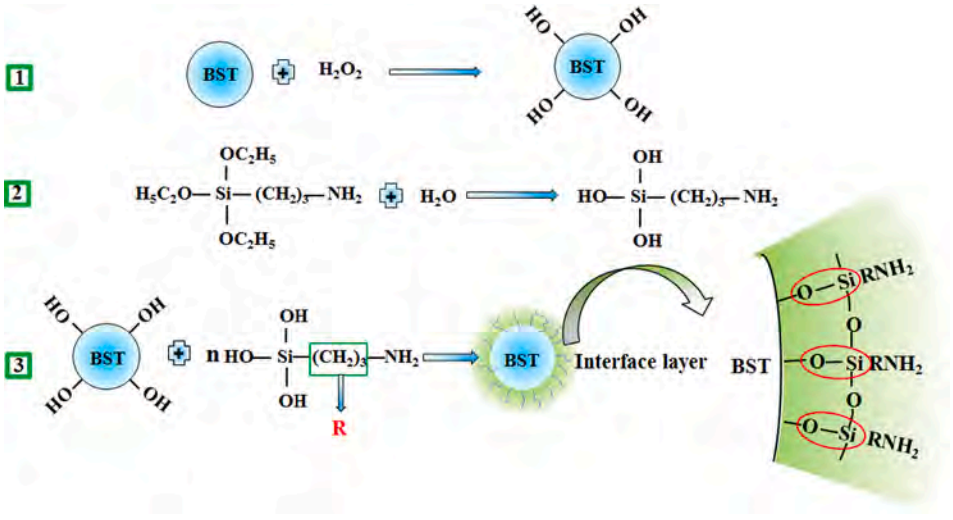

Fig. 13. Schematic of hydroxylation of BST particles, hydrolysis reaction of KH550 and BST coupling reaction with KH550 [122].

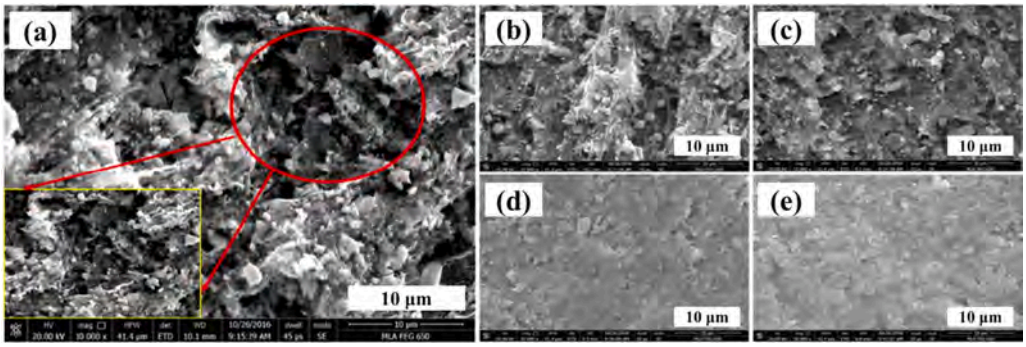

Fig. 14. SEM images of BST/PVDF composites at different HP temperature [123] (a) RT, (b) 80 °C, (c) 100 °C, (d) 120 °C, (e) 140 °C.

methods. Most BST/polymer composites that were reported in previous literature were 0–3-type composites. **Xiang et al.** [115] fabricated a 1–3-type $Ba_{0.6}Sr_{0.4}TiO_3$/PMMA composite with a BST rod array in a PMMA matrix by the dice-and-fill technique. For the 1–3-type BST/PMMA tunable composite, the permittivity and composite loss tangent were 1212 and 0.026 at 10 kHz, which is much larger than that of the 0–3-type composites. They prepared $Ba_{0.6}Sr_{0.4}TiO_3$/PMMA with 0–3-, 1–3- and 2–2-type structure [114]. Another 1–3-type $Ba_{0.55}Sr_{0.45}TiO_3$/epoxy resin composite showed an extremely high tunability and low dielectric constant [110], which shows that the structure and properties of the interphase layer are important to the overall dielectric properties of the composite.

3.1.2. Three-phase composites

To prepare high dielectric constant polymer composites for supercapacitors, different particles, including ceramic powders and conductive metals were filled into the ferroelectric polymer even though the volume concentration of ceramic fillers reached 50–60%. An increase in the concentration of ceramic filler led to the appearance of pores, which reduced the dielectric constant and dielectric breakdown strength [139]. According to percolation theory, the dielectric permittivity of the composites improves rapidly by adding fillers with a high electrical conductivity [140–144]. For high dielectric constant materials, three-phase polymer matrix composites that consist of a ceramic, polymer and electrically conductive phase may provide a good strategy [145–148]. Conducting fillers, e.g., Ag, Ni, Fe, W, Cu, carbon black, carbon nanotubes and graphite have been investigated to achieve a high composite dielectric permittivity [149].

Li et al. [100] observed that when the volume content of BST@Ag and BST was 55 vol%, the relative permittivity of the BST@Ag/PVDF composite was 153, which was 73% higher than that of BST/PVDF at 100 Hz. They explained that the remarkable enhancement of dielectric constant of BST@Ag/PVDF composites originated from the space charge polarization in a silver shell and the nano-capacitor network that was formed by interparticle junctions and sample electrodes. **Reddy et al.** [149] prepared a BST-Graphite-PVDF three-component nanocomposite to improve the dielectric permittivity and dielectric tunability. Instead of performing direct ceramic or conductive filler addition to the polymer matrix, BST was first mixed with graphite layers to produce a homogenous dielectric ceramic/conducting interface and then it was added into the PVDF polymer matrix. The maximum dielectric constant was 84.2 in three-component composite films, when both filler ratios of BST were 0.250. Inner electric fields that developed around the conducting phase and microcapacitor networks with dielectric insulating layers increase the dielectric constant. They proposed that the giant dielectric permittivity was influenced by the area of the phase interfaces, which was also dependent on the graphite concentration of the composites. The addition of conductive particles to the two-phase ceramic/polymer composite material exhibits similar laws to the three-phase composite material [146–148].

In summary, the microstructure and interface of BST/polymer composites are critical towards advancing their dielectric properties. Table 2 summarized the dielectric properties of typical BST/polymer composites.

Table 2
Dielectric properties of various BST/polymer composites.

System	BST content (vol%)	Test Frequency	ε_r	tanδ	References
$Ba_{0.7}Sr_{0.3}TiO_3$/HDPE	40	7.26 GHz	12.67	0.0029	[21]
$Ba_{0.7}Sr_{0.3}TiO_3$/BR	39	5 GHz	13.1	0.009	[29]
$Ba_{0.6}Sr_{0.4}TiO_3$@Ag/PVDF	55	100 Hz	153	0.2	[100]
$Ba_{0.55}Sr_{0.45}TiO_3$/PPS	36.4	5 GHz	14.2	0.0055	[113]
$Ba_{0.6}Sr_{0.4}TiO_3$/PMMA	50	10 kHz	28	0.043	[114]
$Ba_{0.6}Sr_{0.4}TiO_3$/PVDF	40	1 kHz	56	0.12	[122]
BST/ER	50.5	1 GHz	28.5	0.00085	[134]
$Ba_{0.5}Sr_{0.5}TiO_3$/P(VDF-CTFE)	30	1 kHz	49	0.08	[137]
$Ba_{0.5}Sr_{0.5}TiO_3$/GE/PVDF	25	100 Hz	84.2	0.064	[149]
$Ba_{0.6}Sr_{0.4}TiO_3$/ABS	40	1 kHz	18	0.082	[150]
BMAZ/PVDF	40	1 kHz	34	0.02	[151]
BST/COC	45.8	2.55 GHz	13.8	0.00015	[152]

3.2. Theoretical models for dielectric constant of BST/polymer composites

In ceramic/polymer composites, high dielectric properties are provided by ceramic fillers, whereas a good flexibility comes from the polymer matrix. Compared with single phases, the composite properties show different trends in electrical properties. The precise prediction and simulation of the dielectric properties (such as the dielectric constant and dielectric tunability) of ceramic/polymer composites are important in the design and preparation of dielectric composites. Successful simulation and prediction can provide an understanding of the mechanism, reduce the randomness in material preparation and improve the research and development efficiency. Several dielectric theoretical models have been used to predict the dielectric properties of composite materials.

Dielectric theoretical models used ε_c and ε_p for the dielectric constant of the ceramic and polymer, respectively, and δ_c and δ_p as the volume fraction of the ceramic and polymer, respectively.

3.2.1. Lichtenecker model

The Lichtenecker rule [153] is the most common dielectric theoretical model that is used to predict the dielectric constant of a ceramic/polymer composites (see Eq. (7)), and is also referred to as the logarithmic mixing rule.

$$\log\varepsilon_{\mathrm{r}} = \delta_{\mathrm{c}}\log\varepsilon_{\mathrm{c}} + \delta_{\mathrm{p}}\log\varepsilon_{\mathrm{p}} \tag{7}$$

Lichtenecker's idea is based on the Wiener theory for bounds of the effective composite dielectric function or conductivity [154] and is the intermediate form of the series and parallel combination laws for dielectric composites, which is more suitable for composite materials with small dielectric constant difference between the ceramic and polymer phases [155]. When the ceramic phase content is large, this equation is no longer applicable. The modified Lichtenecker model (Eq. (7)), which was optimized from Eq. (7) is more applicable to ceramic/polymer composites with a large difference in two parts and a high volume content of ceramic:

$$\log\varepsilon_r = \log\varepsilon_p + \delta_c(1-k)\log\left(\frac{\varepsilon_c}{\varepsilon_p}\right) \tag{8}$$

where k is the universal factor. The typical value of k is 0.3 in an excellent dispersibility composite system. This model is based on a random distribution of ceramics in the polymer matrix and the volume fraction of ceramics must be less than 0.75.

3.2.2. Maxwell's model

For spherical inorganic particles with a high permittivity, which is dispersed homogeneously in the low dielectric constant organic matrix, according to Maxwell's model [155], the composite dielectric constant can be calculated from:

$$\varepsilon_r = \frac{\delta_p\varepsilon_p\left(2/3 + \varepsilon_c/3\varepsilon_p\right) + \delta_c\varepsilon_c}{\delta_p\left(2/3 + \varepsilon_c/\varepsilon_p\right) + \delta_c} \tag{9}$$

Maxwell's model is suitable for ceramic-phase particles that are surrounded by a polymer matrix, but it cannot explain why the dielectric constant of the composites increases suddenly when the ceramic phase increases to a certain value, i.e., the matrix could not be judged when the ceramic volume fraction was close to that of the polymer. Unlike a single ceramic, the ceramic powder in the composite materials agglomerates easily, and the degree of agglomeration increases gradually with an increase in ceramic content, which causes a significant deviation between the theoretical and experimental values. Therefore, the dielectric constant cannot be determined accurately by this model in the above situation.

3.2.3. Maxwell-Garnett model

Equation (10) is used to predict the relative dielectric constant with a higher accuracy, and is termed the Maxwell–Garnett equation [156–159].

$$\varepsilon_r = \varepsilon_p\left[1 + \frac{3\delta_c(\varepsilon_c - \varepsilon_p)}{(1-\delta_c)(\varepsilon_c - \varepsilon_p) + 3\delta_p}\right] \tag{10}$$

Equation (10) is used only for a composite with spherical fillers. When the particles are not spherical, the geometry of the filler particles should be considered.

Maxwell-Garnett proposed a common way to introduce a factor that describes the geometry of dispersed particles as a depolarization factor, which is related to their deviation from the spherical nature. Thus, a more general formula is displayed [160]. However, this equation applies only to composite materials with $\delta_c < 0.1$.

$$\varepsilon_r = \varepsilon_p\left[1 + \frac{\delta_c(\varepsilon_c - \varepsilon_p)}{A(1-\delta_c)(\varepsilon_c - \varepsilon_p) + \delta_p}\right] \quad \text{for } \delta_c < 0.1 \tag{11}$$

where parameter A is the depolarization. When $A = 1/3$, Eq. (11) converts to Eq. (10).

3.2.4. Jaysundere-Smith model

The Maxwell-Garnett equation is applicable only to the case where the filler concentration is low. The particle spacing is large and the interaction between particles is weak. When the particle concentrations increase, the distance between filler particles is close and

the interaction between filler particles cannot be ignored. Moreover, the electrical field that arises from the uniformly induced distribution of dipole moments is not negligible when the overall field is experienced locally in the matrix. Based on the polarization of adjacent particles, Jaysundere and Smith proposed the following [161]:

$$\varepsilon_r = \frac{\varepsilon_p\delta_p + \varepsilon_c\delta_c\frac{3\varepsilon_p}{(2\varepsilon_p+\varepsilon_c)}\left[1+3\delta_p\frac{(\varepsilon_p-\varepsilon_c)}{2\varepsilon_p+\varepsilon_c}\right]}{\delta_p + \delta_c\frac{3\varepsilon_p}{(2\varepsilon_p+\varepsilon_c)}\left[1+3\delta_p\frac{(\varepsilon_p-\varepsilon_c)}{2\varepsilon_p+\varepsilon_c}\right]} \tag{12}$$

3.2.5. Clausius-Mossotti model

For the two-phase mixture that formed by homogeneous spherical particle dispersion into a continuum, the dielectric composite constant was explained by the Clausius-Mossotti model [162]:

$$\varepsilon_r = \varepsilon_p[1+3\delta_c(\frac{\varepsilon_c-\varepsilon_p}{\varepsilon_c+2\varepsilon_p})] \tag{13}$$

This model approximates ceramic particles in the composite material as spherical, but it is difficult to achieve spherical ceramic filler particles, especially when the particles are agglomerated. The particle shape influences the simulation results, therefore, a huge difference exists between the theoretical and experimental values.

3.2.6. Yamada model

Considering the influence of the shape of ceramic filler, the Yamada model introduced the shape factor n and proposed the calculation of the dielectric constant equation [163], as shown in the figure below:

$$\varepsilon_r = \varepsilon_p[1+\frac{n\delta_c(\varepsilon_c-\varepsilon_p)}{n\varepsilon_p+(1-\delta_c)(\varepsilon_c-\varepsilon_p)}] \tag{14}$$

where n is the ceramic particle shape factor. The value of the shape factor can be determined by adjusting the deviation degree between the theoretical and experimental values. Conversely, the shape factor of the ceramic particles can influence the interface bonding strength between the polymer matrix and ceramic phases directly, and the composite dielectric properties.

3.2.7. Other models

In addition to the 0–3-type connectivity, the dielectric properties of composite materials may be of other types. Therefore, the theoretical calculation of dielectric properties should be based on the filler and matrix type and the connectivity type of the single phase. **Tangantsev et al.** [152,164] described theoretical models of dielectric/ferroelectric composites with different connectivities. For the 1–3-type composite, the dielectric constant and loss can be calculated from Eqs. (15) and (16), which is obtained by using an equivalent electrical circuit that consists of two capacitors that are connected in parallel.

$$\varepsilon_r^{1-3} = \delta_c\varepsilon_c + \delta_p\varepsilon_p \tag{15}$$

$$tan\delta_r^{1-3} = \frac{\delta_c tan\delta_c\varepsilon_c + \delta_p tan\delta_p\varepsilon_p}{\delta_c\varepsilon_c + \delta_p\varepsilon_p} \tag{16}$$

For the 2–2-type composite, the dielectric constant and tanδ as a function of the ceramic content can be obtained by using an equivalent electrical circuit that consists of two capacitors that are connected in series.

$$\varepsilon_r^{2-2} = \left(\frac{\delta_c}{\varepsilon_c}+\frac{\delta_p}{\varepsilon_p}\right)^{-1} \tag{17}$$

$$tan\delta_r^{2-2} = \frac{\delta_c tan\delta_c\varepsilon_p + \delta_p tan\delta_p\varepsilon_c}{\delta_c\varepsilon_p + \delta_p\varepsilon_c} \tag{18}$$

Recently, the dielectric constant of the ceramic/polymer composites was improved by introducing conducting fillers [165,166]. The use of conducting fillers can induce Maxwell-Wagner polarization, which leads to an enhanced dielectric constant. Classical mixing rules, except for percolation theories, cannot be used to explain this enhancing phenomenon. A metal–insulator transition can be found when the content of conducting fillers reaches the percolation threshold. The dielectric constant often follows the following relationship [167,168]:

$$\varepsilon_r \propto (\delta_0-\delta_c)^{-q} \quad \text{for } \delta_c < \delta_0$$

where δ_0 is the concentration of conducting particles when the percolation threshold is reached.

The dielectric properties of the composites are influenced by many factors, such as the morphology, dispersion and interface bonding between two phases. Thus, it is difficult to reflect the dielectric properties accurately by these models. Increased attention is required to consider the physical truth of composites and choose an appropriate model to describe the dielectric properties of certain ceramic/polymer composites.

3.3. Fabrication processing of BST/Polymer composites

The preparation process is critical to the performance of ceramic/polymer functional composites, especially in the field of functional device applications. Processing methods, such as the solution route and tape-casting method, melt-compounding method, in situ polymerization process and inject printing method are used commonly, and other methods, such as the dice-and-fill method show typical processing for 1–3-type composites. A brief description and typical example of each processing method is given below.

3.3.1. Solution route and the Tape-casting method

The higher viscosity of the mixture usually appears when a high filler concentration is used in the composites, which makes melt mixing. In contrast, solution processing can be used smoothly to incorporate filler into the polymer matrix. This process involves the dispersion of polymer and filler in a solvent. N,N-dimethylformamide (DMF) has been explored to manufacture BST/polymer composite solution that contains PVDF [22,24,25,27], P(VDF-CTFE) [127], P(VDF-TrFE-CTFE) [133] and PI [102]. After the polymer is dissolved in DMF, BST fillers particles are mixed with polymer solution. Solution processes can be efficient at dispersing fillers in the polymer solution.

Together with BST and polymer mixed solution, tape casting is used extensively to make BST/polymer composite films. In tape casting, which is sometimes referred to as the doctor-blade process, the slurry is spread over a surface by using a carefully controlled blade. The orientation distribution of the ceramic powders in ceramic/PVDF composites is used mostly to enhance the dielectric response. The ceramic particles must be well aligned in the polymer matrix. Tape casting is an effective way to make the filler alignment directional. For example, PVDF-based nanocomposite films that were filled with surface-fluorinated $Ba_{0.6}Sr_{0.4}TiO_3$ nanofibers (F-BST NF) were prepared by tape casting [25]. A 10-μm-thick film was obtained after heating and quenching. Fig. 15 shows schematic diagrams of the fabrication of F-BST NF/PVDF nanocomposites. **Wang et al.** [169] prepared PVDF-based composite films with plate-like BST particles. After tape casting, the degree of alignment of plate-like BST particles reached 59.4%. Other types of BST/polymer composites film, such as BST nanocubes/PVDF [98], BST nanotubes/PVDF [27], BST nanoparticles/P(VDF-CTFE) [127] and plate-like BST/P(VDF-TrFE-CTFE) [133] were prepared by tape casting.

Tape casting is an outstanding manufacturing process because of its merits. Tape casting results in the easy generation of large samples and ensures a relatively uniform powder distribution. The casting tape sample thickness is tunable over a wide range from 0.1 to 3000 μm [170]. The sample can be produced in the laboratory and industrially, and be reprocessed into the desired shape and stack, which makes solution combined with tape casting an effective method for producing BST/polymer composites industrially.

3.3.2. Melt-compounding method

To mix BST powders with highly viscous fluids, especially thermoplastic melts such as PE, PVDF and COC, high shear forces are used to break BST powder agglomeration and improve BST dispersion. Twin-screw extrusion is the most popular method for processing ceramic/polymer composites owing to its good dispersive and distributive mixing capability [150,151,171]. **Sonoda et al.** [134] mixed BST powders in ER at 60 rpm for 30 min and extruded these from a die. The as-prepared composites had a uniform dispersion [135]. BST/PPS composites were prepared by feeding BST powders into molten PPS by a gravimetric twin-screw feeder at 310~320 °C.

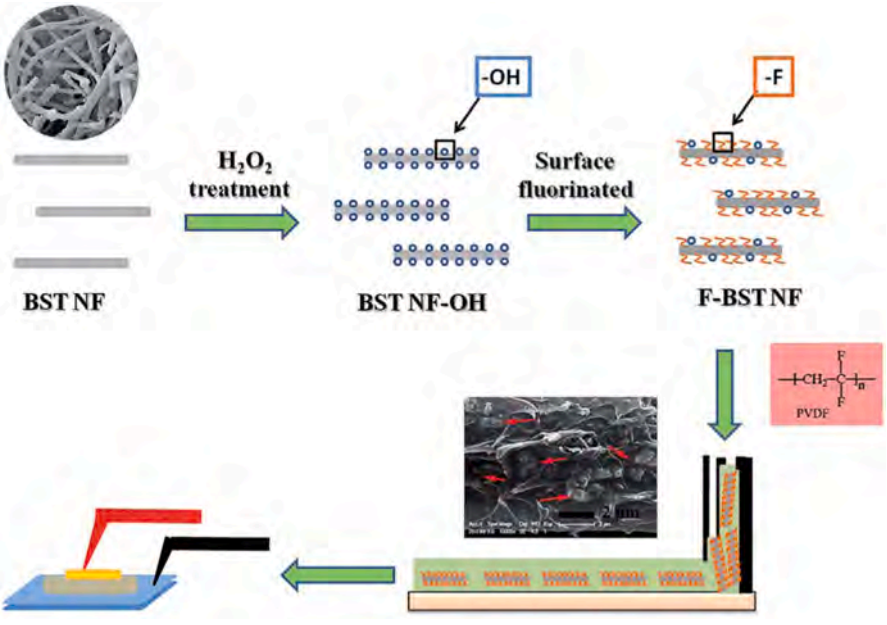

Fig. 15. Schematic diagrams of F-BST NF/PVDF nanocomposite fabrication [25].

After compounding, 20~30-mm-wide and 0.2~0.3-mm-thick samples were extruded through the die (290 °C). Mechanical stirring or milling could also be used to blend the ceramic polymer powders. **Zhang et al.** [21] prepared BST/HDPE composites by mixing BST and HDPE powders in a planetary mill. The composite powder was extruded at 180 °C and 30 rpm using a conic twin-screw extruder, and after hot pressing, the composite disk was made by cycling at 200 MPa and 220 °C under uniaxial pressure for 30 min. The advantages of the extrusion molding method are a high production speed and the low cost of each part. However, the viscosity of the melt composite with a higher filler concentration is usually high, which makes melt compounding more difficult.

3.3.3. *In situ polymerization*

To fabricate ceramic/polymer composites, in situ polymerization processes are usually applied to obtain a better compatibility between filler and matrix, which leads to improved electrical and mechanical properties. **Sambyal et al.** [172] used this method to prepare a polyaniline/barium–strontium-titanate/expanded graphite (PANI/BST/EG, PBE) multiphase composite as shown in Fig. 16. The PBE composites were prepared using aniline/BST/EG as the dispersed phase, deionized water as the continuous phase, dodecylbenzene sulfonic acid (DBSA) to form micelles and an oxidant to initiate the polymerization reaction at the micelle–water interface. **Zha et al.** [103] prepared PI/BST composite films by two steps: (1) a BST/poly (amic acid) precursor film made by solution casting. (2) PI/BST films from the thermal imidization process. **Beier et al.** [104] prepared polyimide/BST by using in situ polymerization, where the BST suspension was blended with 1,3-bis(4-amino phenoxy)benzene (BAPB) and pyromellitic dianhydride (PMDA) monomers before spin casting and thermal imidization. Strong interfacial interactions between matrix and filler could be ensured for homogenous filler dispersion in situ polymerization. However, some issues remained, such as limited reaction systems, intractable reaction conditions and byproducts during the in situ polymerization process.

3.3.4. *Inkjet printing*

Inkjet printing is a computer-controlled printing method that creates flexible components by a digital model and is a promising technology for the selective deposition of functional components [114,173–175]. A suitable stable composite ink with an excellent printability ink is critical. **Mikolajek et al.** [114] prepared a BST/PMMA composite capacitor via inject printing. A PMMA solution was prepared in butanone and mixed with the BST dispersion to obtain an ink with a 50:50 vol ratio of BST and PMMA. They also investigated the printability of the composite ink to fabricate small structures, the drying behavior of the ink at different temperatures and the composite thick-film morphology. The developed composite ink was used to prepare capacitors as shown in Fig. 17.

3.3.5. *Dice-and-Fill method*

For 1–3-type BST/polymer composites, the sintered BST ceramics were cut and filled with polymer and polished. BST rods array

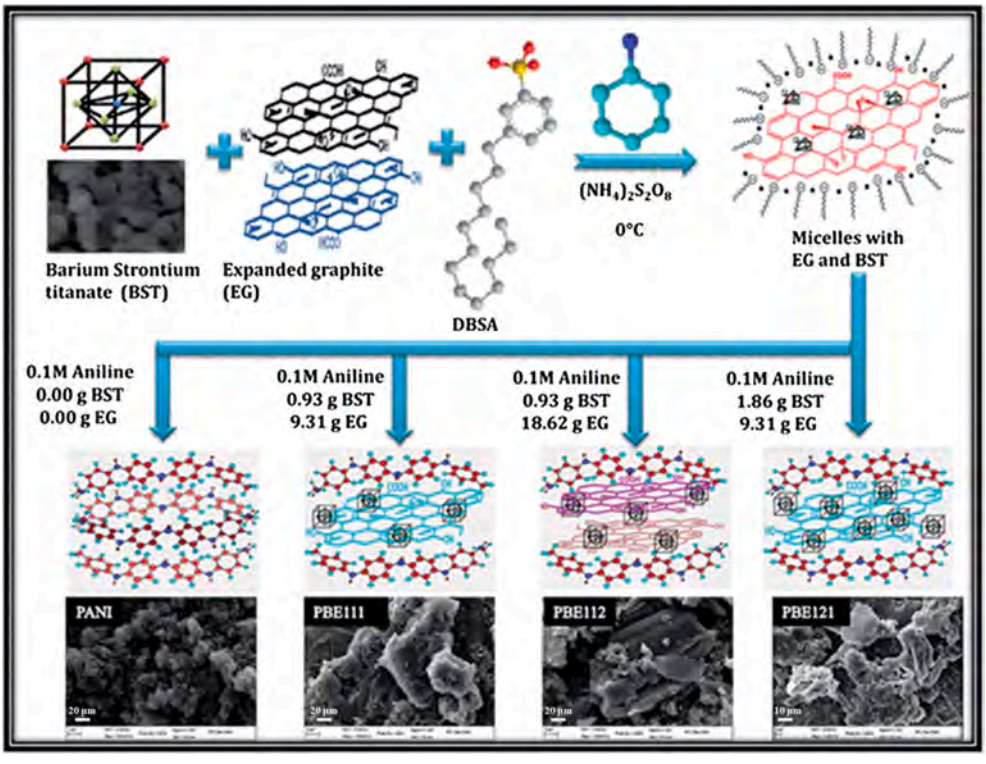

Fig. 16. Schematic representation of BST nanoparticle-decorated EG sheets filled with PANI by in situ polymerization of aniline using APS as oxidant in the presence of DBSA [172].

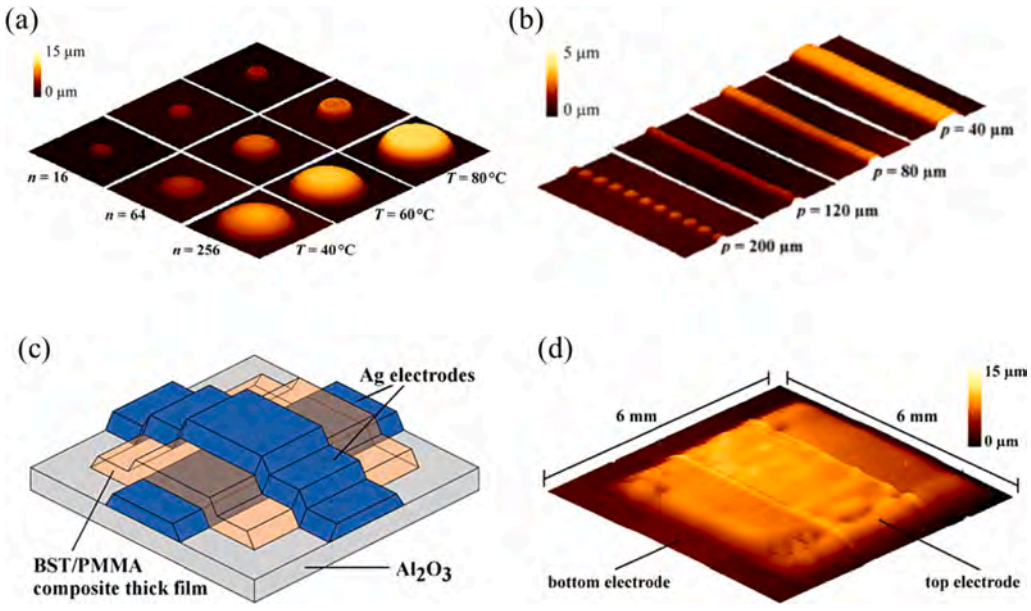

Fig. 17. BST/PMMA composites used for inkjet printing. (a) Topography of drop structures with different sizes, (b) topography of lines printed with different droplet spacings at 60 °C, (c) schematic parallel-plate capacitor layout, (d) topography of all-inkjet-printed MIM capacitor [114].

with widths of 1 mm and spaced 1.55 mm apart were cut by sintered BST bulk ceramics. The BST rod array with a ceramic base was filled with PMMA solution. After the PMMA solidified, the 1–3-type BST/PMMA composite was cut into 1-mm-thick flakes [115], as shown in Fig. 18. Another 1–3-type of BST/Resin Epoxy composite was also prepared by this method [110].

In summary, the preparation process has an important effect on the dielectric composite properties. The physical, chemical, mechanical and thermal characteristics of the composite system should be considered when using the preparation method and operation conditions.

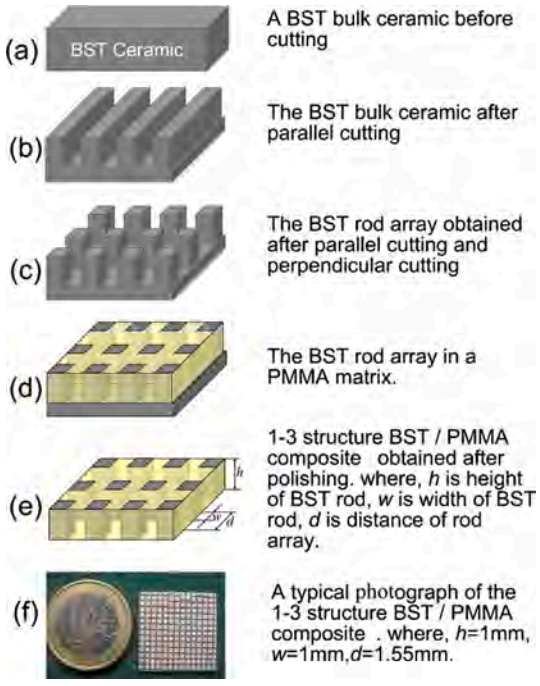

Fig. 18. Process of 1–3-type BST/PMMA composite synthesis, (a) BST bulk ceramic, (b) series of parallel cuts, (c) second series of perpendicular cuts, (d) filled with PMMA solution, (e) cut into flakes, (f) typical photograph of top view of 1–3-type BST/PMMA composite. [105].

4. Effects of BST fillers on dielectric properties of BST/Polymer composites

4.1. Concentration effect

The increased dielectric permittivity of the ceramic/polymer composites resulted because of the relatively high permittivity of the ceramic powders. The dielectric constant of the composites was tuned easily by adjusting the concentration of ceramic fillers. These composites possess a relatively low dielectric loss. An increase in interfacial area between the individual phases existed in the composites as a higher content of ceramic filler [121]. The interfacial polarization has a significant influence on the dielectric properties. **Zhang et al.** [108] reported that the dielectric constant of modified BST/ABS composites increased from 4.5 to 18 with an increase in BST filler from 10 vol% to 40 vol%. Interfacial polarization occurred in the inner microstructure of the BST/ABS composites as shown in Fig. 19.

Lots of defects at the interface between BST and ABS and carriers such as the electrons, holes and ion vacancies are assembled easily toward the defects. Restrained carriers migrate with difficulty and distribute randomly without an applied electric field. The interfacial polarization is caused by the produced and ordered electric dipole moments with the applied electric field. As a result, the interfacial polarization reaction increases and contributes to a higher composite dielectric constant with more interfaces when the ceramic loading volume increases. Fig. 20 shows the dielectric constant and loss variation with frequency for BST/ABS composite films with different BST contents measured at RT. The decrease in dielectric constant is thought to be responsible for the weakening of the interface polarization and dipole orientation resulted from the increase in frequency with the same BST content. The results also demonstrated that dielectric loss increased from 0.021 to 0.082 at 1 kHz because of the increased interaction strength of interfacial polarization as the ceramic fillers volume increased [108].

Because of the interaction between ceramics and polymer, the improvement in dielectric properties of THE BST/polymer composites has been investigated extensively. **Hu et al.** [121] reported that the dielectric constant of the BST/PVDF composites increased from 16 to 40 at 1 kHz, whereas the dielectric loss first decreased and then increased with an increase in BST filler from 10 vol% to 40 vol%. The composite dielectric permittivity with 40 vol% BST measured at 10^2, 10^3, 10^4, 10^5 and 10^6 Hz was 50, 40, 33, 30 and 27, respectively, which showed a strong frequency dependence. **Hu et al.** [75] reported on multi-doped (Mg, Al, and Zn) BST ceramic particles (BMAZ) filled with PVDF resin composites. The dielectric constant and dielectric loss of the composites changed from 10 to 34 and 0.07 to 0.02, respectively, with an increase (i.e., from 10 vol% to 40 vol%) in BMAZ fillers. **Zha et al.** [103] reported that on PI/$Ba_{0.6}Sr_{0.4}TiO_3$ composites that were prepared by in situ polymerization, the composites possessed a dielectric constant of 24 and a loss of 0.004 at 100 Hz when the volume concentration of BST powders was 30%. This result also showed a weak frequency dependence in the BST/PI composite as shown in Fig. 21.

We deduce that conventional ceramic materials have a high level dielectric constant value whereas that of composites remains lower. The interface structure is the main factor. To improve the dielectric properties of the BST/polymer composites, three aspects should be considered; 1) the polymer matrix dominates the electrical characteristics of composites and it is necessary to consider the electrical property of the selected polymer matrix, 2) the critical improvement in interface conjunction between ceramic and polymer, and 3) the designation and optimization of the fabrication process to minimize pores in the BST/polymer composites. **Zhang et al.** [122] reported that the dielectric permittivity of BST/PVDF composite film can be improved by modified BST powders with KH550. When the KH550 content was 4 wt%, a BST/PVDF composite with 40 vol% BST powder showed the higher dielectric constant (56 at 1 kHz) and enhanced the energy storage density (5.28 J/cm^3), with a lower dielectric loss (0.12 at 1 kHz) compared with BST/PVDF composites without using modified BST powders.

Conducting filler introduction can increase the dielectric permittivity of polymer composites markedly. **Reddy et al.** [149] reported that the dielectric permittivity increased with an increase in BST loading and reached a maximum of 84.2 in $Ba_{0.5}Sr_{0.5}TiO_3$/graphite(G)/PDVF three-component composite films with a low frequency dependence, which is 45% higher than the value measured for two-phase composite films, as shown in Fig. 22. They explained that the enhancement in dielectric constant resulted because of the existence of microcapacitor networks that were created by conducting fillers. The introduction of conducting phases into ceramic/

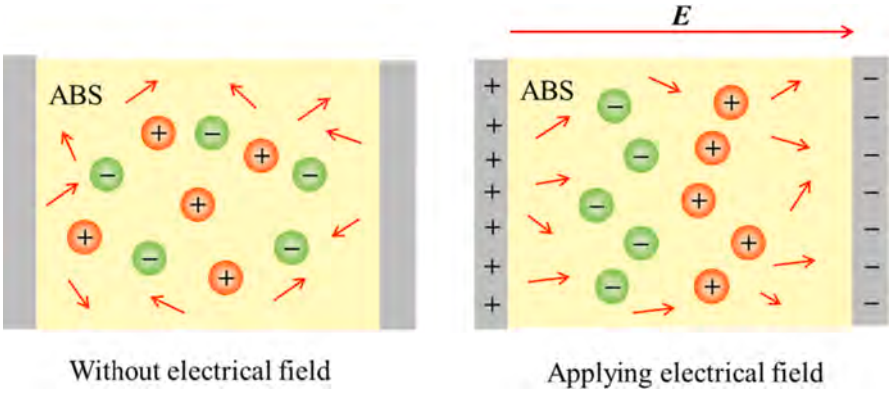

Fig. 19. Model of interfacial polarization in BST/ABS composites [143].

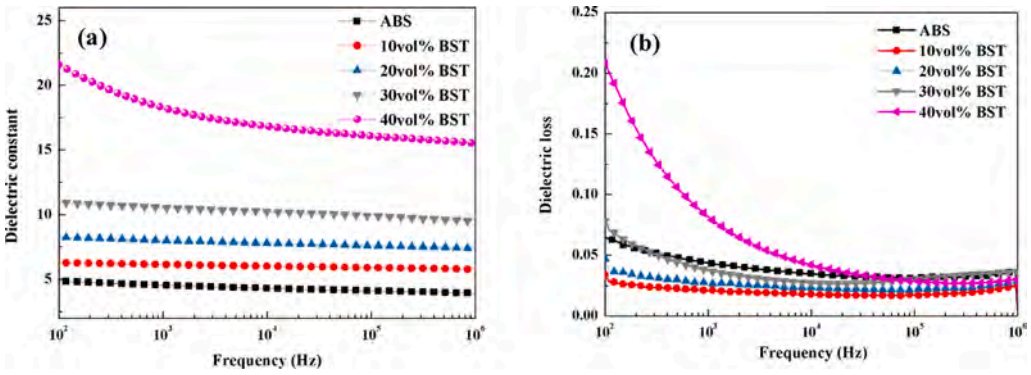

Fig. 20. Frequency dependence of dielectric properties of BST/ABS composites: (a) Dielectric constant, (b) dielectric loss [108].

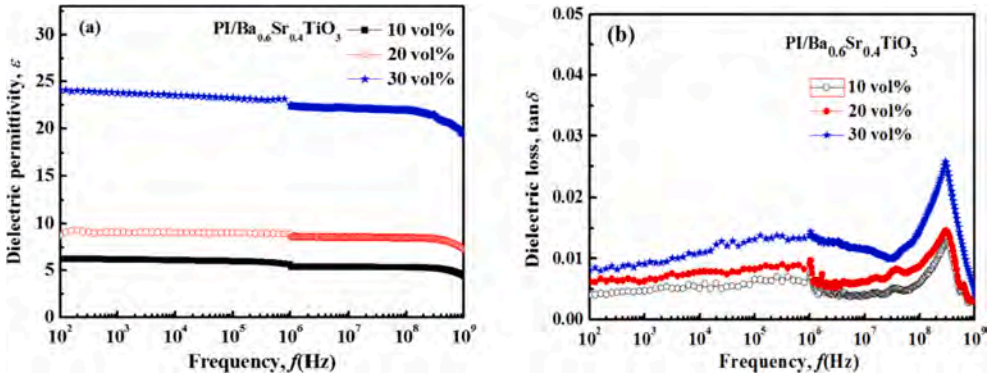

Fig. 21. Frequency dependence of (a) dielectric permittivity and (b) loss tangent of PI/$Ba_{0.6}Sr_{0.4}TiO_3$ composite films with volume fraction of $Ba_{0.6}Sr_{0.4}TiO_3$ loading [103].

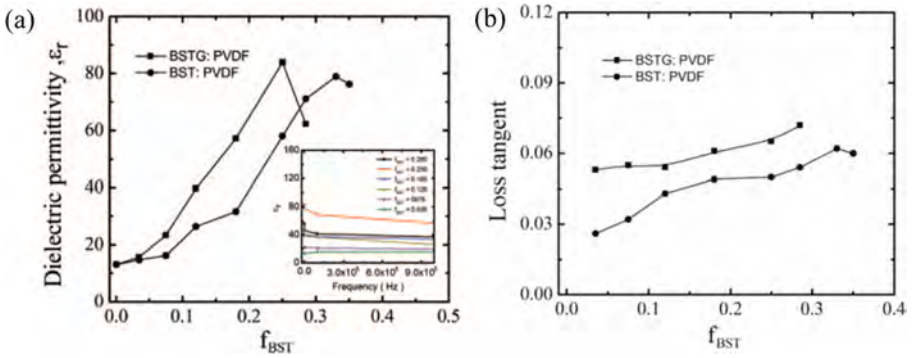

Fig. 22. (a) Dielectric permittivity, (b) loss tangent of composites as a function of BST at RT at 100 Hz. Inset in (a) frequency dependence of dielectric permittivity for three-component composites with various values of f_{BST} [149].

polymer composites was accompanied by drawbacks, such as a high conduction loss and low dielectric breakdown strength.

Li et al. [100] prepared a type of surface-functionalized BST nanoparticle (50~100 nm) with a silver coating, filled the particles into a PVDF polymer matrix and investigated the dielectric properties of the BST@Ag/PVDF composites that differed from direct addition of bare BST powders or conductive fillers to the polymer matrix. Fig. 23 shows that the maximum dielectric constant was 153, which was accompanied by a high dielectric loss of ~0.2. The enhancement in dielectric constant is attributed to space–charge polarization in a silver shell and the nanocapacitor network that was formed by interparticle junctions and sample electrodes. A decreasing trend in apparent density was used to explain the decrease in dielectric constant for the composites when the BST fraction was >55 vol%. The loss tangent showed the same change rule as the dielectric constant.

The dielectric properties of composites in the lower (below 1 MHz or 1 GHz) and higher frequency region (above 1 GHz) were

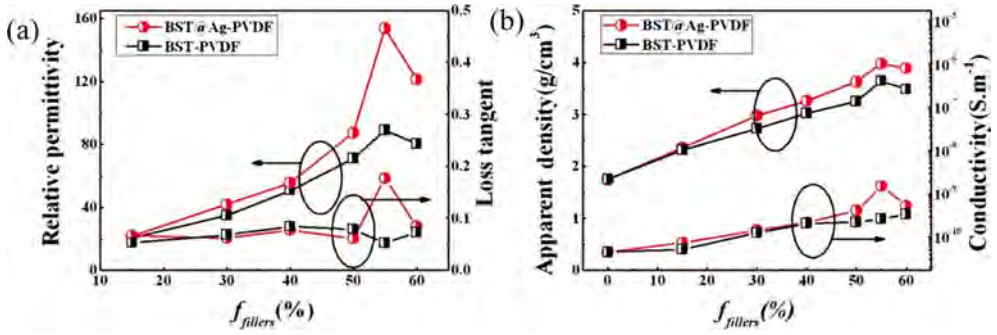

Fig. 23. (Color online) Relative permittivity and loss tangent (a) and apparent density and conductivity (b) of BST@Ag measured at RT and 100 Hz [100].

investigated. **Hu et al.** [176] reported that the dielectric constant and loss tangent of the composites increased gradually with an increase in $Ba_{0.55}Sr_{0.45}TiO_3$ loading on the $Ba_{0.55}Sr_{0.45}TiO_3$/PPS composites. A rising trend of BST/PPS composite dielectric constant at 1 GHz (4.8~13.5) can be obtained, whereas the BST loading increased from 30 wt% to 70 wt%. The dielectric loss showed an increasing change rule (0.0012 to 0.0025). **Osińska et al.** [177] reported that the dielectric properties of the BST/PVDF composite for the volume fraction of BST powders >20% changed significantly for small ($f = 10$ kHz~1 MHz) and high ($f = 3$~10 GHz) frequencies. The abrupt increase in permittivity may indicate an excess percolation threshold, as shown in Fig. 24.

In summary, the increase in BST fillers can improve the dielectric constant and dielectric loss of the BST/polymer composite. If the BST loading is too high, the dielectric properties are counterproductive. Conductive filler introduction can improve the dielectric properties compared with the use of pure ceramic fillers, whereas an increase in dielectric loss and drop in dielectric breakdown strength makes the practical application far more challenging.

4.2. Size effect

The small fillers lead to an exceptionally large interfacial area in the composites. Thus, the properties of the ceramic/polymer composites can be influenced by controlling the degree of interaction between the polymer and the fillers. The smaller filler facilitates a more homogenous composite. For example, a large polarization and high breakdown electric field in the P(VDF-CTFE)/BST composites has been reported [136]. A high discharged energy density of 6.5 J/cm^3 at a breakdown field of 250 MV/m was obtained in the composite film with 10 wt% BST nanoparticles. The higher discharge energy density results because of the strong binding force between the modified BST nanoparticles and the matrix, which results in a uniform dispersion of BST powder on the nanometer scale. A comparison of the BST/COC composites with $Ba_{0.55}Sr_{0.45}TiO_3$ at the micrometer scale and $Ba_{0.5}Sr_{0.5}TiO_3$ at the nanometer scale was investigated [111]. Composites with a lower loading of common and nano-BST powders had the same relative permittivity. When the BST loading exceeded 15 vol%, the nanosized BST/COC had a higher dielectric constant, whereas it generated a higher dielectric loss. Because of the high surface area of the nanosized powders, the polarizability also increased; more surface area was connected to the polymer matrix, which formed a large "interaction zone" that changed the polymer behavior. The charge can accumulate at the interface between the nanosized powder and polymer matrix. Hence, the increase in dielectric constant of the BST/COC nanocomposite can be attributed to a high nanosized BST polarizability.

A different study reported conflicting results [178] in BST/PVDF composites with micron- and nanosized BST fillers. Fig. 25 shows

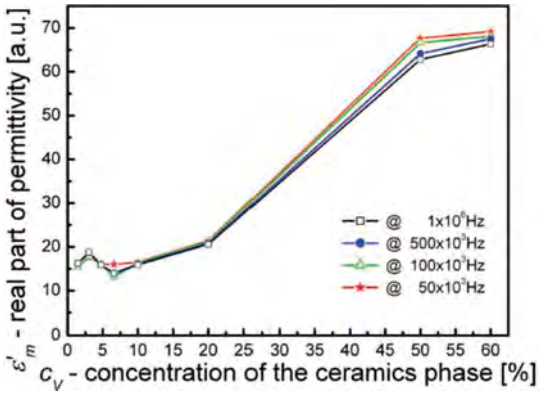

Fig. 24. Dependence of real part of dielectric permittivity on volume fraction of ceramic phase for BST/PVDF composite at different frequencies [177].

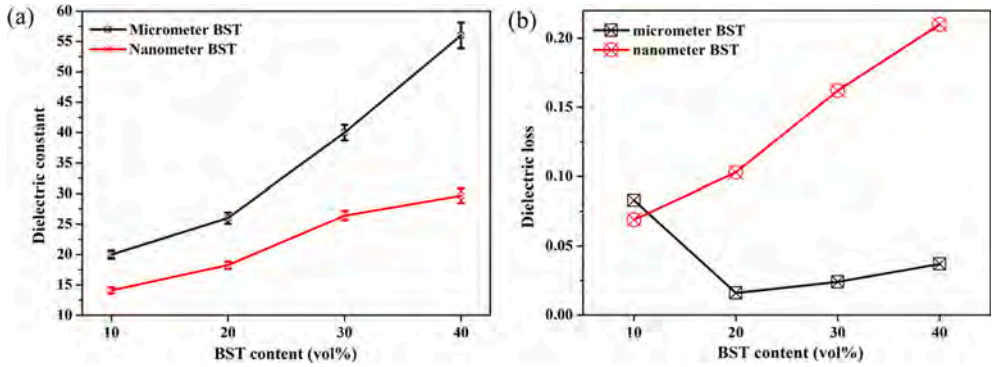

Fig. 25. Dielectric constant and dielectric loss of BST/PVDF micro- and nanocomposites with different BST contents at 1 kHz, (a) dielectric constant, (b) dielectric loss [178].

the effect of filler size on the dielectric properties of BST/PVDF composites. The dielectric constants of the nanocomposites are lower than those of the microcomposites, mainly because the ferroelectric domain walls in a single BST nanocrystal size will be reduced or even disappear, so the effect of domain wall vibration that contributes to the dielectric constant will be attenuated. The nanocomposite dielectric loss is higher than that of the microcomposites, because, in the polymer composition, the morphology and measurement conditions differ between the BST/COC and BST/PVDF composites. The influence of BST size on the dielectric properties needs further investigation.

4.3. Shape effect

Ceramic fillers with different shapes influence the dielectric properties of the ceramic/polymer composites [179]. Different polarization performances appear with various interfacial areas between ceramics and polymers that are created by different ceramic shapes. Different filler shapes can lead to different composite connectivity types. Filler types include spherical, cubic, fiber and plate-like particles in BST/polymer composites, in which zero-dimensional sphere-like fillers are used most. Part of the mixing rules used to describe the dielectric properties of composite materials is given in Section 3.2. Common rules are only suited to composites with spherical ceramic fillers. The Maxwell-Garnett and Yamada models are revised models to explain the dielectric behavior of composites, which contains information about the particle shape.

4.3.1. Zero-dimension BST

Several studies on the dielectric properties of BST/polymer composites with amorphous zero-dimension micron- and nanosized have been reported as mentioned above. However, the effect of some zero-dimension BST fillers with special shapes on the dielectric properties of BST/polymer composites has rarely been reported. **Adireddy et al.** [98] prepared BST cube-shape particles (BST NCs) with an average size of ~15 nm by a solvothermal reaction. The BST NCs/PVDF films were obtained by casting. The unique dielectric-polymer films showed an enhanced dielectric constant (>27) and a dielectric breakdown strength (E_b) of 285 MV/cm with a 30 vol% loading BST NC powder. Fig. 26 shows that the linear hysteresis loop behavior and resulting dielectric energy density for BST NCs/PVDF was 9.7 J/cm^3. They proposed that the strong nanoparticle-polymer matrix interfacial interaction is the main reason for the improved dielectric properties. **Liu et al.** [96] reported modified $Ba_{0.6}Sr_{0.4}TiO_3$/PVDF nanocomposites in which the BST NC size was

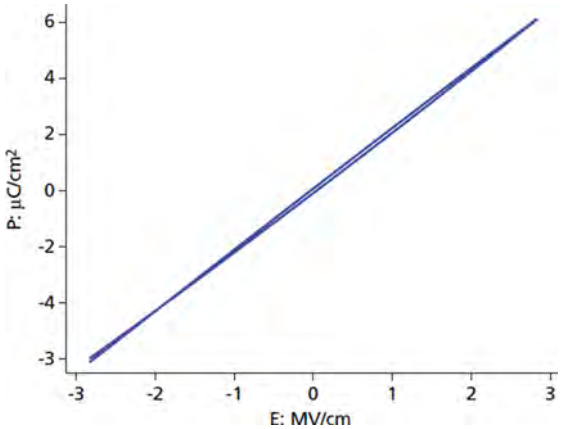

Fig. 26. Electric field-dependent polarization hysteresis loop of BST NPs/PVDF films [98].

~110 nm. They simulated the dielectric constant according to the theoretical models that were presented previously as shown in Fig. 27. The Maxwell-Garnett model and Lichtenecker model deviated from the experimental data when the volume fraction of BST-NPs powder exceeded 10%. The Yamada model is applicable over the entire concentration range. The shape factor of $n = 15$, $\varepsilon_c = 1000$ and $\varepsilon_p = 7.9$ agreed well with the experimental data.

Xu et al. [180] prepared a hollow-sphere BST (HS-BST) with a good spherical morphology, uniform size and accurate proportion of Ba/Sr using a template-assisted method as shown in Fig. 28. The particle size and shell thickness of the HS-BST particles can be adjusted by controlling the synthesis conditions, including the carbon sphere size, reactant concentrations, reaction time and temperature and hydrolytic inhibitor content. HS-BST particles with an average particle size of 0.44, 1.50 and 2.57 μm were obtained. **Guo et al.** [181] prepared HS-BST/PVDF composite materials on this basis using a tape-casting method. The micro-HS-BST was easier to separate from the polymer matrix than the nanoparticles. With the decrease in HS-BST particle size, the dielectric constant and loss of the HS-BST/PVDF composites decreased, whereas the dielectric breakdown strength increased initially and then decreased. The shape factor n of the HS-BST particles ranged from 2 to 2.5, which corresponds to a diameter of 0.44~2.57 μm, and a shell thickness of 40~500 nm. For HS-BST/PVDF composites with nano-HS-BST fillers (~440 nm), the dielectric constant and dielectric loss at 1 kHz were 14 and 0.03, respectively, with a high dielectric tunability of 4.26%, which showed potential application to produce flexible capacitors and tunable electronic devices.

4.3.2. One-dimensional BST fiber and tube

Extensive studies have been conducted on the synthesis and characterization of ceramic/polymer nanocomposites that contain one-dimensional $Ba_{1-x}Sr_xTiO_3$ particles with different morphologies, including nanotubes [27], nanofibers [22,24–26,182] and nanowires [28,29,183]. A critical obstacle in using nanoscale fillers is that they are difficult to disperse well in most polymer matrices because of the strong interaction among one-dimensional nanopowders. Significant effort has been expended to find a suitable process to disperse one-dimensional nanoparticles into the polymer matrix. One of the more effective ways is to create interfacial bonding between nanopowders and polymer matrixes. For this purpose, nanopowder surfaces were modified with certain organic groups, such as ammonium persulfate (APS) [22], silane coupling agent KH550 [121,122,184], tetrabutyl titanate coupling agent [21], polyhedral oligomeric silsesquioxane (POSS) [23], isopropyl dioleic(dioctyl- phosphate) titanate (NDZ10-1) [24] and perfluorooctyltrichloro silane [137]. This method can be used for nanoscale particles and other filler types. The increase in interfacial bonding promotes nanopowder dispersion, which improves the dielectric properties.

Liu et al. [22] reported on the excellent dielectric properties in surface-functionalized $Ba_{0.6}Sr_{0.4}TiO_3$ nanofibers/poly(vinylidene fluoride) (BST NF/PVDF). Fig. 29 shows typical surface and cross-sectional SEM images of the nanocomposite filled with BST nanofibers using untreated BST NF and BST nanofibers modified by APS (BST NF-APS). Fig. 29 (a) and (b) shows typical surface SEM images of nanocomposites with untreated BST NF and those with surface-modified BST NF (the BST NF content is 5 vol%). The adhesion between the BST NF and PVDF was weak. Voids and debonding between the BST NF and PVDF occurred in the nanocomposites. Some voids and pores were visible in the BST NF/PVDF nanocomposite film. The surface-modified BST-NF nanocomposite membrane had almost no small holes and was well dispersed in the nanocomposite membrane. Fig. 29 (c), (d) shows the surface SEM images of the 7.5 vol% BST NF-APS/PVDF nanocomposites and cross-sectional SEM of 5 vol% BST NF-APS/PVDF nanocomposites. The SEM image shows that BST NF-APS with a larger aspect ratio was dispersed uniformly in the PVDF matrix because of the enhanced compatibility of BST NF with the polymer matrix, and the orientation of BST NF-APS tends to the surface of the nanocomposite film inner direction. Compared with BST NF/PVDF, the BST NF-APS/PVDF nanocomposite film showed improved dielectric properties. The excellent dispersibility of the filler and the good interfacial adhesion between the surface-modified filler and the matrix increase the dielectric constant and reduce the dielectric loss.

When spherical or amorphous fillers are used to improve the dielectric properties, such as the dielectric permittivity and energy storage density, a higher ceramic filler loading is needed. Unfortunately, the composites may exhibit a deteriorated dielectric breakdown strength, mechanical properties and processing. Compared with spherical ceramic fillers, ceramic fillers with large aspect

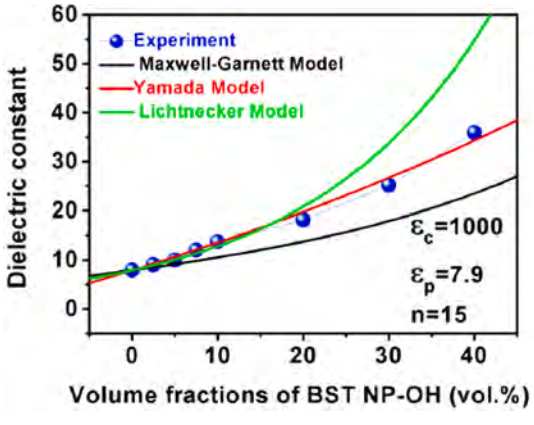

Fig. 27. Theoretical and experimental dielectric constants of composites as a function of content of BST-NPs-OH powders [96].

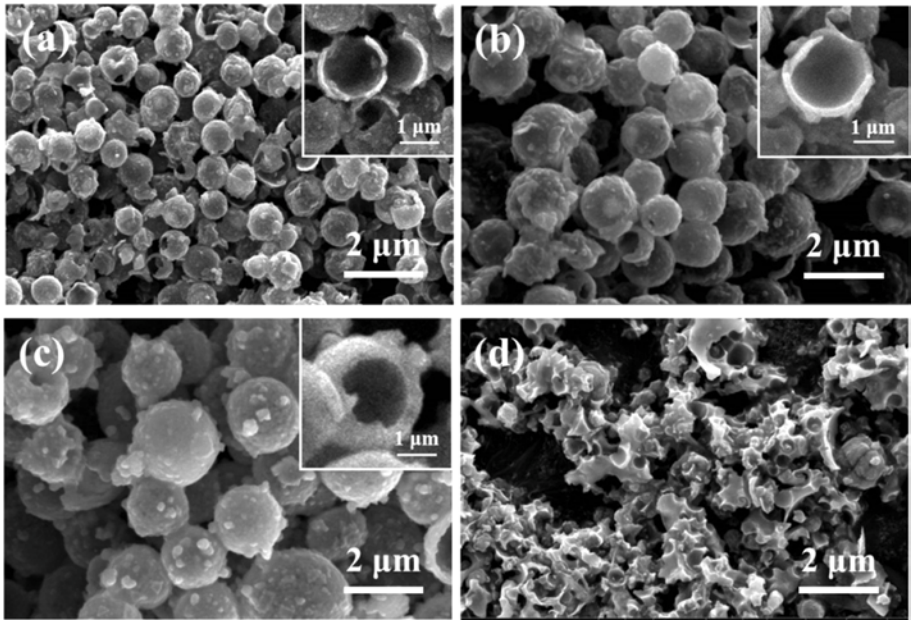

Fig. 28. SEM images of HS-BST for different metal-ion concentrations. (a) 0.002 mol/L, (b) 0.003 mol/L, (c) 0.004 mol/L, (d) 0.005 mol/L [180].

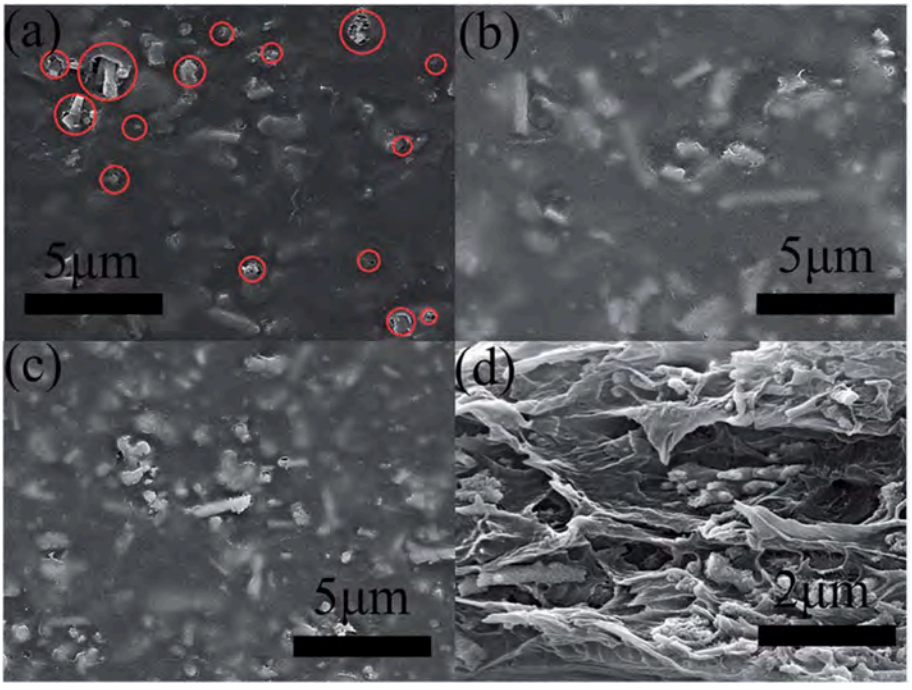

Fig. 29. Surface SEM of BST NF/PVDF nanocomposites that contain (a) 5 vol% BST NF/PVDF, (b) 5 vol% BST NF-APS/PVDF, (c) 7.5 vol% BST NF-APS/PVDF, (d) cross-section SEM of 5 vol% BST NF-APS/PVDF [22].

ratios can increase the dielectric properties of nanocomposites at lower concentrations because of their large dipole moments. **Song et al.** [185] proposed a micromechanical model and conducted experiments that showed that a greater dielectric constant could be obtained easily by using higher aspect ratio fillers rather than nanoparticles at the same volume fraction. Thus, a novel strategy has been developed by using one-dimensional BST fillers to enhance the dielectric energy storage density in nanocomposites. In many papers, an improved energy storage density of the BST/polymer composites (5.24~14.86 J/cm^3) was observed [22,34,35,186].

4.3.3. Two-dimensional Plate-Shaped BST

Plate-like BST particles are difficult to synthesize because of their high-symmetry lattice structure. In our recent research work [169,187], plate-like $Ba_{0.6}Sr_{0.4}TiO_3$ (P-BST) powders with a radial size of ~11 μm and a thickness of ~100 nm were synthesized using plate-like $Bi_4Ti_3O_{12}$ precursor by a two-step molten salt method. Flexible P-BST/PVDF composites were fabricated by tape casting and hot pressing. The P-BST powders were easy to orientate in PVDF matrix using tape casting, which resulted in an optimized microstructure, as shown in Fig. 30. Fig. 30 (a) to (d) shows that the textured arrangement of the particles (in the matrix) increases with an increase in particle size from 5.29 μm to 11.27 μm because the shear force that is generated during casting forces the P-BST particles to texture along the direction of the casting belt. A larger particle size yields a greater sensitivity to shear force. The excellent microstructure enhanced the dielectric properties significantly. The dielectric constant and energy storage of the P-BST/PVDF composites increased and dielectric loss decreased with an increase in average particle size in which the concentration of P-BST was 40 vol%, as shown in Table 3. The plate-like BST particles were parallel and isolated by a polymer layer as a medium between the platelet, which could form microcapacitors in the PVDF matrix. The excellent uniform dispersion of platelets and the existence of many microcapacitors in the PVDF matrix contribute to the high dielectric properties.

Table 4 summarizes the dielectric properties of some examples based on composites with different filler sizes and shapes. The BST filler is a key factor that affects the dielectric properties of the BST/polymer functional composites. These results indicate that the composite dielectric properties can be tuned by filler concentration, size, shape and fabrication process. The choice of a suitable filler and process method is necessary to obtain the required dielectric properties.

5. Dielectric tunability of BST/Polymer composites

5.1. Recent developments in evolution dielectric tunability of functional materials

A large electrical field dependent dielectric constant can be used for tunable devices. BST ceramics are often used as tunable materials because of their high tunability properties. Fig. 31 summarizes the dielectric constant and dielectric tunability (T_0) based on Eq. (4) of functional materials with BST, PVDF and composites [30–40,187–193]. Points at the rectangle in the top right corner represent doped and composite ceramics. Fig. 31 shows that the dielectrics with a high tunability usually possess a high permittivity. However, the practical application of dielectric tunable devices requires a low dielectric constant and high tunability, especially in the microwave band [41,42]. The attraction point should be in the shadow region. The dielectric constant of the BST/polymer was less than 100 and the dielectric tunability was relatively high. Therefore, it is very desirable if the BST/polymer composites possess a suitable dielectric constant and a high tunability. Current research on high-dielectric tunable materials focuses mainly on BST-based

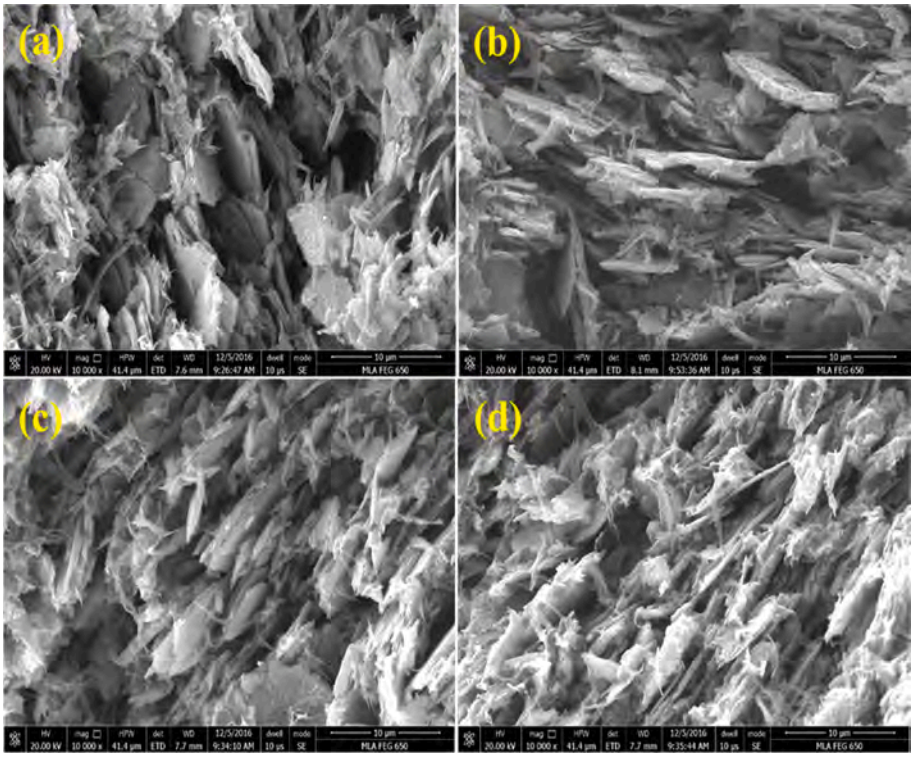

Fig. 30. SEM micrographs of 40 vol% P-BST/PVDF composites with different average particle sizes (a) P-BST 5.29 μm, (b) P-BST 7.86 μm, (c) P-BST 9.96 μm, (d) P-BST 11.27 μm [169]

Table 3
Dielectric properties of P-BST/PVDF composites.

Properties	P-BST	P-BST	P-BST	P-BST
Particle size (μm)	5.29	7.86	9.96	11.27
ε_r at RT at 1 kHz	58.0	60.0	61.2	62.2
Tanδ at RT at 1 kHz	0.066	0.056	0.047	0.042
Breakdown strength E_b (kV/mm)	134.1	140.7	146.3	151.9
Energy storage density U (J/cm^3)	4.61	5.26	5.80	6.36

Table 4
Dielectric properties of BST/PVDF composite with various ceramic filler shapes.

Material	Ceramic shape	BST (vol%)	ε_r (1 kHz)	tanδ (1 kHz)	Energy storage density (J/cm^3)	Ref.
BST/PVDF	Nanofibers	2.5	13	0.019	6.8	[22]
		7.5	21.78	0.013	–	
	Nanotubes	10	48.2	0.07	7.9	[27]
	Nanowires	7.5	–	–	14.86	[28]
	Nanocube shape	35	27	–	9.7	[98]
	Amorphous nanosize	40	29.7	0.210	3.29	[108]
	Amorphous microsize	40	56	0.12	0.36	[121]
	Plate shape	40	62.2	0.042	6.36	[169]

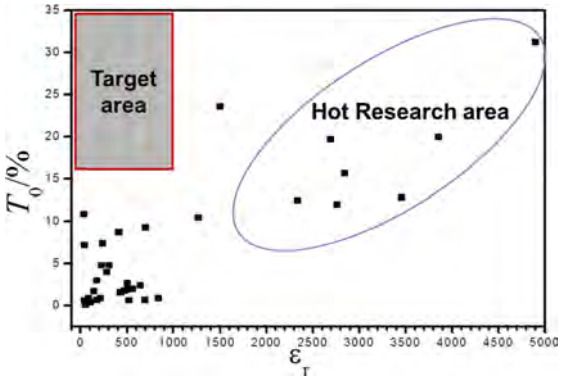

Fig. 31. Dielectric constant and dielectric tunability (T_0) of functional materials in recent decades.

ceramics, as introduced in Section 2.3. However, limited research exists on the dielectric tunability of BST/polymer functional materials.

For the 0–3-type ceramic/polymer composites, the filler concentration has a significant influence on the dielectric tunability. **Hu et al.** [121] reported that the dielectric tunability T_0 of BST/PVDF composites increase from 3.2% to 7.2% under a bias voltage of 1.0 kV/mm with BST filler contents that increased from 10 vol% to 40 vol%. The tunability of 40 wt% (MgO-Al_2O_3-ZnO co-doped BST)/

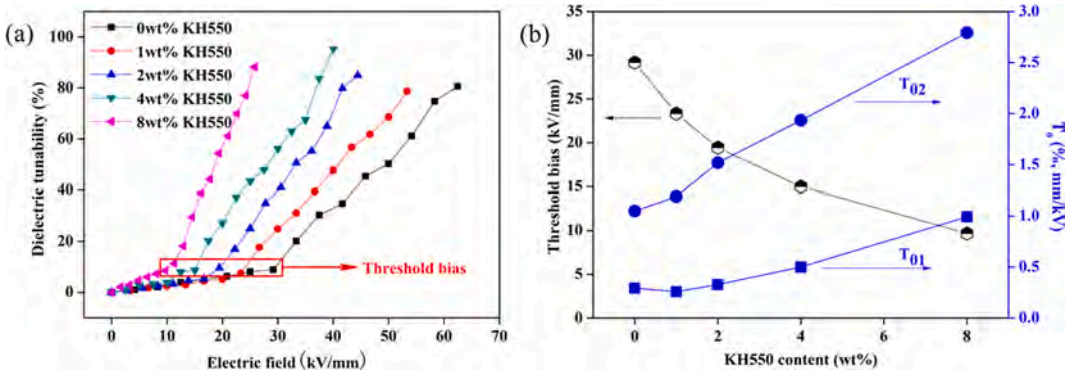

Fig. 32. Dielectric tunability (a) and threshold bias (b) of 40 vol% BST/PVDF composites modified with different KH550 contents at RT (1 kHz) [122].

PVDF composites reached 10.9% under the same bias [187]. The dielectric tunability of the BST/ABS composites filled with 40 vol% BST powders reached 3.36% (2 kV/mm) [108], and the dielectric tunability of the BST/ABS-PVDF composites filled with 40 vol% BST powders reached 20% (16 kV/mm) [175]. **Zhang et al.** [122] proposed a threshold bias in the plot of the dielectric tunability versus applied electric DC field with different filler contents as shown in Fig. 32.

Fig. 32 shows the dielectric tunability of 40 vol% BST/PVDF composite samples at 1 kHz at RT. The dielectric tunability increases with an increase in bias voltage, as shown in Fig. 32(a). The maximum dielectric tunability reaches 95.2% at a low electric bias of 40 kV/mm when the KH550 content is 8 wt% BST powder. Fig. 32(a) shows that initially, the dielectric tunability increases slowly with an increase in bias, and the dielectric tunability increases sharply after the electric field is larger than a specific electric field, which is defined as the threshold bias. Because two parts are present in the single plot of Fig. 32 (a) separated by the threshold bias, the dielectric tunabilities under unit electronic bias of BST/PVDF composites, T_{01} and T_{02}, were calculated as shown in Fig. 32 (b). T_{01} and T_{02} increased with an increase in KH550 content, accompanied by a decreasing threshold bias. A smaller threshold bias results in a better dielectric tunable property. Therefore, a high dielectric tunability can be obtained at a relatively low electric bias. For example, the threshold bias of BST/PVDF composites with 8 wt% KH550 was 9.68 kV/mm, and a high tunability of 88.2% could be obtained at a 25.8 kV/mm electric bias.

The analogous phenomenon mentioned above can also be observed in BST/PVDF with nanosized BST particles [178]. Thus, a new criterion EP_{80} with a synthetic consideration of the threshold electric bias is proposed to evaluate the dielectric tunability of the BST/PVDF composites [169]. EP_{80} means an electric field when the dielectric tunability of the composites reaches 80%. For composites with the same thickness, a smaller EP_{80} corresponds to a better dielectric tunability. A small EP_{80} and a low threshold electric bias benefit practical application. As an example, **Wang et al.** [169] fabricated P-BST/PVDF composites with different ceramic particle sizes. The particle sizes of P-BST5, P-BST10, P-BST15 and P-BST20 are 5.29 μm, 7.86 μm, 9.96 μm and 11.27 μm, respectively. Through testing and calculating the dielectric tunability of the composite material, the EP_{80} and threshold electric bias were obtained, as shown in Fig. 33. The threshold electric bias decreases from 20 kV/mm to 14 kV/mm and the EP_{80} of the P-BST/PVDF composites ranged from 43.5 kV/mm to 29 kV/mm with an increase in average plate-like particle size. The EP_{80} decreased by up to 50%. The results confirm that the plate-like particle size influences the P-BST/PVDF composite tunability. The large plate-like P-BST particles show oriented arrangements in the PVDF matrix, which results in an improved dielectric tunability.

The dielectric tunability of the BST/polymer composites depends on the connectivity of the ceramic and polymer. **Xiang et al.** [115] prepared a 1–3-type BST/PMMA composite and investigated its tunability as shown in Fig. 34. The composite tunability was 36% at 16 kV/cm. No threshold bias exists in this composite type, which differs from the 0–3-type composites. Analogous results are present in the 1–3-type BST/epoxy composites [110].

5.2. Theoretical models for dielectric tunability of Ceramic/Polymer composites

An accurate prediction and simulation of dielectric properties of ceramic/polymer composites are of significance and are important in the design and fabrication of dielectric materials. Several models were used to predict the dielectric constant of the composites, which could reduce the uncertainty in the preparation process and improve the efficiency of research and development, as described in Section 3.2.

According to research into ceramic/PVDF composites, the logarithmic mix law, Maxwell's theory model, Clausius-Mossotti model and Yamada model have been used often to perform numerical simulations of the dielectric constant of composites. Our research group simulated the experimental data of the dielectric constant of BST/PVDF [121] and BMAZ/PVDF [187] composites by different models. After comparing the experimental and simulated permittivity from several theoretical models, the permittivity curves that were obtained by the Yamada model had a preferable matching with an adjustment of shape factor. The other models displayed more errors because of various assumptions, and the logarithmic law shows the greatest deviation, as shown in Fig. 35. The deviation between the experimental and simulated dielectric constant in BST/PVDF and BMAZ/PVDF composites is small when the shape factor values of the ceramic particles are 4 and 1.5, respectively. These observations indicate that the shape factor is important to predict the dielectric properties of composites accurately. Thus, the law of permittivity of ceramic/polymer composite systems with changing ceramic contents can be fitted by correcting the error between experimental and simulated values by adjusting the shape factor of ceramic particles in the Yamada model.

For the dielectric tunability (T_u), it can be concluded that a functional relationship must exist between the composite dielectric tunability and ceramic dielectric tunability and permittivity based on the previous dielectric tunability experimental data. According to the thermodynamic phenomenological theory of Devonshire [114], the composite dielectric tunability (T_{u1}) theoretical rules can be obtained as follows:

$$\varepsilon_{(E)} = \frac{\varepsilon_{(0)}}{1 + 2\beta\varepsilon_{(0)}\varepsilon_0 P^2_{(E)}} \tag{19}$$

$$P_{(E)} = \varepsilon_0[\varepsilon_{(E)} - 1]E \approx \varepsilon_0\varepsilon_{(0)}E \tag{20}$$

$$T_u = 1 - \frac{1}{1 + 2\beta\varepsilon_{(0)}\varepsilon_0 P^2_{(E)}} \approx 2\beta\varepsilon^3_{(0)}\varepsilon^3_0 E^2 \tag{21}$$

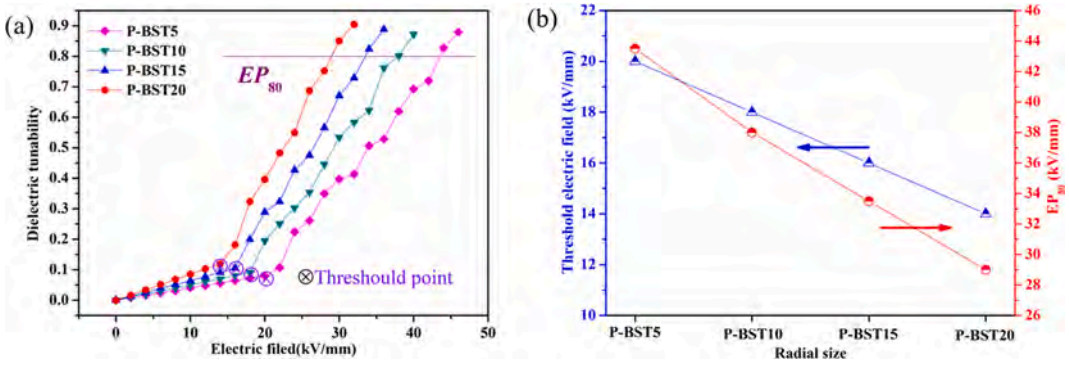

Fig. 33. Dielectric tunability (a) threshold electric field and EP_{80} (b) of 40 vol% P-BST/PVDF composites with different average particle sizes [169].

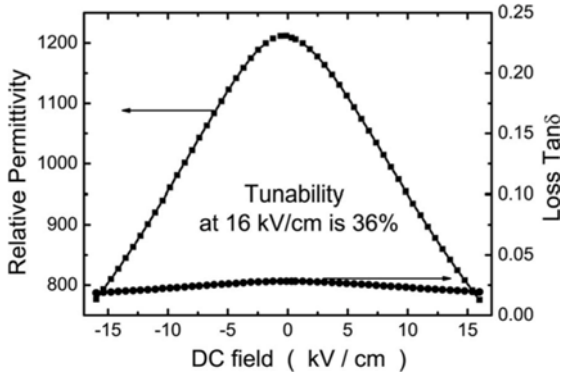

Fig. 34. Bias dependence of dielectric constant and loss tangent of BST/PMMA composite at 10 kHz [115].

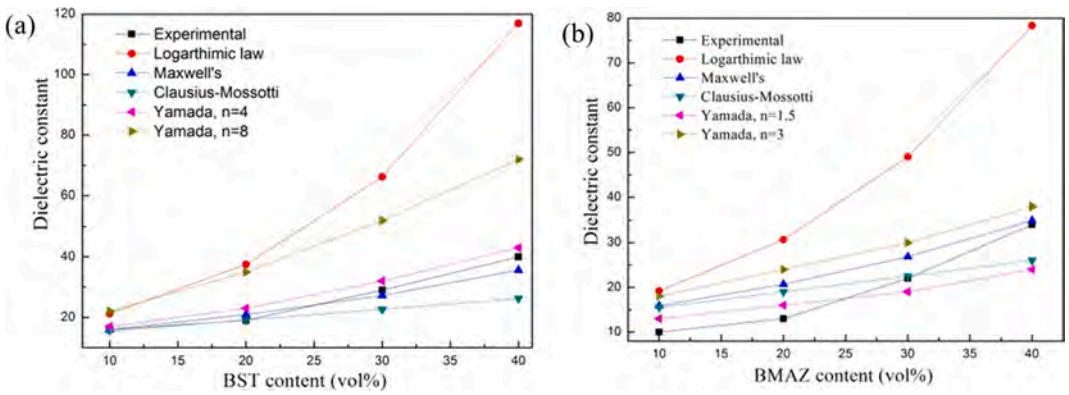

Fig. 35. Experimental and simulated dielectric constant of (a) BST/PVDF [121] and (b) BMAZ/PVDF [187] composites.

Table 5
Experimental and theoretical dielectric tunability of BST/PVDF composites.

Properties	10 vol% BST	20 vol% BST	30 vol% BST	40 vol% BST
ε_2 (BST)	3558	3558	3558	3558
T_{u2} (BST)	25%	25%	25%	25%
ε_1 (BST/PVDF)	16	19	29	40
Experimental value T_{u1} (BST/PVDF)	3.2×10^{-2}	3.9×10^{-2}	4.5×10^{-2}	7.2×10^{-2}
Theoretical value T_{u1} (BST/PVDF)	2.3×10^{-8}	3.8×10^{-8}	1.3×10^{-7}	3.5×10^{-7}

$$T_{u1} = 2\beta\varepsilon_{(0)}^{3}E^{2}\varepsilon_{1}^{3} = 2\beta\varepsilon_{(0)}^{3}E^{2}\varepsilon_{2}^{3}\left(\frac{\varepsilon_1}{\varepsilon_2}\right)^{3} = T_{u2}\left(\frac{\varepsilon_1}{\varepsilon_2}\right)^{3} \tag{22}$$

where $\varepsilon_{(0)}$ and $\varepsilon_{(E)}$ are the dielectric constants under a zero-DC electric field and a specific electric field, respectively; $P_{(E)}$ is the polarization in a given electric field; ε_0 is the vacuum permittivity; E is the given electric field; T_{u1} and ε_1 are the dielectric tunability and dielectric constant of the composites, respectively; T_{u2} and ε_2 are the dielectric tunability and dielectric constant of ceramic and β is the phenomenological coefficient of the materials.

The dielectric tunability of the BST/PVDF composite materials was calculated by Eq. (22), as shown in Table 5. The experimental data are higher than the theoretical values, e.g., the composite with a 40% volume fraction BST yielded experimental data of 7.2%, whereas the theoretical value was five orders of magnitude lower than the experimental data at 3.5×10^{-7}. A careful analysis of the Devonshire phenomenological theory model showed that the composites and ceramic phenomenological coefficient were considered identical during the derivation process from Eq. (21) to Eq. (22). However, a significant difference exists between composite and ceramic phenomenological coefficients in a real situation, which can be proven again with the simulated and experimental data of BMAZ/PVDF composites shown in Table 6. It is necessary to modify the Devonshire theory model to make it fit BST/polymer composites.

A modified theoretical model for dielectric tunability is proposed as follows:

$$T_{u1} = 2\beta_1\varepsilon_{(0)}^{3}E^{2}\varepsilon_{1}^{3} = 2\left(\frac{\beta_1}{\beta_2}\right)\beta_2\varepsilon_{(0)}^{3}E^{2}\varepsilon_{2}^{3}\left(\frac{\varepsilon_1}{\varepsilon_2}\right)^{3} = T_{u2}\left(\frac{\beta_1}{\beta_2}\right)\left(\frac{\varepsilon_1}{\varepsilon_2}\right)^{3} \tag{23}$$

where T_{u1}, ε_1 and β_1 are the dielectric tunability, dielectric constant and phenomenological coefficient of the composite, respectively. T_{u2}, ε_2 and β_2 are the dielectric tunability, dielectric constant, and phenomenological coefficient of the ceramic filler, respectively. The following can be deduced from Eq. (23):

(1) There is a direct proportional relationship between the dielectric tunability of the composites and ceramic filler.
(2) If the concentration of the polymer is zero, which implies pure ceramic materials, so $\beta_1 = \beta_2$, $\varepsilon_1 = \varepsilon_2$, and $T_{u1} = T_{u2}$.
(3) If the dielectric constant of composites is close to that of the ceramics, Eq. (23) is changed to Eq. (24):

$$T_{u1} \approx T_{u2}\left(\frac{\beta_1}{\beta_2}\right) \tag{24}$$

Equation (24) shows that the dielectric tunability of the composite has a significant positive correlation with the ceramic phase, and its value depends on the phenomenological coefficient ratio between the composites and the ceramic.

(4) If the difference in permittivity between the composites and the ceramic is large, the difference in dielectric constant for the dielectric tunability between the polymer and ceramics can be compensated by the phenomenological coefficient ratio between the composites and ceramic (β_1/β_2).

The dielectric tunability of the BST/polymer composites in References [121–123,174,178,187] agrees with the four rules above. The phenomenological coefficient ratio between composites and ceramic can be obtained by calculating the dielectric tunability ratio of the experimental and theoretical values. BST/PVDF [121] and BMAZ/PVDF [187] composites were used as examples. The dielectric tunability data of the composites were used to simulate the phenomenological coefficient ratio, and the simulated results are shown in Table 7. The changes in phenomenological coefficient ratio for the composite and ceramic with the ceramic content can be obtained as shown in Fig. 36. There is an approximately linear relationship between the phenomenological coefficient ratio and ceramic content in these two composite types. According to the curves, two approximate linear functional relationships were fitted as follows:

$$\text{BST/PVDF composites} \quad \beta_1/\beta_2 = -4300\delta_c + 1800000 \tag{25}$$

$$\text{BMAZ/PVDF composites} \quad \beta_1/\beta_2 = -8700\delta_c + 340000 \tag{26}$$

where β_1/β_2 is the phenomenological coefficient ratio between the composites and the ceramic and δ_c is the volume fraction of the ceramic phase.

Fig. 36 shows that the phenomenological coefficient ratio almost decreases linearly with an increase in ceramic content. The

Table 6
Experimental and theoretical dielectric tunability of BMAZ/PVDF composites.

Properties	10 vol% BMAZ	20 vol% BMAZ	30 vol% BMAZ	40 vol% BMAZ
ε_2 (BMAZ)	1307	1307	1307	1307
T_{u2} (BMAZ)	41.5%	41.5%	41.5%	41.5%
ε_1 (BMAZ/PVDF)	10	13	22	34
Experimental value T_{u1} (BMAZ/PVDF)	4.3×10^{-2}	6.5×10^{-2}	8.6×10^{-2}	10.9×10^{-2}
Theoretical value T_{u1} (BMAZ/PVDF)	1.6×10^{-7}	4.1×10^{-7}	2.0×10^{-6}	7.4×10^{-6}

Table 7
Phenomenological coefficient ratio of composites and ceramics.

β ratio	10 vol%	20 vol%	30 vol%	40 vol%
β_1/β_2 (BST/PVDF)	1.4×10^6	1.0×10^6	0.3×10^6	0.2×10^6
β_1/β_2 (BMAZ/PVDF)	2.7×10^5	1.6×10^5	0.4×10^5	0.2×10^5

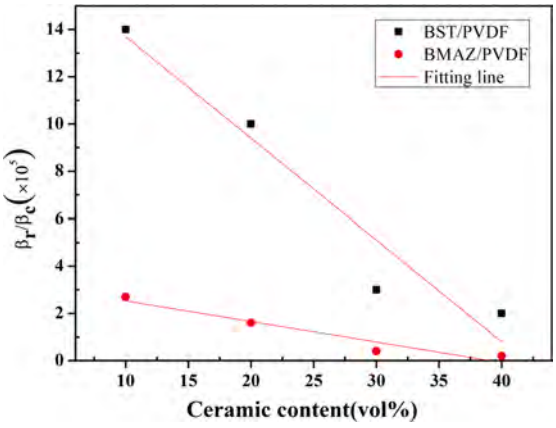

Fig. 36. Ceramics volume fraction dependence of phenomenological coefficient ratio of composites and ceramics.

phenomenological coefficient ratio decreases systematically under the equivalent ceramic content. The connectivity between the ceramic and polymer and the ceramic fillers influences the composite structure and properties significantly, which lays a theoretical foundation for further accurate prediction of the dielectric tunability.

The values that were simulated by the Yamada model are closer to the experimental data compared with the results that were simulated by the other dielectric theory models, so the Yamada dielectric model was introduced into Eq. (23) and then the dielectric tunability for the BST/polymer composite changed to the following format:

$$T_{u1} = T_{u2}\left(\frac{\beta_1}{\beta_2}\right)\left(\frac{\varepsilon_1}{\varepsilon_2}\right)^3 = T_{u2}\left(\frac{\beta_1}{\beta_2}\right)\left(\varepsilon_p/\varepsilon_1\left[1+\frac{n\delta_c(1-\varepsilon_p/\varepsilon_1)}{n\varepsilon_p/\varepsilon_1+(1-\delta_c)(1-\varepsilon_p/\varepsilon_1)}\right]\right)^3 \tag{27}$$

where ε_p is the dielectric constant of polymer matrix and n is the shape factor. The dielectric constant ratio of the organic matrix and

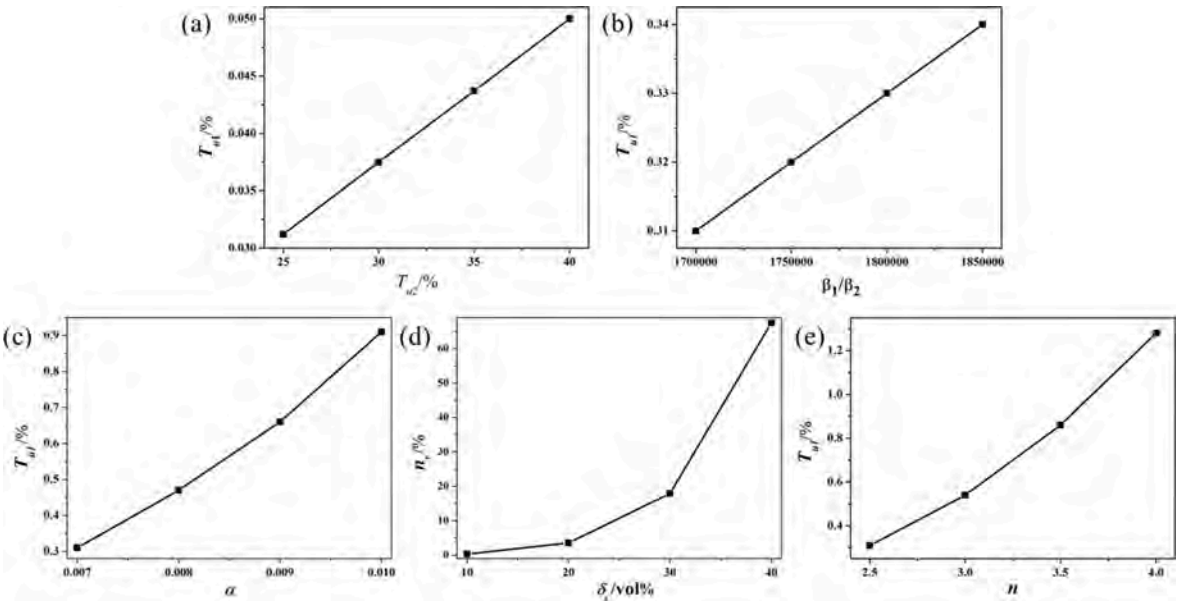

Fig. 37. Dependence of influencing factors on dielectric tunability of composite.

ceramic (a, $a = \varepsilon_p/\varepsilon_1$) is introduced into Eq. (27) and the equation can be rewritten as:

$$T_{u1} = T_{u2}\left(\frac{\beta_1}{\beta_2}\right)\left(a + \frac{a\delta_c(1-a)}{na + (1-\delta_c)(1-a)}\right)^3 \tag{28}$$

A new dielectric tunable theoretical equation that combined the Yamada dielectric model and the modified Devonshire phenomenological theoretical model is proposed:

$$T_{u1} \approx T_{u2}\left(\frac{\beta_1}{\beta_2}\right)\left(a \cdot \frac{\delta_c}{1-\delta_c} \cdot n\right)^3 \tag{29}$$

where T_{u1} and β_1 are the dielectric tunability and phenomenological coefficient of the composite, respectively; T_{u2} and β_2 are the dielectric tunability and phenomenological coefficient of the ceramic, respectively; δ_c is the volume fraction of the ceramic, a is permittivity ratio of the organic matrix and the ceramic and n is the shape factor of the ceramic particles.

Five factors influence the dielectric tunability of the BST/polymer composites: T_{u2}, β_1/β_2, a, δ_c and n. A significant positive correlation exists between the dielectric tunability and these five factors. According to the experimental and fitted data of BST/PVDF, the ranges of T_{u2}, β_1/β_2, a, δ_c and n are 25~40%, 1.7~1.85 $\times$ 10^6, 0.007~0.01, 10~40 vol% and 1.5~4, respectively. The composite dielectric tunability simulation values can be obtained by substitution of the above data into Eq. (29) as shown in Fig. 37. During each simulation, one variable kept changing, and the other variable achieved a minimum value within the limit.

Among these factors, T_{u1} and a are independent and the phenomenological coefficient between polymer and ceramics is related to the concentration of ceramics. The shape factor n can be changed, but its physical interpretation requires further investigation. Within the given system, once the parameters T_{u2} and a reach a certain value, the phenomenological coefficient between the polymer and ceramics is determined. Thus, the shape factor of the ceramic particles (n) affects the dielectric tunability of a certain ceramic/polymer composite with the same filler content.

6. Applications for BST/polymer composites

The outstanding properties of BST/polymer composites make them applicable over a wide range. Various promising applications have been specified and future development directions have been forecast. Increased attention has been given to BST/polymer composites in the application of embedded capacitor materials [24–27,96,98,100]. Traditionally, BST is used for capacitors. However, many disadvantages cannot be ignored, such as the expensive processing and difficulty in implementation over large PCB substrate areas. Embedded electronic devices are difficult to process, which limits their application. Polymers are low cost, have a high dielectric breakdown strength, are easily produced, and are compatible with PCB process, whereas their dielectric permittivity typically is low. Fig. 38 shows schematics of discrete and embedded passives [182]. If these capacitor components are embedded in the PCB, the printed circuit board size would be reduced significantly. The BST/polymer composites combine the advantages of an excellent dielectric constant from the ceramic phase and a good processibility from the polymer matrix, which has great potential for the development of embedded capacitors [182,183].

Wearable electronic devices show great market prospect. As one core component of wearable electronic devices, the sensor will exert a significant influence on the future design and function of the wearable electronic device [12,148,194–197]. Compared with traditional electrical sensors, flexible wearable sensors have the advantages of being light, thin, portable and highly integrated. BST/polymer composites can be considered as a capacitance signal transduction sensor. The BST/polymer composite has an excellent flexibility and good deformability, which makes it applicable to wearable and other flexible electronic devices, as shown in Fig. 39.

Energy storage is an important development aspect in modern industry. Functional dielectric BST/polymer composites can be applied in the field of large power energy storage devices because of their high energy storage density [22,98,103,136]. Compared

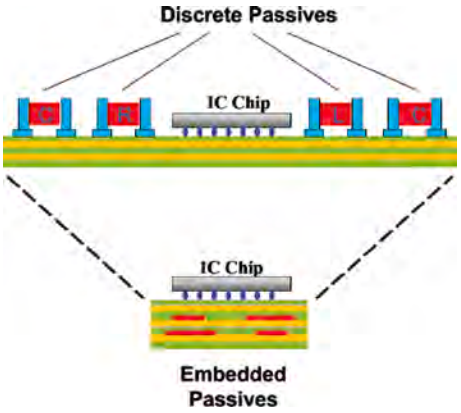

Fig. 38. Schematic of discrete and embedded passives [182].

Fig. 39. Photograph of flexible ferroelectric BST/polymer composite tape [198].

with other energy storage devices, such as batteries, the dielectric energy storage materials have a high power [24], which means that the energy can be released in a short time. **Tang et al.** [184] reported an ultra-high energy storage density BST/PVDF nanocomposite using $Ba_{0.2}Sr_{0.8}TiO_3$ nanowires. The nanocomposites had an ultra-high energy density of 14.86 J/cm^3 at 450 MV/m and provided a microsecond discharge time that was faster than commercial biaxial oriented polypropylene capacitors as shown in Fig. 40. The good properties, with the large energy storage density and rapid discharge speed, make the BST/polymer composites good candidates for military applications, especially in new weapons, such as laser guns and electromagnetic guns.

BST/polymer composites can be used in microwave tunable devices, such as phase shifters, tunable filters and steerable antennas [199–201], especially at the microwave frequency because of its well-known advantages of a low dielectric constant, high tunability and low dielectric loss at the microwave frequency [202,203]. To establish the optimal trade-off between a high tunability and a low permittivity, many non-ferroelectric oxides (such as MgO, La_2O_3, Mg_2SiO_4, ZnO and Al_2O_3) have been added to the ABO_3-type perovskite. However, previous literature has shown that it is difficult to maintain the tunability at the same level while decreasing the permittivity [29–39]. BST/polymer composites have shown successful potential application because of the variable BST/polymer composite dielectric constant. Many efforts on the high dielectric tunability BST/polymer composites have been explored [110,121,122,115,169,174,178].

BST/polymer composites are suitable for wireless sensor networks because of their reconfigurable sensing antenna, promising wireless sensor networks type, ability to monitor the surrounding environment by transmitting and receiving information through electromagnetic waves. Some special BST/polymer composites possess an excellent microwave performance and a high environmental sensitivity. For example, **Zhang et al.** [21] fabricated a Radio Frequency I Dentification (RFID) sensor antenna for wireless temperature sensing by using HDPE/BST composites as the substrate. The resonant frequency of the antenna changes with the temperature. The temperature of the resonant frequency of the RFID sensor antenna was ~700 ppm/°C, which could monitor the variation in environmental temperature by detecting the shift in resonant frequency.

Recently, functional materials with large electronic and caloric effects have attracted attention [204–209]. The ECE phenomenon is defined as a reversible change in temperature (ΔT) or isothermal entropy (ΔS) and the induction of isothermal heat (Q) of a polarized material in response to the application of an applied electric field under adiabatic or isothermal conditions. The EC has been observed in various ferroelectric ceramics and polymers, in which large spontaneous polarization can become an electric field to generate ΔT

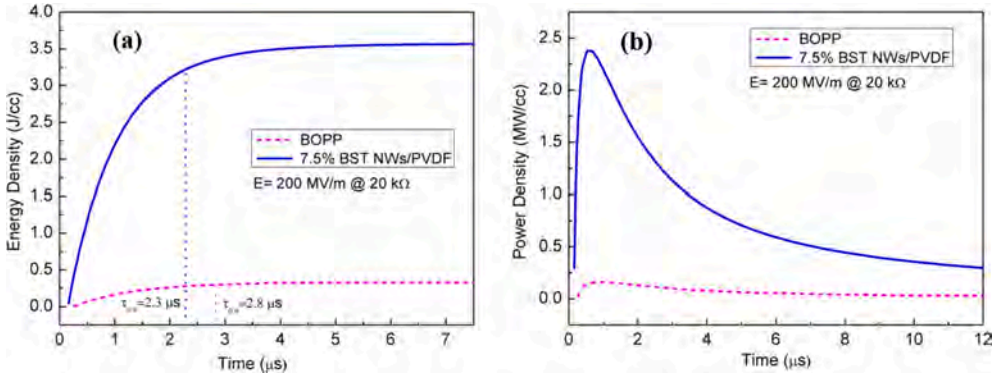

Fig. 40. Typical (a) discharged energy density and (b) power density profiles for nanocomposites with 7.5% BST NWs and commercial BOPP. Load resistor RL is 20 kΩ, and the electrical field is 200 MV/m [184].

and ΔS. Ferroelectric polymers are among the most promising EC materials for cooling applications. However, the introduction of the EC effect in ferroelectric polymers requires a large electric field (E). The calculation of $|Q|/|\Delta E|$, $|\Delta T|/|\Delta E|$ and $|\Delta S|/|\Delta E|$ compared with ferroelectric ceramics shows that the EC polymer strength is lower [204]. An EC response in BST materials near the paraelectric to ferroelectric range is most effective around the phase transition according to a first-principles-derived approach combined with the Wang-Landau algorithm [205]. Thus, ferroelectric BST/polymer composites can serve as a novel class of EC materials that are soluble and display a pronounced EC under a modest electric field. **Zhang et al.** [207–209] reported the EC performance of ~6-μm-thick $Ba_{0.67}Sr_{0.33}TiO_3$/P(VDF-TrFE-CFE) nanocomposite films and characterized at ambient temperature as shown in Fig. 41. The EC strength was improved substantially with BST introduction, i.e., a composite with 10 vol% BST exhibits a $|Q|/|\Delta E|$ of 326.7 kJ/(MV·m^2) at 75 MV/m, which more than doubles that of the best EC polymer represented P(VDF-TrFE-CFE) and approaches that of PMN-PT thin films (~348 kJ MV^{-1} m^{-2}). Ferroelectric BST/ polymer composite could find wide application in cooling devices for advanced electronics, energy efficiency and environmentally friendly refrigeration.

Inkjet printing is a promising technology for the selective deposition of functional components, such as electronic circuits, light emitting devices (LEDs) or dielectric films. Recently, BST/polymer composites including BST/PPS [210], BST/COC [112], BST/PMMA [114] and BST/PEG-DA [120] were used for inkjet printing. **Mikolajek et al**. prepared BST/PMMA with a 50:50 vol ratio which is suitable for printing larger films and for printing small line structures with a uniform topography. The prepared composite thick films showed a homogeneous thickness of 7.2 mm. The temperature treatment after each electrode printing step was set to 150 °C, which offers the future possibility to print on flexible substrates, such as PET substrates. A relative permittivity of 28 and dielectric loss of 0.043 were obtained at $f = 10$ kHz.

BST/polymer composites tend to have broad application prospects [211–218]. A significant improvement in BST/polymer composites has been made in the field of energy storage capacity and high dielectric tunability characteristics. A simple outlook for applications of the BST/polymer composite is shown in Fig. 42.

7. Concluding remarks and future perspectives

This paper reviews the fundamentals of BST materials, the process, energy storage and dielectric properties, and focuses on the dielectric tunability of BST/polymer composites. The concluding remarks are as follows.

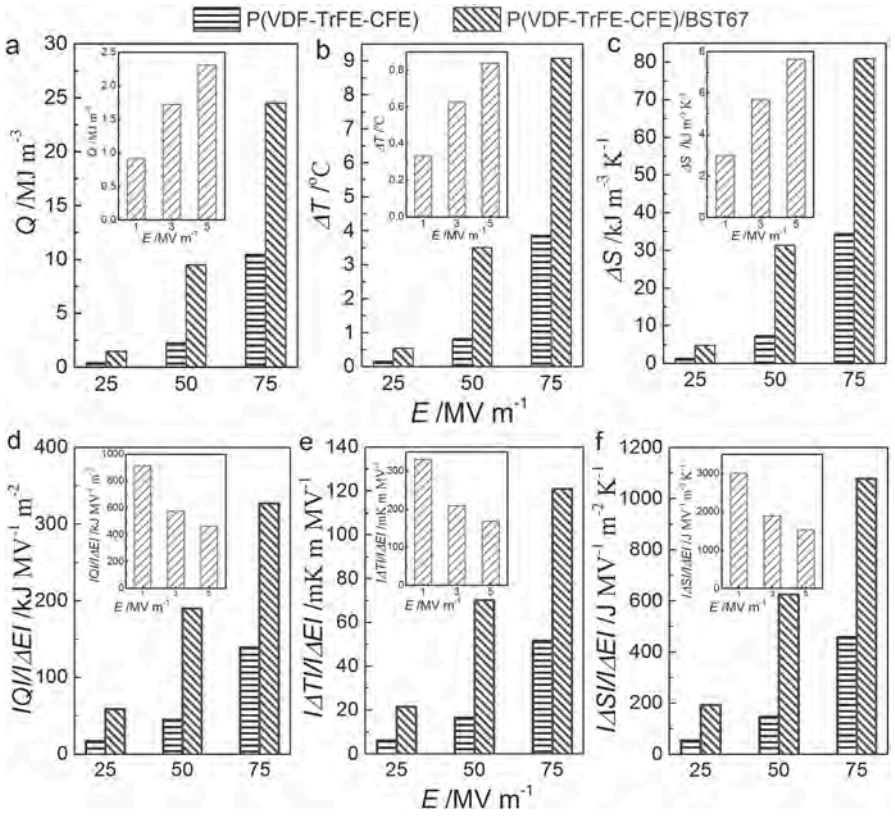

Fig. 41. Comparison of EC of $Ba_{0.67}Sr_{0.33}TiO_3$ (inset), P(VDF-TrFE-CFE), and BST/P(VDF-TrFE-CFE) (10 vol% of BST) nanocomposites at low electric fields (25–75 MV m^{-1}) (a) Q, (b) ΔT, (c) ΔS, (d) |Q|/|ΔE|, (e) |ΔT|/|ΔE|, (f) |ΔS|/|ΔE| [207].

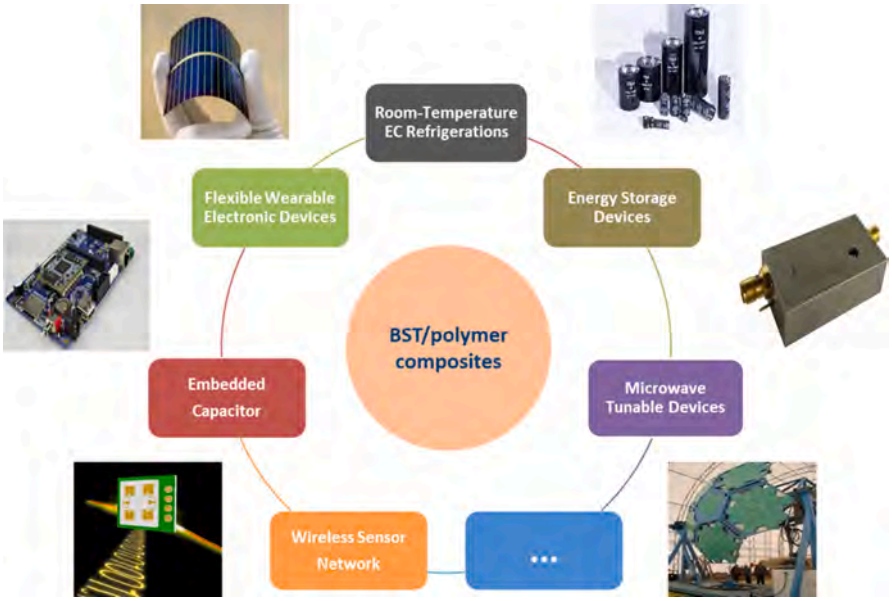

Fig. 42. Outlook for applications of the BST/polymer composite.

1) BST materials are a ferroelectric solid–solution material. BST ceramics exhibit excellent dielectric properties: a high dielectric constant, a Ba/Sr composition-dependent Curie temperature T_c, and a high tunability of dielectric behavior. However, they also have drawbacks, such as a poor-flexibility high dielectric loss under microwave frequency and a low energy storage density, which does not satisfy their application in electric devices.
2) BST/polymer composites have many advantageous properties and the properties depend on the microstructure and interface between the BST fillers and polymers. A better filler-polymer compatibility improves the composite microstructure stability. Various methods, such as filler modification, filler functionalization and hot processing, were used to improve the composite microstructure and interface. Appropriate surface modification of inorganic fillers is important to promote interfacial interaction between fillers and polymer matrix and filler dispersion in the polymers. Surface modification may also minimize defect or void content in the composite by using a specific process, such as hot pressing.
3) The size, shape and concentration of BST fillers has a significant effect on the dielectric properties. The dielectric properties are normally enhanced with an increase in BST filler content. However, the high BST content may generate more defects in the composites, and thus their dielectric properties worsened with a high ceramic particle loading. The dielectric properties of the BST/polymer can be improved significantly by introducing BST fillers with a large specific surface area, such as nanofibers and nanotubes. The dielectric properties are sensitive to the concentration of one-dimensional nanosized particles. The outstanding dielectric properties of these BST/polymer nanocomposites can be obtained at a low filler concentration because of the existence of a percolation structure. Three-phase composites that consist of conducting fillers, BST ceramic particles and polymer may be good candidates to acquire good dielectric properties because of microcapacitor formation in the inner structure.
4) Many theoretical models have been presented to describe the properties of polymer-matrix composites. Besides the modified Maxwell-Garnett and Yamada models, few models consider the shape factor. The other models assume a spherical particle shape. The dielectric constant of the BST/polymer composites can be predicted by using the Yamada model and by adjusting the shape factor of the ceramic filler.
5) The investigation of composite dielectric tunability focuses mainly on the 0–3-type BST/PVDF-based composites. The BST filler concentration and shape affect the dielectric tunability. The dielectric tunable theoretical model for the 0–3-type composites was proposed after introducing the Yamada model into the modified Devonshire phenomenological theory. Five influencing factors, namely, n_c, β_r/β_c, a, δ_c and n affect the composite dielectric tunability significantly. The proposed theoretical model provides essential information on the dielectric tunability instead of applying a trial-and-error experimental strategy on dielectric functional ceramic/polymer composites, which is an important improvement for the future development of tunable microwave dielectric device applications.

Based on the above discussion, future perspectives are as follows:

1) The ceramic/polymer matrix interface has a significant impact on the dielectric properties of the functional dielectric composites. Extensive attention should be given to the BST/polymer composite interface.
2) Advantages, such as a high dielectric breakdown strength, rapid charge/discharge, simple processing and cost-effectiveness make BST/polymer composites suitable for use as capacitors compared with other electrical energy storage devices. However, their

energy densities are lower than that of electrochemical devices, such as batteries and double-layer supercapacitors. So, it is worth developing high energy storage density BST/polymer composites. High breakdown dielectric strength is a key issue.

3) Fabrication of BST/polymer composites with different connectivities, such as 1–2, 1–3 and 2–3, can be interesting for different structures. The structural design of BST/polymer composites and the preparation of a sandwich, gradient and other multilayer structure is noteworthy.
4) The dielectric tunability cannot meet practical applications and needs to be improved further. It is also necessary to investigate the dielectric tunability of ceramic/polymer composites, especially with the different BST filler sizes and shapes.
5) Many investigations have been undertaken in the normal frequency range. The dielectric properties and dielectric tunability of the BST/polymer at sub-THz or even at THz conditions and their application at a high frequency should be addressed.
6) It is worth drawing attention to the application of BST/polymer composites in smart flexible wearable electronic devices, aerospace and biomedical fields.

Declaration of Competing Interest

The authors declare that they have no known competing financial interests or personal relationships that could have appeared to influence the work reported in this paper.

Acknowledgements

This work was supported by the China-Poland International Collaboration Fund of National Natural Science Foundation of China (No. 51961135301), National Natural Science Foundation of China (No. 51702259 and 52072301), the Fundamental Research Fund for the Central Universities (No. 3102019GHJD001, 3102019MS0406), the International Cooperation Foundation of Shaanxi Province China (No. 2017KW-025, 2020KW-032), the “111” Project (No. B20028), and the Polish National Science Centre (No 2018/30/Q/ST8/00205).

References

[1] Ezhilvalavan S, Tseng TY. Progress in the developments of (Ba, Sr)Ti$_O$3 (BST) thin films for Gigabit era DRAMS. Mater Chem Phys 2000;65:227–48.
[2] Hou Y, Tian DX, Chu BJ, et al. Flexoelectric response of (1–x)BaTiO$_3$-xSrTiO$_3$ ceramics. Ceram Int 2020;46:12928–32.
[3] Kim D, Choi Y, Allen M, et al. A wide-band reflection-type phase shifter at S-band using BST coated substrate. IEEE Trans Microw Theory Tech 2002;50:2903–9.
[4] Yu SH, Li LX, Zheng HR, et al. Ba$_{0.6}$Sr$_{0.4}$TiO$_3$-Bi$_{1.5}$Mg$_{1.0}$Nb$_{1.5}$O$_7$ composite thin film capacitors with enhanced tunable performance for tunable device applications. Mater Lett 2015;161:517–9.
[5] Altynnikov AG, Gagarin AG, Tumarkin AV, et al. Characterization of the properties of Barium-Strontium Titanate films and controlled elements based on them in the frequency range of 1–60 GHz. Tech Phys Lett 2019;45:540–3.
[6] Huang W, Chen Y, Li X, et al. Ultrahigh recoverable energy storage density and efficiency in barium strontium titanate-based lead-free relaxor ferroelectric ceramics. Appl Phys Lett 2018;113:203902-1–5.
[7] Ma R, Cui B, Wang YJ, et al. The energy storage properties of fine-grained Ba$_{0.8}$Sr$_{0.2}$Zr$_{0.1}$Ti$_{0.9}$O$_3$ ceramics enhanced by MgO and ZnO-B$_2$O$_3$-SiO$_2$ coatings. Mater Res Bull 2019;111:311–9.
[8] Yu SH, Zhang CM, Wu MY, et al. Ultra-high energy density thin-film capacitors with high power density using BaSn$_{0.15}$Ti$_{0.85}$O$_3$/Ba$_{0.6}$Sr$_{0.4}$TiO$_3$ heterostructure thin films. J Power Sources 2019;412:648–54.
[9] Lu X, Tong Y, Talebinezhad H, et al. Dielectric and energy-storage performance of Ba$_{0.5}$Sr$_{0.5}$TiO$_3$-SiO$_2$ ceramic-glass composites. J Alloy Compd 2018;745:127–34.
[10] Selmi A, Mascot M, Jomni F, et al. Investigation of interfacial dead layers parameters in Au/Ba$_{0.85}$Sr$_{0.15}$TiO$_3$/Pt capacitor devices. J Alloy Compd 2020;826:154048.
[11] Solodukha AM, Grigoryan GS. Negative capacitance effect in the low-frequency impedance of barium strontium titanate semiconductor ceramics. Inorg Mater 2019;55:401–4.
[12] Patil RP, Gaikwad SS, Karanjekar AN, et al. Optimization of strontium- doping concentration in BaTiO$_3$ nanostructures for room temperature NH$_3$ and NO$_2$ gas sensing. Mater Today Chem 2020;16:100240.
[13] Zhu J, He J, Lu JJ, et al. Resistive switching characteristics of resistive random access memory based on a Ba$_x$Sr$_{1-x}$TiO$_3$ thin film grown by a hydrothermal method. IEEE Electr Device L 2019;40:1411–4.
[14] Immergut EH, Brandrup J, McDowell W. Polymer handbook. New York: Wiley; 2008.
[15] Dang ZM, Yuan JK, Zhai JW, et al. Fundamentals, processes and applications of high-permittivity polymer-matrix composites. Prog Mater Sci 2012;57.
[16] Lu X, Zhang L, Tong Y, et al. BST-P(VDF-CTFE) nanocomposite films with high dielectric constant, low dielectric loss, and high energy-storage density. Compos Part B 2019;168:34–43.
[17] Xu PP, Luo SB, Yu JY, et al. Simultaneously enhanced permittivity and electric breakdown strength of polyacrylonitrile composites by introducing ultralow content BaSrTiO$_3$ nanofibers. Adv Eng Mater 2019;1900817.
[18] Lu X, Zou XW, Shen JL, et al. High energy density with ultrahigh discharging efficiency obtained in ceramic-polymer nanocomposites using a non-ferroelectric polar polymer as matrix. Nano Energy 2020;70:104551.
[19] Newnham RE. Composite electroceramics. Ferroelectrics 1986;68:1–32.
[20] Newnham RE, Skinner DP, Cross LE, et al. Connectivity and piezoelectric-pyroelectric composites. Mater Res Bull 1978;13:525–36.
[21] Zhang L, Qiao Q, Yue ZX, et al. A new HDPE/BST polymer-ceramic composite for wireless temperature sensing. Ceram Int 2015;41:S471–5.
[22] Liu SH, Zhai JW. A small loading of surface-modified Ba$_{0.6}$Sr0.$_4$TiO$_3$ nanofiber-filled nanocomposites with enhanced dielectric constant and energy density. RSC Adv 2014;4:40973–9.
[23] Pan MJ, Gorzkowski E, McAllister K, et al. Dielectric properties of polyhedral oligomeric silsesquioxane (POSS)-based nanocomposites at 77k. IOP Conf Ser: Mater Sci Eng 2011;18:082006.
[24] Pan ZB, Yao LM, Zhai JW, et al. Fast discharge and high energy density of nanocomposite capacitors using Ba$_{0.6}$Sr$_{0.4}$TiO$_3$ nanofibers. Ceram Int 2016;42:14667–74.
[25] Liu SH, Xiao S, Xiu SM, et al. Poly(vinylidene fluoride) nanocomposite capacitors with a significantly enhanced dielectric constant and energy density by filling with surface fluorinated Ba$_{0.6}$Sr$_{0.4}$TiO$_3$ nanofibers. RSC Adv 2015;5:40692–9.

[26] Liu SH, Xue SX, Zhang WQ, et al. The influence of crystalline transformation of $Ba_{0.6}Sr_{0.4}TiO_3$ nanofibers/poly (vinylidene fluoride) composites on the energy storage properties by quenched technique. Ceram Int 2015;41:S430–4.
[27] Liu SH, Xue SX, Zhang WQ, et al. Significantly enhanced dielectric property in PVDF nanocomposites flexible films through a small loading of surface-hydroxylated $Ba_{0.6}Sr_{0.4}TiO_3$ nanotubes. J Mater Chem A 2014;2:18040–6.
[28] Liu FH, Li Q, Cui J, et al. High-energy-density dielectric polymer nanocomposites with trilayered architecture. Adv Funct Mater 2017;27:1606292.
[29] Tang HX, Sodano HA. Ultra high energy density nanocomposites capacitors with fast discharge using $Ba_{0.2}Sr_{0.8}TiO_3$ nanowires. Nano Lett 2013;13:1373–9.
[30] Bian YL, Zhai JW. Low dielectric loss $Ba_{0.6}Sr_{0.4}TiO_3/MgTiO_3$ composite thin films prepared by a sol-gel process. J Phys Chem Solids 2014;75:759–64.
[31] Wu JM, Wang XH, Fan YN, et al. Microstructures and dielectric properties of $Ba_{0.6}Sr_{0.4}TiO_3$-MgO ceramics prepared by non-aqueous gelcasting and dry pressing. Mater Res Bull 2011;46:2217–21.
[32] Wang HZ, Dong YX, Wang ZM, et al. High tunable dielectric properties of Zn and Mg alternately doped $Ba_{0.6}Sr_{0.4}TiO_3$ film varactors. J Alloy Compd 2018;745:651–8.
[33] Kim KT, Kim C, Senior DE, et al. Microwave characteristics of sol-gel based Ag-doped $(Ba_{0.6}Sr_{0.4})TiO_3$ thin films. Thin Solid Films 2014;565:172–8.
[34] Wang T, Gao F, Hu GX, et al. Synthesis $Ba_{0.6}Sr_{0.4}TiO_3$-$ZnNb_2O_6$ composite ceramics using chemical coating method. J Alloy Compd 2010;504:362–6.
[35] Singh J, Krupanidhi SB. Multilayer $Bi_{1.5}Zn_{1.0}Nb_{1.5}O_7/Ba_{0.6}Sr_{0.4}TiO_3/ Bi_{1.5}Zn_{1.0}Nb_{1.5}O_7$ thin films for tunable microwave applications. Appl Surf Sci 2011;257:2214–7.
[36] Liao JX, Xu ZQ, Wei XB, et al. Influence of preheating on crystallization and growing behavior of Ce and Mn doped $Ba_{0.6}Sr_{0.4}TiO_3$ film by sol-gel method. Surf Coat Tech 2012;206:4518–24.
[37] Jiang HT, Shen B, Zhai JW, et al. Influence of low concentration $MgCo_2(VO_4)_2$ addtion on microwave dielectric properties of $Ba_{0.6}Sr_{0.4}TiO_3$ ceramics. Ceram Int 2012;38S:S183–6.
[38] Liao WF, Liang RH, Wang GS, et al. Dielectric and tunable properties of bulk columnar $Ba_{0.6}Sr_{0.4}TiO_3$/MgO composites. Ceram Int 2013;39:891–5.
[39] Lu X, Tong Y, Zhang L, et al. High dielectric tunability in composites prepared using SiO_2 coated $Ba_{0.5}Sr_{0.5}TiO_3$ nanoparticles. Ceram Int 2018;44:9875–9.
[40] Vilarinho PM, Fu Z, Kingon AI, et al. Low loss tunable dielectric $BaNd_2Ti_5O_{14}$- $(Ba_{0.5}Sr_{0.5})TiO_3$ composite thick films. Scripta Mater 2018;155:160–3.
[41] Sherman VO, Tagantsev AK, Setter N, et al. Model of a low-permittivity and high-tunability ferroelectric based composite. Appl Phys Lett 2007;90:162901.
[42] Zhou K, Boggs SA, Ramprasad R, et al. Dielectric response and tunability of a dielectric-paraelectric composite. Appl Phys Lett 2008;93:102908.
[43] Bhalla AS, Guo R, Roy R, et al. The perovskite structure-a review of its role in ceramic science and technology. Mat Res Innovat 2000;4:3–26.
[44] Reveŕon H, Elissalde C, Aymonier C, et al. Continuous supercritical synthesis and dielectric behaviour of the whole BST solid solution. Nanotechnology 2006;17:3527–32.
[45] Zhou LQ, Vilarinho PM, Baptist JL, et al. Dependence of the structural and dielectric properties of $Ba_{1-x}Sr_xTiO_3$ ceramic solid solutions on raw material processing. J Eur Ceram Soc 1999;19:2015–20.
[46] Jain A, Panwar AK, Jha AK, et al. Structural, dielectric and ferroelectric studies of $Ba_{1-x}Sr_xTiO_3$ ceramics prepared by mechanochemical activation technique. J Mater Sci: Mater Electron 2016;27:9911–9.
[47] Kongtaweelert S, Sinclair DC, Panichphant S, et al. Phase and morphology investigation of $Ba_xSr_{1-x}TiO_3$ (x = 0.6, 0.7 and 0.8) powders. Curr Appl Phys 2006;6:474–7.
[48] Jona F, Shirane G. Ferroelectric Crystals. Pergamon Press; 1962.
[49] Rios S, Ruediger A, Jiang AQ, et al. Orthorhombic strontium titanate in $BaTiO_3$-$SrTiO_3$ superlattices. J Phys: Condens Matter 2003;15:L305–9.
[50] Kim SW, Choi HI, Lee MH, et al. Electrical properties and phase of $BaTiO_3$-$SrTiO_3$ solid solution. Ceram Int 2013;39:S487–90.
[51] Alexandru HV, Berbecaru C, Ioachim A, et al. BST solid solutions, temperature evolution of the ferroelectric transitions. Appl Surf Sci 2006;253:354–7.
[52] Yamada T, Takuwa I, Kamo T, et al. Influence of Ba/Sr ratio in compressively-strained (Ba, Sr)Ti_O3(001) films on the ferroelectric phase transition. J Ceram Soc Jpn 2013;121:690–2.
[53] Śmiga W, Sitko D, Piekarczyk W, et al. Composition-related structural, thermal and mechanical properties of $Ba_{1-x}Sr_xTiO_3$ ceramics ($0 \leq x \leq 0.4$). Phase. Transit 2015;88:716–25.
[54] Fu CL, Yang CR, Chen HW, et al. Microstructure and dielectric properties of $Ba_xSr_{1-x}TiO_3$ ceramics. Mater Sci Eng B 2005;119:185–8.
[55] Kim TS, Oh MH, Kim CH, et al. Influences of indium tin oxide layer on the properties of RF magnetron-sputtered $(BaSr)TiO_3$ thin films on indium Tin oxide-coated glass substrate. Jpn J Appl Phys 1993;32:2837–41.
[56] Granqvist CG, Hunderi O, et al. Optical properties of nltrafine gold particles. Phys Rev B 16:3513–34.
[57] Kondo SY, Yamada T, Tagantsec AK, et al. Large impact of strain on the electro-optic effect in (Ba, Sr)TiO_3 thin films: experiment and theoretical comparison. Appl Phys Lett 2019;115:092901.
[58] Zhu SY, Li J, Xing JJ, et al. Cathodoluminescence characteristics of a novel core-rim structure in Bidoped (Sr, Ba)Ti_O3 ceramics. Ceram Int 2019;45:8027–31.
[59] Edmondson BI, Kwon S, Ortmann JE, et al. Composition and annealing effects on the linear electro-optic response of solution-deposited barium strontium titanate. J Am Ceram Soc 2020;103:5700–5.
[60] Rashad MM, Turky AO, Kandil AT, et al. Optical and electrical properties of $Ba_{1-x}Sr_xTiO_3$ nanopowders at different Sr^{2+} ion content. J Mater Sci: Mater Electron 2013;24:3284–91.
[61] Zhang XF, Xu Q, Huang YH, et al. Dielectric properties of low-temperature sintered $Ba_{0.6}Sr_{0.4}TiO_3$ derived from citrate method. Mater Sci Eng 2011;20:012016.
[62] Zhang MH, Wang H, Yang HB, et al. Dielectric properties of low-temperature sintered $Ba_{0.6}Sr_{0.4}TiO_3$ thick films prepared by reactive sintering method. J Alloy Compd 2011;509:L344–7.
[63] Ćirković J, Vojisavljević K, Nikolić N, et al. Dielectric and ferroelectric properties of BST ceramics obtained by a hydrothermally assisted complex polymerization method. Ceram Int 2015;41:11306–13.
[64] Wu T, Pu YP, Gao P, et al. Influence of Sr/Ba ratio on the energy storage propertiesand dielectric relaxation behaviors of strontium barium titanate ceramics. J Mater Sci: Mater Electron 2013;24:4105–12.
[65] Singh AK, Barik SK, Choudhary RNP, et al. Ac conductivity and relaxation mechanism in $Ba_{0.9}Sr_{0.1}TiO_3$. J Alloy Compd 2009;479:39–42.
[66] Ostapchuk T, Petzelt J, Hlinka J, et al. Broad-band dielectric spectroscopy and ferroelectric soft-mode response in the $Ba_{0.6}Sr_{0.4}TiO_3$ solid solution. J Phys: Condens Matter 2009;21. 474215-474214.
[67] Jonscher AK. Dielectric relaxation in solids. London: Chelsea Dielectric Press; 1983.
[68] Liou JW, Chiou BS. Effect of direct-current biasing on the dielectric properties of barium strontium titanate. J Am Ceram Soc 1997;80:3093–9.
[69] Qiu J, Liu GZ, Wolfman J, et al. Structure and dielectric characteristics of continuous composition spread $Ba_{1-x}Sr_xTiO_3$ thin films by combinatorial pulsed laser deposition. Ceram Int 2016;42:6408–12.
[70] He YY, Xu YB, Liu T, et al. Microstructure and dielectric tunable properties of $Ba_{0.6}Sr_{0.4}TiO_3$-Mg_2SiO_4-MgO composite. IEEE Trans Ultrason Ferroelectr Freq Control 2010;57:1505–12.
[71] Cui JD, Dong GX, Yang ZM, et al. Low dielectric loss and enhanced tunable properties of Mn-doped BST/MgO composites. J Alloy Compd 2010;490:353–7.
[72] Chung UC, Elissalde C, Maglione M, et al. Low-losses, highly tunable $Ba_{0.6}Sr_{0.4}TiO_3$/MgO composite. Appl Phys Lett 2008;92:042902.
[73] Zhang JJ, Zhai JW, Chou XJ, et al. Relaxor behavior and dielectric properties of $(1–x)Ba_{0.6}Sr_{0.4}TiO_3$-$xMg_{0.7}Zn_{0.3}TiO_3$ composite ceramics for tunable microwave applications. Solid State Commun 2008;147:392–6.
[74] Liu P, Ma JL, Meng L, et al. Preparation and dielectric properties of BST-Mg_2TiO_4 composite ceramics. Mater Chem Phys 2009;114:624–8.
[75] Hu GX, Gao F, Liu LL, et al. Microstructure and dielectric properties of highly tunable $Ba_{0.6}Sr_{0.4}TiO_3$/MgO/Al_2O_3/ZnO composite. J Alloy Compd 2012;518:44–50.
[76] Zhu XP, Shi P, Lou XJ, et al. Remarkably enhanced energy storage properties of lead-free $Ba_{0.53}Sr_{0.47}TiO_3$ thin films capacitors by optimizing bottom electrode thickness. J Eur Ceram Soc 2020;40:5475–82.
[77] Dong GZ, Fan HQ, Jia YX, et al. Dielectric temperature stability and energy storage performance of B site Sn^{4+} doped BNKBST ceramics. J Mater Sci: Mater Electron 2020;31:13620–7.

[78] Tunkasiri T, Rujijanagul G, et al. Dielectric strength of fine grained barium titanate ceramics. J Mater Sci Lett 1996;15:1767–9.
[79] Young A, Hilmas G, Zhang SC, et al. Effect of liquid-phase sintering on the breakdown strength of barium titanate. J Am Ceram Soc 2007;90:1504–10.
[80] Wu ZH, Liu HX, Cao MH, et al. Effect of BaO-Al_2O_3-B_2O_3-SiO_2 glass additive on densification and dielectric properties of $Ba_{0.3}Sr_{0.7}TiO_3$ ceramics. J Ceram Soc Ton 2008;116:345–9.
[81] Liebault J, Vallayer J, Goeuriot D, et al. How the trapping of charges can explain the dielectric breakdown performance of alumina ceramics. J Eur Ceram Soc 2001;21:389–97.
[82] Hu GX, Gao F, Liu LL, et al. Microstructure and dielectric properties of $Ba_{0.6}Sr_{0.4}TiO_3$-$MgAl_2O_4$ composite ceramics. Ceram Int 2011;37:1321–6.
[83] Li DX, Shen ZY, Li ZP, et al. *P-E* hysteresis loop going slim in $Ba_{0.3}Sr_{0.7}TiO_3$-modified $Bi_{0.5}Na_{0.5}TiO_3$ ceramics for energy storage applications. J Adv Ceram 2020;9:183–92.
[84] Huang YH, Liu B, Li J, et al. Improved energy storage performance of $Ba_{0.4}Sr_{0.6}TiO_3$ nanocrystalline ceramics prepared by using oxalate co-precipitation and spark plasma sintering. Mater Res Bull 2019;113:141–5.
[85] Huang JJ, Zhang Y, Ma T, et al. Correlation between dielectric breakdown strength and interface polarization in barium strontium titanate glass ceramics. Appl Phys Lett 2010;96:042902.
[86] Liu BB, Wang XH, Zhang RX, et al. Energy storage properties of ultra-fine-grained $Ba_{0.4}Sr_{0.6}TiO_3$-based ceramics sintered at low temperature. J Alloy Compd 2017;691:619–23.
[87] Song Z, Liu HX, Zhang SJ, et al. Effect of grain size on the energy storage properties of $(Ba_{0.4}Sr_{0.6})TiO_3$ paraelectric ceramics. J Eur Ceram Soc 2014;34:1209–17.
[88] Song Z, Liu HX, Hao H, et al. The Effect of grain boundary on the energy storage properties of $(Ba_{0.4}Sr_{0.6})TiO_3$ paraelectric ceramics by varying grain sizes. IEEE T Ultrason Ferr 2015;62:609–16.
[89] Zhang Y, Huang JJ, Ma T, et al. Sintering Temperature Dependence of energy-storage properties in (Ba, Sr)Ti_O3 glass-ceramics. J Am Ceram Soc 2011;94:1805–10.
[90] Wang XR, Zhang Y, Ma T, et al. Influence of AlF_3 Concentration on microstructures and energy storage properties of barium strontium titanate glass ceramics. Int J Appl Ceram Technol 2013;10:301–6.
[91] Zhang WQ, Wang JW, Xue SX, et al. Effect of La_2O_3 additive on the dielectric properties of barium strontium titanate glass-ceramics. J Mater Sci: Mater Electron 2014;25:4145–9.
[92] Xiu SM, Xiao S, Zhang WQ, et al. Effect of rare-earth additions on the structure and dielectric energy storage properties of $Ba_xSr_{1-x}TiO_3$-based barium boronaluminosilicate glass-ceramics. J Alloy Compd 2016;670:217–21.
[93] Wu YJ, Huang YH, Wang N, et al. Effects of phase constitution and microstructure on energy storage properties of barium strontium titanate ceramics. J Eur Ceram Soc 2017;37:2099–104.
[94] Wu T, Pu YP, Chen K, et al. Dielectric relaxation behavior and energy storage properties in $Ba0_{.4}Sr_{0.6}Zr_{0.15}Ti_{0.85}O_3$ ceramics with glass additives. Ceram Int 2013;39:6787–93.
[95] He DL, Wang Y, Zhang LY, et al. Poly(vinylidene fluoride)-Based composites modulated via multiscale two-dimensional fillers for high dielectric performances. Compos Sci Technol 2018;159:162–70.
[96] Liu SH, Xiu SM, Shen B, et al. Dielectric properties and energy storage densities of poly(vinylidenefluoride) nanocomposite with surface hydroxylated cube shaped $Ba_{0.6}Sr_{0.4}TiO_3$ nanoparticles. Polymers 2016;8:45–51.
[97] Hu XP, Zhou Y, Liu J, et al. Improved flexoelectricity in PVDF/barium strontium titanate (BST) nanocomposites. J Appl Phys 2018;123:154101-1–7.
[98] Adireddy S, Puli VS, Sklare SC, et al. PVDF-$BaSrTiO_3$ nanocomposites for flexible electrical energy storage devices. Emerg Mater Res 2014;3:265–70.
[99] Xie YC, Jiang WR, Fu T, et al. Achieving high energy density and low loss in PVDF/BST nanodielectrics with enhanced structural homogeneity. Acs Appl Mater Inter 2018;10:29038–47.
[100] Li KC, Wang H, Xiang F, et al. Surface functionalized $Ba_{0.6}Sr0_{.4}TiO_3$/pol(vinylidene fluoride) nanocomposites with significantly enhanced dielectric properties. Appl Phys Lett 2009;95:202904.
[101] Liou JW, Chiou BS. Dielectric tunability of barium strontium titanate/silicone-rubber composite. J Phys Condens Matter 1998;10:2773–86.
[102] Hamciuc C, Hamciuc E, Asandulesa M, et al. Study on dielectric behavior and harvesting properties of new $Ba_{0.5}Sr_{0.4}Ca_{0.1}TiO_3$/poly(ether imide) composite films. Mater Res Bull 2018;102:70–8.
[103] Zha JW, Liu Q, Dang ZM, et al. Tailored wide-frequency dielectric behavior of polyimide composite films with $Ba_xSr_{1-x}TiO_3$ perovskites ceramic particles. IEEE T Dielect El In 2015;23:113–9.
[104] Beier CW, Sanders JM, Brutchey RL, et al. Improved breakdown strength and energy density in thin-film polyimide nanocomposites with small barium strontium titanate nanocrystal fillers. J Phys Chem C 2013;117:6958–65.
[105] Olszowy M, Pawlaczyk C, Markiewicz E, et al. Dielectric and pyroelectric properties of $BaTiO_3$-PVC composites. Phys Stat Sol (a) 2005;202:1848–53.
[106] Chiang CK, Popielarz R. Polymer composites with high dielectric constant. Ferroelectrics 2002;275:1–9.
[107] Badheka P, Magadala V, Devaraju NG, et al. Effect of dehydroxylation of hydrothermal barium titanate on dielectric properties in polystyrene composite. J Appl Polym Sci 2006;99:2815–21.
[108] Zhang KN, Gao F, Xu J, et al. Fabrication and dielectric properties of $Ba_{0.6}Sr_{0.4}TiO_3$/acrylonitrile–butadiene–styrene resin composites. J Mater Sci: Mater Electron 2017;28:8960–8.
[109] Abbas SM, Chandra M, Verma A, et al. Complex permittivity and microwave absorption properties of a composite dielectric absorber. Compos Part A 2006;37:2148–54.
[110] Liang RH, Liao WF, Wu JW, et al. Extremely high tunability of low dielectric constant 1–3 type (Ba, Sr)Ti_O3/resin epoxy. J Am Ceram Soc 2012;95:2120–3.
[111] Hu T, Juuti J, Jantunen H. Dielectric properties of BST/polymer composite. J Eur Ceram Soc 2007;27:3997–4001.
[112] Haghzadeh M, Akyurtlu A. All-printed, flexible, reconfigurable frequency selective surfaces. J Appl Phys 2016;120:184901.
[113] Palukuru KV, Sanoda K. Inkjet-printed RF structures on BST-polymer composites: an application of a monopole antenna for 2.4 GHz wireless local area network operation. Int J Appl Ceram Technol 2011;8:940–6.
[114] Wang H, Xiang F, Li KC. Ceramic-Polymer $Ba_{0.6}Sr_{0.4}TiO_3$/Poly(Methyl Methacrylate) composites with different type composite structures for electronic technology. Int J Appl Ceram Tec 2010;7:435–43.
[115] Xiang F, Wang H, Li KC. Dielectric tunability of $Ba_{0.6}Sr_{0.4}TiO_3$/poly(methyl methocrylate) composites in 1-3-type structure. Appl Phys Lett 2007;91:192907.
[116] Wongwilawan S, Ishida H. Dielectric properties at microwave frequency in barium strontium titanate/poly(benzoxazine/urethane) composite films. Ferroelectrics 2013;452:84–90.
[117] Zhang L, Zhao J, Huang EQ, et al. Preparation and dielectric properties of $(Ba_{0.5}Sr_{0.4}Ca_{0.1})TiO_3$/Polystyrene composites. J Appl Polym Sci 2015;132:41398.
[118] Shang JL, Hu GJ, Zhang T, et al. Effect of polyethylene glycol content on the optical properties of $Ba_{0.9}Sr_{0.1}TiO_3$ multilayers. J Am Ceram Soc 2009;92:539–41.
[119] Jang Y, Lee WH, Park YD, et al. High field-effect mobility pentacene thin-film transistors with nanoparticle polymer composite/polymer bilayer insulators. Appl Phys Lett 2009;94:183301.
[120] Timo R, Raheleh A, Joachim RB, et al. Polymerizable ceramic ink system for thin inkjet-printed dielectric layers. ACS Appl Mater Inter 2020;12:2974–82.
[121] Hu GX, Gao F, Kong J, et al. Preparation and dielectric properties of poly(vinylidene fluoride)/$Ba_{0.6}Sr_{0.4}TiO_3$ composites. J Alloy Compd 2015;619:686–92.
[122] Zhang QQ, Gao F, Zhang CC, et al. Enhanced dielectric tunability of $Ba_{0.6}Sr_{0.4}TiO_3$/Poly(vinylidene fluoride) composites via interface modification by silane coupling agent. Compos Sci Technol 2016;129:93–100.
[123] Wang L, Gao F, Zhang KN, et al. Effect of hot pressing temperature on dielectric and energy storage properties of $Ba_{0.6}Sr_{0.4}TiO_3$/poly(vinylidene fluoride) composites. IEEE T Dielect El In 2017;24:704–11.
[124] Zhang L, Wu PX, Li YT, et al. Preparation process and dielectric properties of $Ba_{0.5}Sr_{0.5}TiO_3$-P(VDF-CTFE) nanocomposites. Compos B 2014;56:284–9.
[125] Liu FH, Li Q, Li ZY, et al. Ternary PVDF-based terpolymer nanocomposites with enhanced energy density and high power density. Compos Part A-Appl S 2018;109:597–603.

[126] Rahman MA, Chung GS. Synthesis of PVDF-graphene nanocomposites and their properties. J Alloy Compd 2013;581:724–30.
[127] Wu PX, Zhang L, Shan XB, et al. Microstructure and dielectric response of $BaSrTiO_3$/P(VDF-CTFE) nanocomposites. Mater Lett 2015;159:72–5.
[128] Gadinski MR, Li Q, Zhang GZ, et al. Understanding of relaxor ferroelectric behavior of poly(vinylidene fluoride-trifluoroethylene-chlorotrifluoroethylene) terpolymers. Macromolecules 2015;48:2731–9.
[129] Qian K, Lv XG, Chen S, et al. Interfacial engineering tailoring the dielectric behavior and energy density of $BaTiO_3$/P(VDF-TrFE-CTFE) nanocomposites by regulating a liquid-crystalline polymer modifier structure. Dalton Trans 2018;47:12759–68.
[130] Capsal JF, Galineau J, Le MQ, et al. Enhanced electrostriction based on plasticized relaxor ferroelectric P(VDF-TrFE-CFE/CTFE) blends. J Polym Sci Part Pol Phys 2015;53:1368–79.
[131] Lu SG, Neese B, Chu BJ, et al. Large electric tunability in poly(vinylidene fluoride-trifluoroethylene) based polymers. Appl Phys Lett 2008;93:042905.
[132] Meng N, Zhu XJ, Mao R, et al. Nanoscale interfacial electroactivity in PVDF/PVDF-TrFE blended films with enhanced dielectric and ferroelectric properties. J Mater Chem C 2017;5:3296–305.
[133] Guo YT, Meng N, Zhang YM, et al. Characterization and performance of plate-like $Ba_{0.6}Sr_{0.4}TiO_3$/Poly(vinylidene fluoride – trifluoroethylene - chlorotrifluoroethylene) composites with high permittivity and low loss. Polymer 2020;203:122777.
[134] Sonoda K, Hu T, Juuti J, et al. Fabrication and properties of composites from BST and polypropylene-*graft*-poly(styrene-*stat*-divinylbenzene). J Eur Ceram Soc 2010;30:381–4.
[135] Sonoda K, Juuti J, Moriya Y, et al. Modification of the dielectric properties of 0–3 ceramic-polymer composites by introducing surface active agents onto the ceramic filler surface. Compos Stru 2010;92:1052–8.
[136] Xia WM, Xu Z, Wen F, et al. Electrical energy density and dielectric properties of poly(vinylidene fluoride-chlorotrifluoroethylene)/$BaSrTiO_3$ nanocomposites. Ceram Int 2012;38:1071–5.
[137] Wu PX, Zhang L, Shan XB, et al. Microstructure and dielectricre sponse of $BaSrTiO_3$/P(VDF-CTFE) nanocomposites. Mater Lett 2015;159:72–5.
[138] Arbatti M, Shan XB, Cheng ZY, et al. Ceramic–polymer composites with high dielectric constant. Adv Mater 2007;19:1369–72.
[139] Bai Y, Cheng ZY, Bharti V, et al. High-dielectric-constant ceramic-powder polymer composites. Appl Phys Lett 2000;76:3804–6.
[140] Dang ZM, Zhang YH, Tjong SC, et al. Dependence of dielectric behavior on the physical property of fillers in the polymer-matrix composites. Synthetic Met 2004;146:79–84.
[141] Li YJ, Xu M, Feng JQ, et al. Dielectric behavior of a metal-polymer composite with low percolation threshold. Appl Phys Lett 2006;89:072902.
[142] Lu J, Moon KS, Xu J, et al. Synthesis and dielectric properties of novel high-k polymer composites containing in-situ formed silver nanoparticles for embedded capacitor applications. J Mater Chem 2006;16:1543–8.
[143] Dang ZM, Peng B, Xie D, et al. High dielectric permittivity silver/polyimide composite films with excellent thermal stability. Appl Phys Lett 2008;92:112910.
[144] Todd MG, Shi FG, et al. Characterizing the interphase dielectric constant of polymer composite materials: effect of chemical coupling agents. J Appl phys 2003; 94:4551–7.
[145] Kuriger RJ, Alam MK, Anderson DP, et al. Processing and characterization of aligned vapor grown carbon fiber reinforced polypropylene. Compos A 2002;33: 53–62.
[146] Devaraju NG, Lee BI, et al. Dielectric behavior of three phase polyimide percolative nanocomposites. J Appl Polym Sci 2006;99:3018–22.
[147] Shen Y, Yue Z, Li M, et al. Enhanced initial permeability and dielectric constant in a double-percolating $Ni_{0.3}Zn_{0.7}Fe_{1.95}O_4$-Ni-polymer composite. Adv Funct Mater 2005;15:1100–3.
[148] Patil R, Ashwin A, Radhakrishnan S, et al. Novel polyaniline/PVDF/$BaTiO_3$ hybrid composites with high piezo-sensitivity. Sensors Actuat A: Phys 2007;138: 361–5.
[149] Reddy VA, Dabra N, Hundal JS, et al. Tunability in threecomponent $Ba_{0.5}Sr_{0.5}TiO_3$-graphite-poly(vinylidene fluoride) nano-composite films. Sci Adv Mater 2014;6:235–42.
[150] Hu GH, Hoppe S, Feng L, et al. Reactive compounding: mixing and compounding of polymers: theory and practice. 2nd ed. Munich: Hanser publisher; 2009. p. 1019–80.
[151] Hu GH. Reactive polymer processing: fundamentals of REX. Encyclopedia of materials: science and technology. Amsterdam 2001:8049–57.
[152] Tagantsev AK, Sherman VO, Astafiev KF, et al. Ferroelectric materials for microwave tunable applications. J Electroceram 2003;11:5–66.
[153] Goncharenko AV, Lozovski VZ, Venger EF, et al. Lichtenecker's equation: applicability and limitations. Opt Commun 2000;174:19–32.
[154] Zakri T, Laurent JP, Vauclin M, et al. Theoretical evidence for Lichtenecker's mixture formulae' based on the effective medium theory. J Phys D: Appl Phys 1998;31:1589–94.
[155] Thomas P, Varughese KT, Dwarakanath K, et al. Dielectric properties of poly(vinylidene fluoride)/$CaCu_3Ti_4O_{12}$ composites. Compos Sci Technol 2010;70: 539–45.
[156] Wagner KW. The after effect in the dielectrics. Arch Electrotech 1914;2:378–80.
[157] Smith GB. Dielectric constant for mixed media. J Phys D: Appl Phys 1977;10:39–43.
[158] Tuncer E, Gubanske SM, Nettelblad B, et al. Dielectric relaxation in dielectric mixtures: application of the finite element method and its comparison with mixture formulas. Appl Phys 2001;89:8092–100.
[159] Shalev VM. Electromagnetic properties of small-particle composites. Phys Rep 1996;272:61–137.
[160] Vanbeek LKH. Dielectric behaviour of heterogeneous systems. Prog Dielect 1967;7:69–114.
[161] Jayasundere N, Smith BV. Dielectric constant for binary piezoelectric 0–3 composites. J Appl Phys 1993;73:2462–6.
[162] Dinulović M, Rašuo B. Dielectric modeling of multiphase composites. Compos Struct 2011;93:3209–15.
[163] Yamada T, Ueda T, Kitayama T. Piezoelectricity of a high-content lead zirconate titanate/polymer composite. J Appl Phys 1982;53:4328.
[164] Sherman VO, Tagantsev AK, Setter N, et al. Ferroelectric-dielectric tunable composites. J Appl Phys 2006;99. 074104~1–074107~10.
[165] Dang ZM, Lin YH, Nan CW, et al. Novel ferroelectric polymer composites with high dielectric constants. Adv Mater 2003;15:1525–9.
[166] Qi L, Bee BI, Chen S, et al. High-dielectric-constant silver-eoxy composites as embedded dielectrics. Adv Mater 2005;17:1777–82.
[167] Jiang MJ, Dang ZM, Xu HP, et al. Giant dielectric constant and resistance-pressure sensitivity in carbon nanotube/rubber nanocomposites with low percolation threshold. Appl Phys Lett 2007;90:042914.
[168] Dang ZM, Fan LZ, Nan CW, et al. Dielectric behavior of novel three-phase carbon nanotube/$BaTiO_3$/PVDF composites. Mater Sci Eng B 2003;103:140–4.
[169] Wang L, Gao F, Xu J, et al. Enhanced dielectric tunability and energy storage properties of plate-like $Ba_{0.6}Sr_{0.4}TiO_3$/poly(vinylidene fluoride) composites through texture arrangement. Compos Sci Technol 2018;158:112–20.
[170] Jabbari M, Bulatova R, Tok AIY, et al. Ceramic tape casting: A review of current methods and trends with emphasis on rheological behaviour and flow analysis. Mater Sci Eng B 2016;212:39–61.
[171] Baker W, Scott C, Hu GH, et al. Reactive polymer blending. Munich: Hanser publisher; 2001. p. 290.
[172] Sambyal P, Singh AP, Verma M, et al. Tailored polyaniline/barium strontium titanate/expanded graphite multiphase composite for efficient radar absorption. RSC Adv 2014;4:12614–24.
[173] Mikolajek M, Reinheimer T, Muth M, et al. Control of the surface morphology of ceramic/polymer composite inks for inkjet printing. Adv Eng Mater 2018;20: 1800318-1–10.
[174] Hu GX, Xu B, Yan XB, et al. Fabrication and electrical properties of textured $Ba(Zr_{0.2}Ti_{0.8})O_3$-$(Ba_{0.7}Ca_{0.3})TiO_3$ ceramics using plate-like $BaTiO_3$ particles as templates. J Mater Sci: Mater Electron 2014;25:1817–27.
[175] Guo YT, Meng N, Xu J, et al. Microstructure and dielectric properties of $Ba_{0.6}Sr_{0.4}TiO_3$/(acrylonitrile- butadiene- styrene)- Poly(vinylidene fluoride) composites. Adv Compos Hybrid Mater 2019;2:681–9.
[176] Hu T, Juuti J, Jantunen H. RF properties of BST-PPS composites. J Eur Ceram Soc 2007;27:2923–6.
[177] Osinska K, Adamczyk M, Dzik J, et al. Fabrication and characterization of BST60//40//PVDF ceramic-polymer composites. Arch Metall Mater A 2011;56: 1083–91.

[178] Wang L, Gao F, Xu J, et al. Fabrication, characterization and dielectric properties of KH550 modified BST/PVDF nanocomposites with high dielectric strength. High Volt 2017;1:1–8.
[179] Huang XY, Sun B, Zhu YK, et al. High-k polymer nanocomposites with 1D filler for dielectric and energy storage applications. Prog Mater Sci 2019;100:187–225.
[180] Xu J, Guo YT, Zhang KN, et al. Monodisperse $Ba_{0.6}Sr_{0.4}TiO_3$ hollow spheres via a modified template-assisted method. Appl Surf Sci 2020;531:147315.
[181] Guo YT, Zhang KN, Meng N, et al. Microstructure and dielectric properties of sub-micron hollow sphere $Ba_{0.6}Sr_{0.4}TiO_3$/PVDF composites. IET Nanodielectrics 2019;2:135–41.
[182] Xu JW. Dielectric nanocomposites for high performance embedded capacitors in organic printed circuit boards. PhD thesis. University of Pennsylvania; 2006.
[183] Windlass H, Raj PM, Balaraman D, et al. Polymer-ceramic nanocomposite capacitors for system-on-package (SOP) applications. IEEE T Adv Packaging 2013;26:10–6.
[184] Tang HX, Sodano HA. Ultra-high energy density nanocomposite capacitors with fast discharge using $Ba_{0.2}Sr_{0.8}TiO_3$ nanowires. Nano Lett 2013;13:1373–9.
[185] Liu SH, Xiao S, Xiu SM, et al. Poly(vinylidene fluoride) nanocomposite capacitors with a significantly enhanced dielectric constant and energy density by filling with surfacefluorinated $Ba_{0.6}Sr_{0.4}TiO_3$ nanofibers. RSC Adv 2015;5:40692–9.
[186] Zhu XP, Guo MY, Sun BW, et al. Significantly enhanced energy storage density of epitaxial $Ba_{0.53}Sr_{0.47}TiO_3$ thin films by optimizing bottom electrode material. Ceram Int 2020;46:13900–6.
[187] Zhang QQ, Gao F, Hu GX, et al. Characterization and dielectric properties of modified $Ba_{0.6}Sr_{0.4}TiO_3$/poly(vinylidene fluoride) composites with high dielectric tunability. Compos Sci Technol 2015;118:94–100.
[188] Song Y, Shen Y, Liu HY, et al. Improving the dielectric constants and breakdown strength of polymercomposites: effects of the shape of the $BaTiO_3$ nanoinclusions, surface modification and polymer matrix. J Mater Chem 2012;22:16491–8.
[189] Zhang KN, Gao F, Xu J, et al. Synthesis of $Ba_{0.6}Sr_{0.4}TiO_3$ platelet crystals based on $Bi_4Ti_3O_{12}$ precursor by topochemical microcrystal conversion. J Alloy Compd 2017;726:955–60.
[190] Zhang HF, Kong LB, Ma CL, et al. Highly enhanced sinterability of fine-grained $Ba_{0.6}Sr_{0.4}TiO_3$-MgO bulk ceramics and in-situ nanocomposite thick films. Ceram Int 2014;40:10475–81.
[191] Yu SH, Lou WT, Zhang CM, et al. (1 1 0)-textured $BaSn_{0.15}Ti_{0.85}O_3$/ $Ba_{0.6}Sr_{0.4}TiO_3$/ $BaZr_{0.2}Ti_{0.8}O_3$ multilayers with enhanced tunable performance. J Alloy Compd 2019;781:689–95.
[192] Zhai JW, Chen H, Chou CC, et al. Peculiarities of temperature and field dependence of tunability in $Ba_{0.6}Sr_{0.4}TiO_3$ ceramics with differing grain sizes. J Alloy Compd 2011;509:6113–6.
[193] Paul F, Menesklou W, Link G, et al. Impact of microwave sintering on dielectric properties of screen printed $Ba_{0.6}Sr_{0.4}TiO_3$ thick films. J Eur Cream Soc 2014;34:687–94.
[194] Iskandar J, Jenie RP, Siregar UJ, et al. Application of thin film barium strontium titanate (BST) in a microcontroller based tool to measure oxygen saturation in blood. Ferroelectrics 2020;554:134–43.
[195] Kurniawan A, Irzaman, Yuliarto B, et al. Application of barium strontium titanate (BST) as a light sensor on led lights. Ferroelectrics 2020;554:160–71.
[196] Godziszewski K, Yashchyshyn Y, Pawlikowska E, et al. Investigations of tunability of ferroelectric ceramic-polymer composites. International Conference on Microwaves 2014:1–3.
[197] Wang Z, Yue JL, Jiang C, et al. Vacancy-induced resistive switching and synaptic behavior in flexible BST@Cf memristor crossbars. Ceram Int 2020;46:21569–77.
[198] Hajisaeid E, Deshmukh S, Burbine SJ, et al. Printed planar tunable composite right/left-handed leaky-wave antenna based on a tunable polymer-BST substrate. Microw Opt Technol Lett 2020;1:1–12.
[199] Gupta R, Gupta V, Tomar M, et al. Structural and dielectric properties of PLD grown BST thin films. Vacuum 2019;159:69–75.
[200] Wang F, Ma WH. Phase stability and dielectric properties of (011) epitaxial ($Ba_{0.6}Sr_{0.4}$) TiO_3 films. J Appl Phys 2019;125:082528.
[201] Chen W, Lee BY, Zhu XH, et al. Tunable ultrahigh dielectric constant (tuHDC) ceramic technique to largely improve RF coil efficiency and MR imaging performance. IEEE T Med Imaging 2020;1:99.
[202] Palukuru VK, Sonoda K, Hagberg J, et al. BST-Polymer composite-based planar inverted-f (pifa) chip antenna for 2.4 GHz Wrist Applications. Integr Ferroelectr 2010;114:17–24.
[203] Chameswary J, Sebastian MT. Butyl rubber–$Ba_{0.7}Sr_{0.3}TiO_3$ composites for flexible microwave electronic applications. Ceram Int 2013;39:2795–802.
[204] Valant M. Electrocaloric materials for future solid-state refrigeration technologies. Prog Mater Sci 2012;57:980–1009.
[205] Bin-Omran S. Thickness dependence of electrocaloric response in ferroelectric thin films. Mater Lett 2017;196:351–3.
[206] Jiang ZY, Zheng XC, Zheng GP, et al. The enhanced electrocaloric effect in P(VDF-TrFE) copolymer with barium strontium titanate nano-fillers synthesized via an effective hydrothermal method. RSC Adv 2015;5:61946–54.
[207] Zhang GZ, Li Q, Gu HM, et al. Ferroelectric polymer nanocomposites for room temperature electrocaloric refrigeration. Adv Mater 2015;27:1450–4.
[208] Zhang GZ, Zhang XS, Yang TN, et al. Colossal room-temperature electrocaloric effect in ferroelectric polymer nanocomposites using nanostructured barium strontium titanates. ACS Nano 2015;9:7164–74.
[209] Zhang GZ, Fan BY, Zhao P, et al. Ferroelectric polymer nanocomposites with complementary nanostructured fillers for electrocaloric cooling with high power density and great efficiency. ACS Appl Eng Mater 2018;1:1344–54.
[210] Palukuru VK, Sanoda K. Inkjet-printed rf structures on BST–polymer composites: an application of a monopole antenna for 2.4 GHz wireless local area network operation. Int J Appl Ceram Technol 2011;8:940–6.
[211] Palupi EK, Umam R, Andriana BB, et al. Micro-Raman analysis of $Ba_{0.2}Sr_{0.8}TiO_3$ (barium strontium titanate) doped of chlorophyll of cassava leaf. Ferroelectrics 2019;540:227–37.
[212] Tariverdian T, Behnamghader A, Milan PB, et al. 3D-printed barium strontium titanate-based piezoelectric scaffolds for bone tissue engineering. Ceram Int 2019;45:14029–38.
[213] Xu SW, Qian WQ, Zhang D, et al. A coupled photo-piezo-catalytic effect in a BST-PDMS porous foam for enhanced dye wastewater degradation. Nano Energy 2020;77:105305.
[214] Li XL, Li Y, Wu LC, et al. Enhanced flexoelectricity in $Ba_{0.6}Sr_{0.4}TiO_3$/epoxy composite. Mater Lett 2020;260:126953.
[215] Faraji S, Hashimoto T, Turner ML, et al. Solution-processed nanocomposite dielectrics for low voltage operated OFETs. Org Electron 2015;17:178–83.
[216] Lim S, Lee KH, Kim H, et al. Optimization of nanocomposite gate insulators for organic thin film transistors. Org Electron 2015;17:144–50.
[217] Qiao Q. Reconfigurable sensing antenna with novel HDPE-BST material for temperature monitoring. IEEE Antenn Wire Pr 2013;12:1420–4.
[218] Yuan SY, Kymissis I. Influence of electromigration on the maximum operating field of (Ba, Sr)Ti_O3/parylene-C composite capacitors. J Vac Sci Technol B 2013;31:060603.

Feng Gao is a Professor in the School of Materials Science and Engineering at Northwestern Polytechnical University (NPU) in China. Feng Gao received degrees of B.E., M.E. and Ph.D. in Materials Science and Engineering from NPU in Xi'an from 1992 to 2002. Following post-doctoral work at Postdoctoral mobile station of Aerospace Science and Technology in NPU from 2003 to 2005, he worked in Pennsylvania State University of America as visiting scholar. He is currently director of the Department of Materials Science and Engineering in NPU, and Chief-scientist of QMUL-NPU Joint Research Institute of Advanced Materials and Structures (AMAS JRI). His main research interests are development of advanced functional ceramics and composite materials, particular those intended for energy, microwave tunable and communication devices.

Kena Zhang got her B.E and M.E. in Materials Science and Engineering from the Fuzhou University and Northwestern Polytechnical University at 2015 and 2018, respectively. Kena Zhang's research mainly focused on electro-composites, including the preparation and dielectric properties of polymer-ceramics for microwave tunable device applications, as well as Phase-field modeling of ferroelectric materials.

YiTing Guo got the B.E and M.E. from the Xi'an University of Technology and Northwestern Polytechnical University at 2015 and 2018, respectively. Now she is a Ph.D. student in Materials Science and Engineering at NPU. She currently works in the Ceramic/polymer composites, including the preparation, dielectric properties and application in energy storage device and microwave tunable device.

Jie Xu is an Assistant Professor in the School of Materials Science and Engineering at Northwestern Polytechnical University (NPU) in China. He received B.E. degree from NPU in 2007, M.E. degree from China Building Materials Academy in 2010 and Ph.D. from Tsinghua University in 2014. He did postdoctoral work in Tsinghua University from 2014 to 2016 and worked in Birmingham University, UK as a visiting scholar from 2015 to 2016. Jie Xu is mainly focused on synthesis of nano-size ceramics powder, colloidal processing of ceramics and advanced sintering techniques.

Mikolaj Szafran, is a Professor of chemical technology, specialization- the technology of advanced ceramics at Faculty of Chemistry Warsaw University of Technology (WUT). Member (Academician) of the World Academy of Ceramics – Class Science. He was graduated from WUT in 1974, Ph.D. in1983, D.Sc. in 2000, and a full professor since 2009. His is working in WUT since 1974; in 1994-1997, ENEA, (Rome, Italy). Member of Ceramic Science Commission of Polish Academy of Science, since 2015. Member of the Board of the European Ceramic Society -since 2009. Member of the Editorial Board of the Journal of Ceramic Science and Technology. He is identified mainly by his work concerning the shaping of advanced ceramics materials (designing, synthesis, and application new water-soluble monomers and new water-dispersible polymeric binders for different methods of the shaping of ceramics), porous ceramic materials, and ceramic-metal and ceramic polymer-composites.